MODELING, OPTIMIZATION AND CONTROL OF SPATIAL UNIFORMITY IN MANUFACTURING PROCESSES

by

RUEY-SHAN GUO

B.S. NATIONAL TAIWAN UNIVERSITY, 1983
M.S. MASSACHUSETTS INSTITUTE OF TECHNOLOGY, 1987

SUBMITTED TO THE DEPARTMENT OF MECHANICAL ENGINEERING IN PARTIAL FULFILLMENT OF THE REQUIREMENTS FOR THE DEGREE OF

DOCTOR OF PHILOSOPHY IN MECHANICAL ENGINEERING

at the

MASSACHUSETTS INSTITUTE OF TECHNOLOGY

September 1991

Signature of Author _____
Department of Mechanical Engineering
September 5, 1991

Certified by _____
Emanuel Sachs
Thesis Supervisor

Accepted by _____
Ain Sonin
Chairman, Departmental Committee on Graduate Students

MODELING, OPTIMIZATION AND CONTROL OF SPATIAL UNIFORMITY IN MANUFACTURING PROCESSES

by

Ruey-Shan Guo

Submitted to the Department of Mechanical Engineering on August 27, 1991 in partial fulfillment of the requirements for the degree of Doctor of Philosophy in Mechanical Engineering.

Abstract

As product quality assumes greater importance, tighter process control must be exercised over each manufacturing process and the output from each process step must be driven as close to target as possible. Process control includes optimization and control, and equipment models which simulate a process and related equipment are created to enable such process control. This thesis is directed at the modeling, optimization, and control of spatial uniformity within a batch of product. Spatial uniformity is important in every manufacturing process as it is often a significant contribution to the total variation of a process. Statistical models and design of experiments are used to derive the models, and off-line optimization and on-line optimization and control, which is also in the context of a process control system under development, are used for the subsequent process control.

Spatial uniformity, or the uniformity of product output characteristics at different locations in a batch of product, is modeled, optimized, and controlled using a methodology called "Multiple Response Surfaces" which may be used to characterize the results of an experimental design. Multiple, low-order polynomial models are used to model the output characteristics at each of several sites within a batch of product. The uniformity model is then obtained by manipulating these multiple models. The Multiple Response Surfaces approach is compared to the traditional method of fitting a single high-order polynomial to the calculated uniformity. Experimental results on several processes, confirm the expectation that similar or improved modeling accuracy is obtained with fewer data points using the new methodology due to the ability to use low-order models. Characteristics of the Multiple Response Surfaces approach including noise immunity and restrictions to classes of model forms are examined both analytically and in application to several semiconductor manufacturing processes, including plasma etching, silicon epitaxy, tungsten CVD and the simulation of polysilicon LPCVD.

Thesis Supervisor: Emanuel Sachs
Title: Associate Professor of Mechanical Engineering

ACKNOWLEDGEMENT

This work would not have been possible without the guidance and support of Professor Emanuel Sachs. His insight and enthusiasm have been the inspiration for my interest in this study. I am personally indebted to him.

I am also grateful to Professor Donald Troxel and Professor Don Clausing for giving useful comments during my thesis committee meetings.

I would like to express my gratitude to Sungdo Ha for sharing his results on plasma etching experiment, Albert Hu for the initial characterization of the epitaxial experiment, and Dr. Paul Langer of AT&T for sharing the results on epitaxial experiment.

My sincere thanks are also due to those who took time to discuss, suggest, and comment. In particular, I am grateful to Sungdo Ha and Albert Hu for the discussion of implementing Multiple Response Surfaces, Armann Ingolfsson and Stephen Thomke for the discussion of multivariate statistics, Dr. Carlos Moreno of Ultramax Corporation for his useful advice in using Ultramax, Joe Hillman of Spectrum Corporation for his valuable comments in performing the tungsten CVD experiment, Bob McCafferty of IBM for the application of Multiple Response Surfaces to a plasma etching tool, and Tim Dalton for the discussion of neural network in application to plasma etching.

This work is supported by DARPA under contract MDA972-88-K-008 and the SEMATECH Massachusetts Center of Excellence under contract 88MC503.

DEDICATION

TO MY PARENTS

TABLE OF CONTENTS

LIST OF FIGURES

LIST OF TABLES

CHAPTER ONE

INTRODUCTION

1.1 Motivation

As product quality assumes greater importance, tighter process control must be exercised over each manufacturing process and the output from each process step must be driven as close to target as possible. Process control includes optimization and control. Optimization is the step of selecting a combination of equipment settings that results in a process with the most preferred combination of output characteristics. Control involves small changes in equipment settings around the optimum point in order to maintain the best output as the process undergoes changes such as drifts and shifts. To enable such process optimization and control, we need models to simulate a process and related equipment.

This thesis is directed at the modeling, optimization, and control of the variation within a batch of product. For example, in a thermoforming process [1], within-a-batch variation might consist of thickness variation across each product. In semiconductor manufacturing processes, within-a-batch variation concerns variation across individual wafers and variation from wafer to wafer in a multiple wafer process such as a tube furnace. In a single wafer process, within-a-batch variation consists of variation across a wafer. Since the variation within a batch is due to variation from one location to another, the term "spatial uniformity" is used in this paper[1].

---

[1] While the focus in this thesis is on the treatment of batch processes, the methodology developed can be applied to continuous processes as well (an example of a contonuous process would be the treatment of a contonuous roll of material). The more general term "spatial uniformity" is therefore preferred.

Spatial uniformity is an issue in every manufacturing process. Its importance stems from the fact that it is often a significant contribution to the total variation of a process, and it generally presents challenges in modeling, optimization, and control. The difficulties associated with modeling, optimizing, and controlling spatial uniformity can be understood by way of examples. Consider the uniformity of thickness in a low pressure chemical vapor deposition (LPCVD) of polysilicon with 150 wafers in a tube furnace [2]. The output from a batch may be idealized as a probability distribution and two such distributions are shown in Fig. 1.1 together with the target value for the thickness. The width of each distribution represents the variation within a batch and the center of the distribution represents the mean of a batch. If we operate the process and observe distribution (a), we would like to reduce the total variation from the process by reducing the variation within a batch (the spread) and adjusting the mean of the batch to the target value. The result would be a distribution such as that shown in (b). The mean may be adjusted to target by changing a single setting, the deposition time. However, the spatial uniformity must be optimized by the proper combination of a number of equipment settings such as gas flow rates, injector positions, and tube pressure. For this reason, the modeling, optimization, and control of spatial uniformity presents a substantial challenge. Another example is plasma etching in a single wafer reactor [2]. In such a case, an end-point signal can be used to control the depth of the etch; however, the etch uniformity may depend on many equipment settings and is more difficult to model, optimize, and control. The third example is the thermoforming process which makes products like yogurt cups. In this case, the average thickness of the cup can be controlled by the volume of the material used; however, the thickness uniformity across the cup must be optimized by equipment settings like pressure, heating temperature, and heating time. Such optimization is important as non-uniformity can often cause the failure of the product (a leakage).

In this work, we define the spatial variation using a metric which normalizes the variation by the mean. The fundamental ratio that we consider is :

$$\frac{\sigma}{\mu} \tag{1.1}$$

where σ is the observed standard deviation and μ is the observed mean of a batch. This ratio is broadly used when uniformities are reported as percentages. Thus, the specification of 5% uniformity is the result of using this metric.

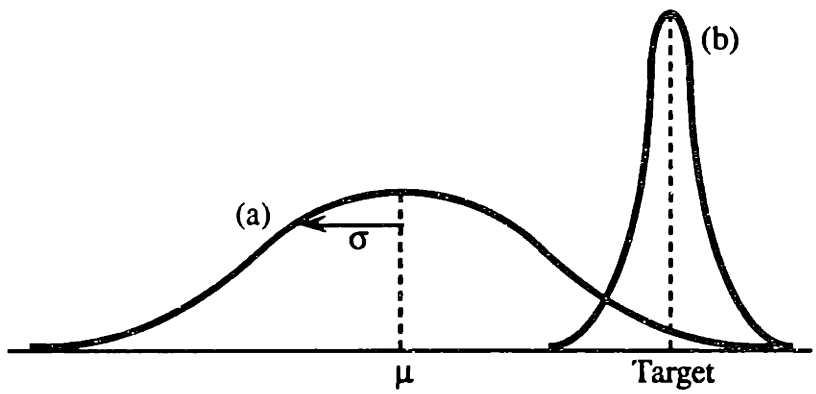

Fig. 1.1 Two distributions (a) before improvement (b) after improvement.

1.2 Objective and Approach

The objective of this work is to develop effective methodologies for modeling spatial uniformity and to use the derived model for subsequent process optimization and control. It will be demonstrated that the developed methodologies are also used in a more general process control system under development.

In this work, the methodologies we use to construct the models are design of experiments and empirical models. The main focus is on a new modeling approach which is called "Multiple Response Surfaces". In most cases, spatial uniformity is not measured

directly but calculated from measurements of output characteristics taken at specified locations. It might be beneficial to fit these primitive output characteristics first and then manipulate these models to construct the model of the spatial uniformity. This is different from the traditional approach of first calculating the value of the spatial uniformity for each experimental run and then fitting an equation to these calculated values.

The new approach will be shown to have the advantages of effective models from a small number of data, rapid adaptation of models after a process disturbance, immunity of models to the presence of noise, and compatibility of the model forms with process knowledge. These advantages are due to the fact that primitive output characteristics are being fitted.

1.3 Outline of the Thesis

The modeling, optimization, and control of spatial uniformity has been an effort to develop a general process control system. The process control system under development is first described in chapter two. The system integrates existing approaches to process control with new methodologies in order to achieve on-line optimization and control of unit processes with consideration of preceding and following process steps. The process control system is based on three core modules : the Flexible Recipe Generator, the Run by Run Controller, and the Real Time Controller.

Chapter three describes the methodologies we use in modeling spatial uniformity. In particular, the procedures of two modeling approaches, Single Response Surface and Multiple Response Surfaces, are explained in detail. In chapter four, the advantages of using the Multiple Response Surfaces approach are discussed and demonstrated through a simulation of LPCVD of polysilicon.

Experimental results are described in chapter five, including applications to silicon epitaxy, tungsten CVD, and plasma etching, all from semiconductor manufacturing unit processes. In chapter six, some of the basic characteristics of the Multiple Response Surfaces approach are examined, including the relationship between robustness and tuning, the curvature effect of the underlying uniformity, saddle point, and the confidence interval of the predictions.

In chapter seven, we describe the alternative ways to implementing Multiple Response Surfaces. This includes the uses of mixed model, neural network, and difference model. At last, conclusions and future work are made in chapter eight.

CHAPTER TWO

PROCESS CONTROL SYSTEM

2.1 Background

Process control is a crucial ingredient in the operation of any manufacturing facility. The techniques and methodologies used for process control determine the effectiveness of each piece of equipment and influence the organization and operation of a facility.

In current practice, process control is implemented in two stages : off-line and on-line. On-line process control includes all approaches where the goal is to improve the process without making any scrap. Off-line process control is taken to include methods where there is no penalty for making scrap.

The most widely employed implementation of off-line process control is off-line optimization using methods of statistical design of experiments [3]. Response surface methods [4][5] and the Taguchi method [6] - [10] are examples of methodologies based on the design of experiments. The key commonality is that experiments are performed by varying many factors simultaneously, thus ensuring an efficient exploration of experimental space. Both methods create models for the purpose of estimating the optimum setting point. These methods can not be used on-line because most of the experiments performed produce scrap. The result is that such optimization methods are infrequently performed, and are used only to determine the best general area for operation and not to fine tune the process. A new methodology which allows for on-line optimization would be extremely beneficial.

As currently practiced, processes are re-tuned only when statistical process control (SPC) [11] indicates a large departure from routine operation and the re-tuning is based on operator experience. An opportunity for improvement is to perform re-tuning on a more frequent basis in order to compensate for small drifts and shifts in the process output. An automated system which changes the equipment settings between product runs based on post-process and *in situ* measurements would provide a framework for accommodating multiple-output responses to multiple-inputs. Such a system would go beyond the capability of human operators who can only consider single-input and single-output problems and would provide consistent and reliable operation. Such control can be done in a feedback mode based on post-process and *in situ* measurements made on a previous batch of wafers processed at the same machine. In addition, such control can be done in a feedforward mode based on post-process measurements made on the same batch of wafers processed at a previous machine.

At the present time, real time control is limited to single-input and single-output loops dedicated to the control of equipment settings. As more *in situ* measurements become realistic, there will be opportunities to further tighten control through expanded real time feedback control.

Currently, automated SPC interpretation is rarely done and equipment diagnostics is mainly through human interpretation. Greater automation is expected in a new system to help identify problems as early as possible.

2.2 System Description

The modular framework of the process control system under development is schematically illustrated in Fig. 2.1. This block diagram represents the control of two

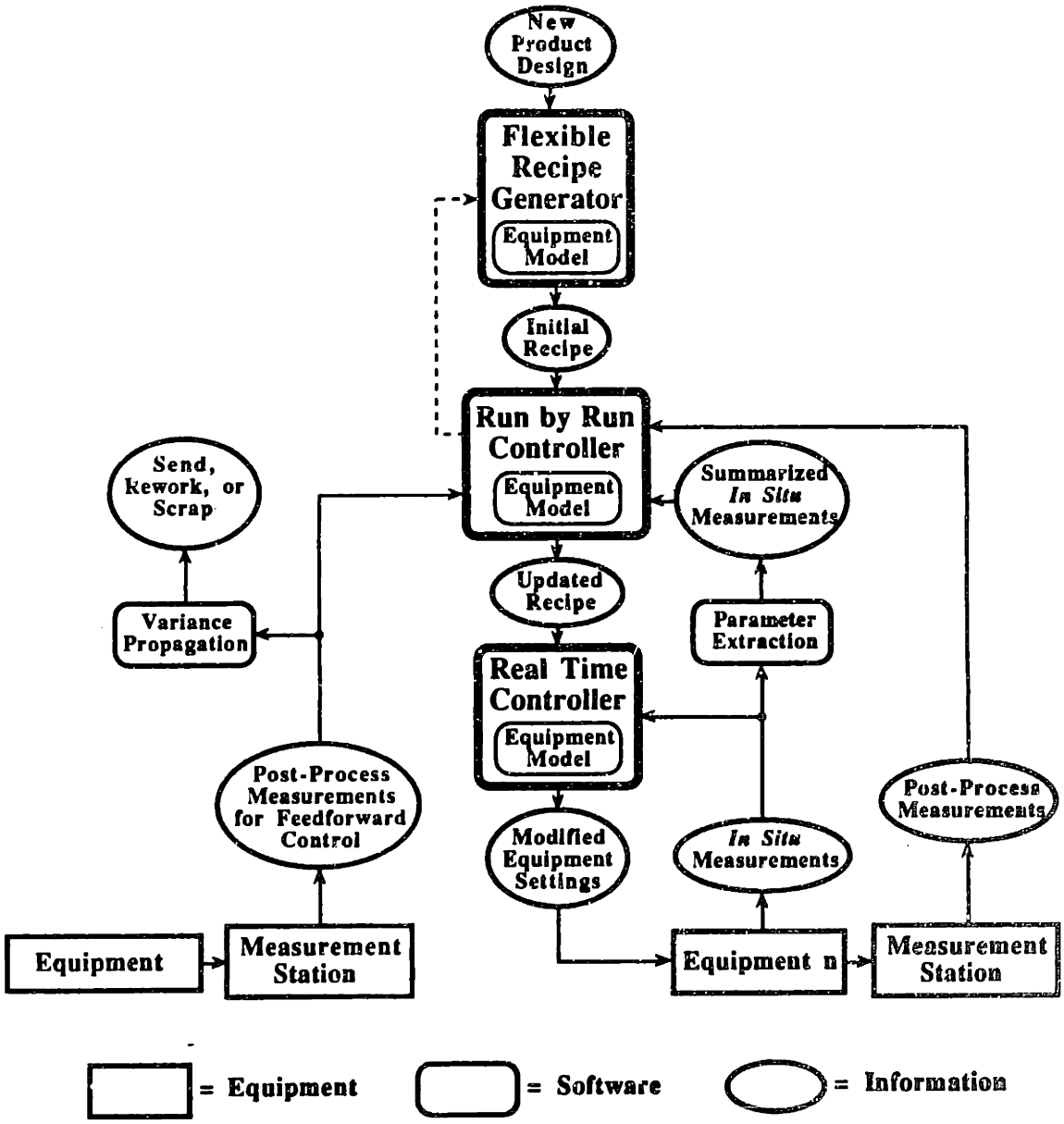

Fig. 2.1 Block diagram for process control system.

sequential pieces of equipment (equipment n-1 and equipment n) somewhere in the process flow corresponding to the manufacturing of a product. The square-cornered boxes represent hardware, the rounded-corner boxes represent software modules, and the ellipses represent information flowing through the system.

Each piece of equipment has post-process and *in situ* measurements associated with it. In specific instances, these measurements might be absent, but, in general, they are available. Post-process measurements are those made on the products after they are removed from the processing equipment. An example of post-process measurements is thickness measurements on deposited films. *In situ* measurements are those made while the process is going on. *In situ* measurements can be of four types: measurements made on the product itself, measurements made on equipment settings, measurements made on the process parameters, and measurements made to characterize the condition of the equipment. An example of an *in situ* product measurement is *in situ* ellipsometry for film thickness. An example of an *in situ* equipment setting measurement is a measurement of gas flow rate. An example of an *in situ* process parameter measurement is a measurement of gas composition. An example of an *in situ* equipment condition measurement is a measurement of thickness of the build-up on the walls of a reactor.

The function of process control has been divided into three core modules. The Flexible Recipe Generator determines an initial operating point in response to a new product design. The Run by Run Controller tunes the recipe between runs based on feedback from post-process and *in situ* measurements. The Real Time Controller further modifies the equipment settings during a process step based on *in situ* measurements. These three modules act to divide up the control function on the basis of the time scale of the response and the range of setting space encompassed. The Flexible Recipe Generator covers the

largest setting space and is invoked only once at the beginning of manufacture of each new design or product. The Run by Run Controller covers a smaller range of space and is invoked after each run of product. The Real Time Controller has the smallest range of setting space and is invoked (in the limit) continuously during each product run.

The Variance Propagation module serves the purpose of making decisions about when to send a batch on, when to rework it, and when to scrap it. This module, in effect, designs the specification limits based on predictions about the probable outcome of continuing to process a batch of product given information about its current condition [12].

2.3 Flexible Recipe Generator

This module responds to each new product design with an indication of the appropriate recipe for the first run. Conceptually, the Flexible Recipe Generator is a substitute for off-line design of experiments and is expected to get the process into the general region of the best performance. One key aspect of the optimization done by the Flexible Recipe Generator is to seek the region of setting space that is most robust against disturbances (least sensitive to disturbances). This role of the Flexible Recipe Generator is after Taguchi's concept of robust operation through parameter design [6]. Following the global optimization performed by the Flexible Recipe Generator, the Run by Run Controller can perform the final tuning needed to locally optimize the process.

Since the Flexible Recipe Generator is designed for the exploration of the global setting space, equipment models constructed should have high accuracy over a large range of setting space. Two alternatives are available for this purpose. One is the construction of multiple piecewise regression models, with each one simulating a separate small setting space. The other is the construction of a mechanistic or semi-empirical model which

simulates the whole setting space. We have implemented our initial Flexible Recipe Generator for LPCVD of polysilicon based on the second approach [13].

2.4 Run by Run Controller

2.4.1 Major Functions

This module starts from the recipe provided by the Flexible Recipe Generator and updates the recipe between product runs. In response to post-process and *in situ* measurements, the Run by Run Controller updates its equipment models and recommends a change in the recipe in order to seek improvement of the process. This sequential adjustment procedure, to seek and stay at an optimum, is similar to the way a process engineer operates a piece of equipment. However, the adjustment by a process engineer is generally done on the basis of guidelines in the equipment supplier's manual and previous experience. Moreover, the control actions are usually limited to single-input and single-output, as a human has difficulty dealing with more complex situations on a quantitative basis. The Run by Run Controller automates and improves on the traditional actions of the process engineer by creating a mathematical formalism which allows for multiple-output responses to multiple-inputs. The Run by Run Controller has two functions [14], one of which is to optimize the process and the other being to control process. These two functions are summarized in Fig. 2.2 and are discussed next.

2.4.2 Optimization

If the process is not yet optimized, the optimization phase of the Run by Run Controller is entered (Fig. 2.2). The goal is to fine-tune the process on-line without making scrap.

The algorithmic basis is the use of sequential design of experiments to update models, which is best explained with a simple example.

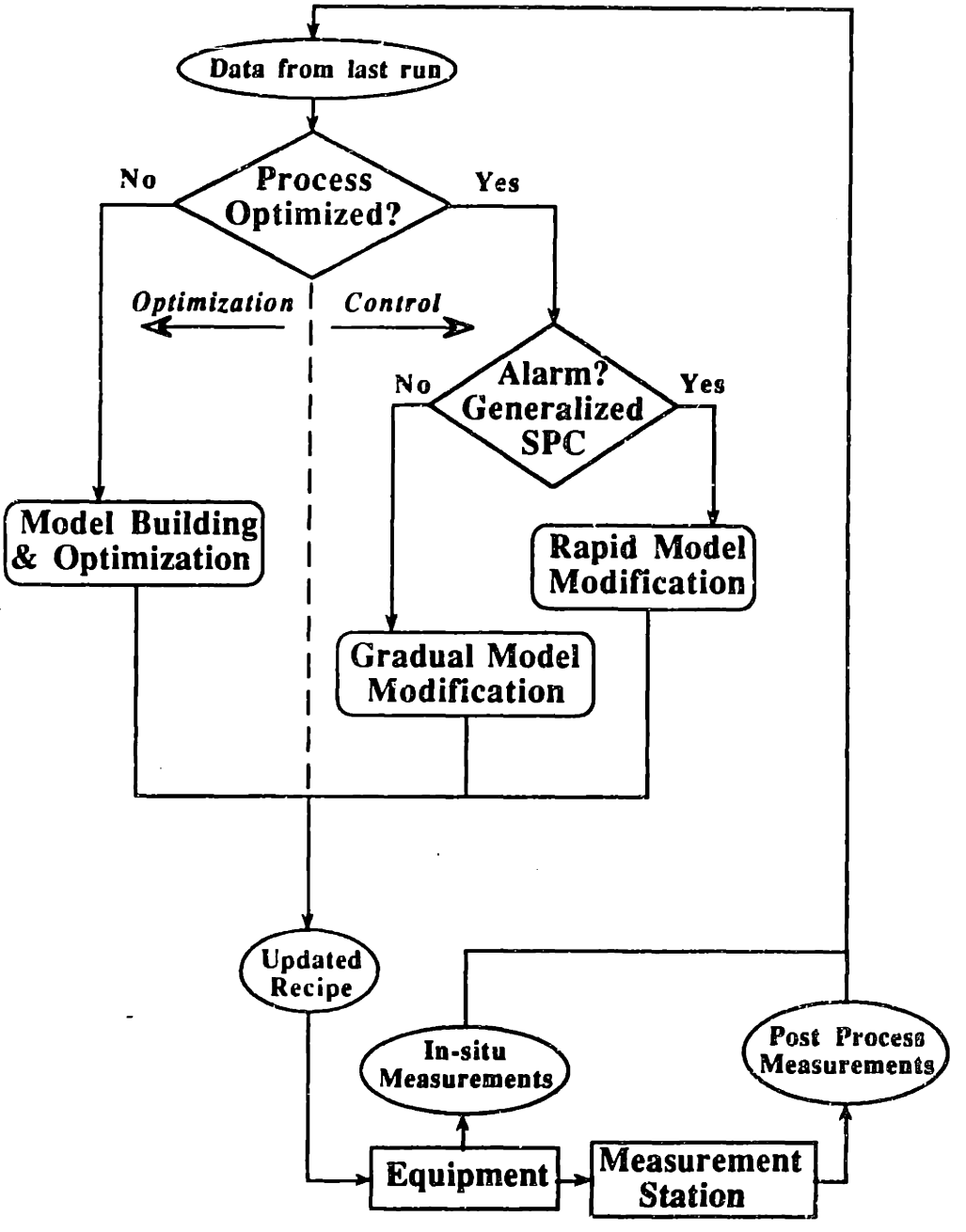

Fig. 2.2 Major functions of Run by Run Controller.

Suppose we want to maximize a production rate (objective function) by adjusting only one equipment setting x_1. The underlying response of the production rate to this equipment setting is assumed to be unknown in the beginning as shown in Fig. 2.3(a). The fundamental procedure of the sequential design of experiments is to sequentially construct the equipment model after each run. Local, weighted regression, which selects and weighs the appropriate data points based on the distance from a reference point in setting space and time, is adopted to ensure higher accuracy in the current region of operation. Suppose we have four data points at some stage in our simple example, a second-order response surface is constructed as shown in Fig. 2.3(b).

The constructed model can now be used to design the next experiment. We might design our next run based on the predicted optimum operating point; however, we usually limit the excursion for the sake of avoiding scrap. As one moves away from the region within which the model is fitted (Fig. 2.3(c)), the error of fit greatly increases, representing the fact that the uncertainty of the fitted model increases and the risk of making scrap increases. We limit the excursion when the projected error of fit exceeds the specification range. We continue climbing the hill as shown in Fig. 2.3(d), with sequential design one run at a time. Note that local weighted regression allows the model to conform to the local behavior of the process.

2.4.3 Control

Once the process is optimized, then the function of the Run by Run Controller switches to control of the process (Fig. 2.2). Control is the process of maintaining the performance at a local optimum in the presence of disturbances to the process such as shifts and drifts.

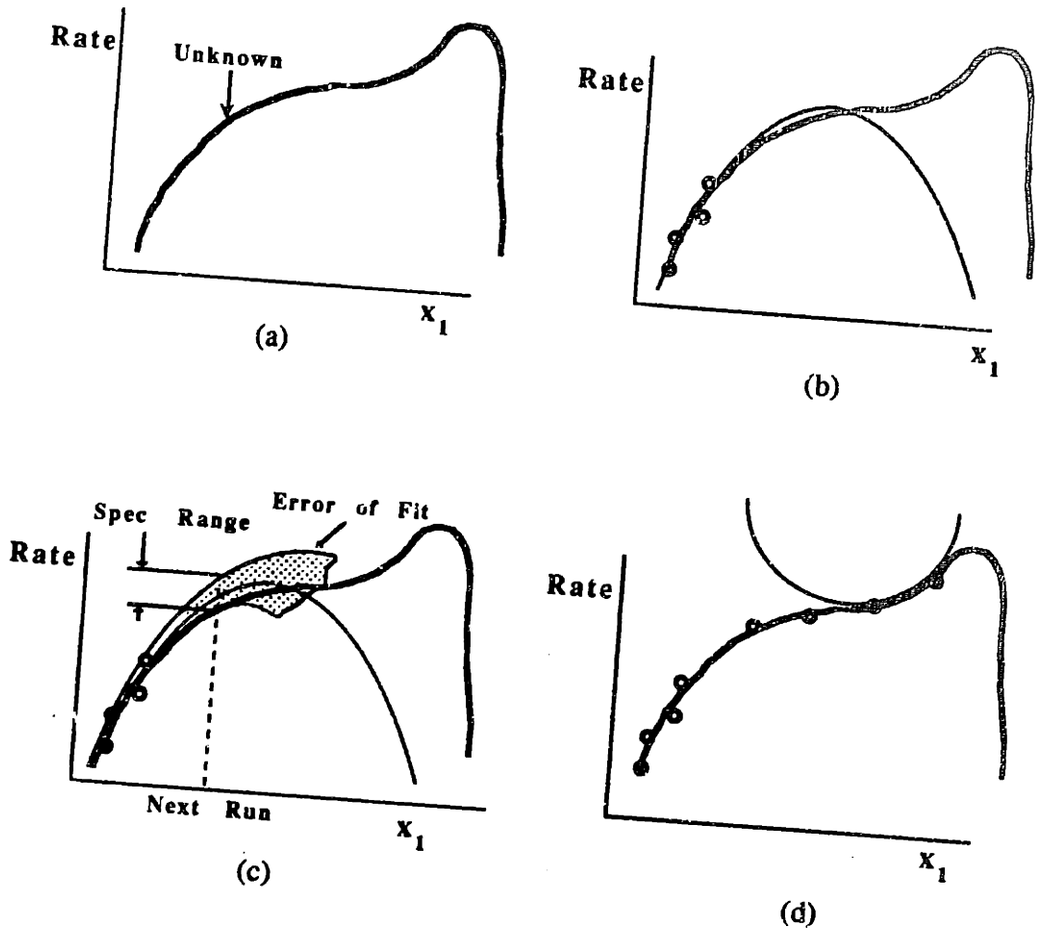

Fig. 2.3 Single-input, single output example illustrating sequential design of experiments for optimization of Run by Run Controller.

Drifts refer to gradual changes of the process over the course of time, while shifts refer to relatively abrupt changes, including step disturbances. In some cases, shifts and drifts can be ascribed to known causes. For example, the build-up of deposition on the inside of a reactor can cause gradual shifting of the process. When a maintenance operation is performed, the process may undergo a sudden shift. In other cases, the cause of a drift or

shift is not easily ascribed, and the presence of the shift or drift must be detected from the data. In other words, the Run by Run Controller includes both process monitoring and process control in one unit [15][16]. In the Run by Run Controller this detection is performed by generalized statistical process control. Generalized statistical process control is a generalization of the standard approach to statistical process control (SPC) which enables the diagnostic capability of SPC to be applied even while the process is being tuned (the recipe is being changed) [14][17]. In traditional SPC, the output is assumed to be a sample from a statistical distribution with a known mean and standard deviation. In generalized SPC, the model is more complex and includes the local dependence of the output on equipment settings as embodied in the models of the Run by Run Controller.

When the process is changing gradually, generalized SPC will indicate that the process is in control and a mode of gradual model modification is entered (Fig. 2.2). In this mode, changes are made to the model on a gradual basis to allow the controller to keep up with a slowly drifting process and modify the recipe to compensate for this slow drift. When generalized SPC detects a rapid change in the process and triggers an alarm, a rapid mode of model modification is entered (Fig. 2.2) so as to respond to the changed process as quickly as possible.

2.4.4 Illustration : Simulation of LPCVD of Polysilicon

In order to test its utility for optimization and control, the Run by Run Controller was applied tc an equipment simulator of LPCVD of polysilicon [18].

The schematic of the reactor is shown in Fig. 2.4. The equipment simulator is a one-dimensional finite difference model which predicts the deposition rate from wafer to wafer down the reactor. The deposition rate uniformity within a batch can be tuned by adjusting

five equipment settings : the silane flow rates of the load injector and the center injector (the total flow rate of the three injectors was fixed), the axial positions of the center injector and the source injector, and the pressure inside the reactor. In the simulations below, 11 equally-spaced monitoring wafers were chosen from the total 150 wafers to calculate the uniformity of one run. Taguchi's signal-to-noise ratio (SN Ratio) [6], which evaluates the ratio of mean to standard deviation as shown in (2.1), was used as the uniformity metric to be maximized[2].

$$\text{SN Ratio} = 10 \log_{10} \left(\frac{\mu}{\sigma}\right)^2 \tag{2.1}$$

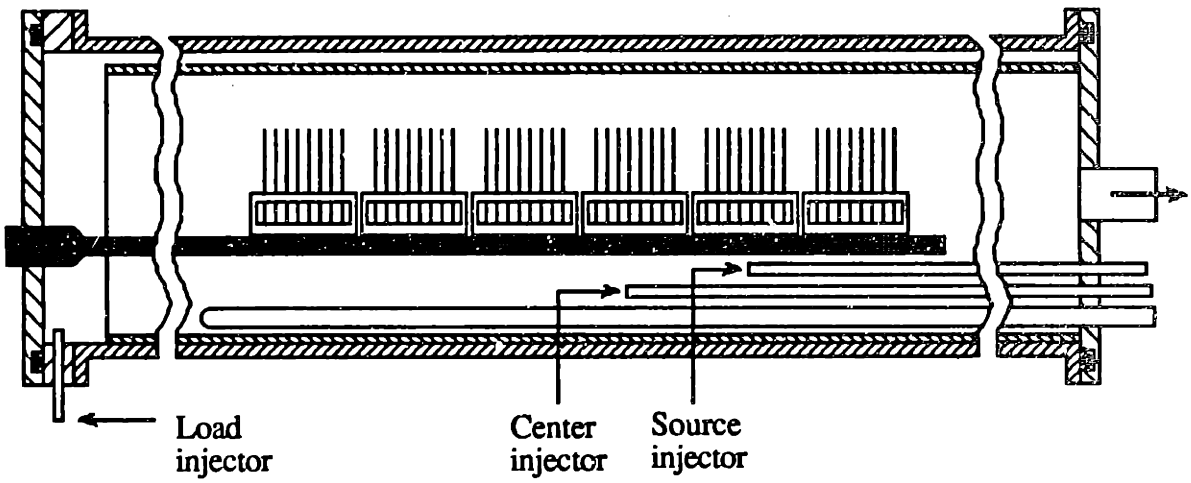

Fig. 2.4 Schematic of LPCVD reactor.

[2] The SN Ratio is a monotonic transformation of the ratio (σ / μ) which may have some advantages in reducing the importance of interaction terms in the models [6][7]. Qualitatively similar results were obtained when (σ / μ) was used as the uniformity metric.

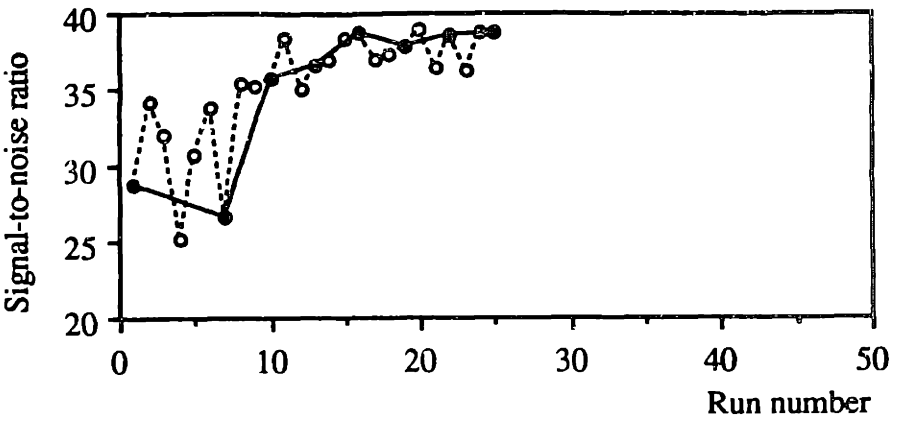

(a) Improvement of SN Ratio

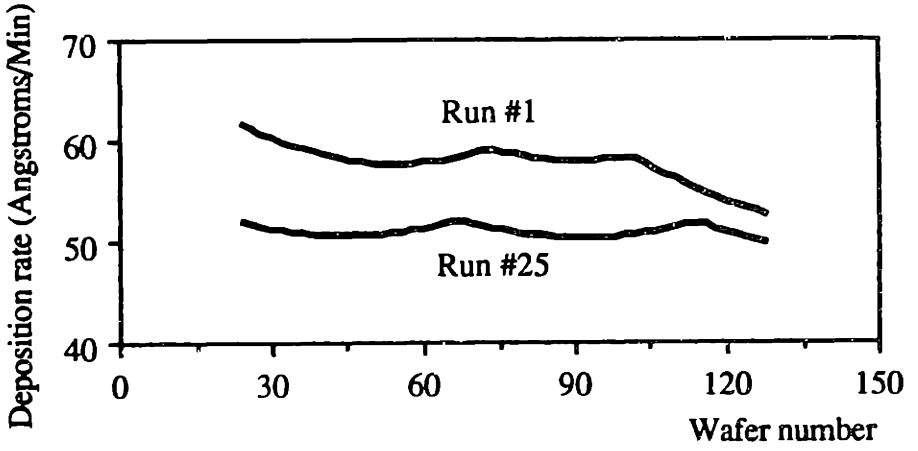

(b) Deposition rate profiles

Fig. 2.5 Run by run optimization of deposition rate uniformity.

Reasonable random disturbances were superimposed on both equipment settings and deposition rate measurements to simulate the real process. A commercial software package called Ultramax [19][20] was used as the basis for the optimization of the Run by Run Controller. An improved modeling approach called "Multiple Response Surfaces" was used to increase the speed of the optimization. Results of the optimization study are shown in Fig. 2.5. Fig. 2.5(a) shows the run by run history of SN Ratio, and demonstrates an overall trend of improvement (solid circles connected by a solid line). Solid circles, which

occur every three cycles after the initial learning phase, correspond to the optimum runs while open circles represent exploration runs which are intentionally designed a little away from the optimum prediction in order to "learn" more about the process. Fig. 2.5(b) shows the deposition rate profiles down the length of the tube corresponding to the first run and the best run (run #25). As can be seen, the best run has a lower mean deposition rate, but a substantially better uniformity, leading to a higher SN Ratio.

In this case of control, a step disturbance which might result from a maintenance operation was simulated by imposing a shift in the position of two injectors. This simulated step disturbance was applied between runs #25 and #26, immediately following a local optimization sequence. Fig. 2.6 shows that the step disturbance resulted in a process that was less well tuned, and that the Run by Run Controller (not Ultramax) was then able to respond and effect a recovery of process uniformity.

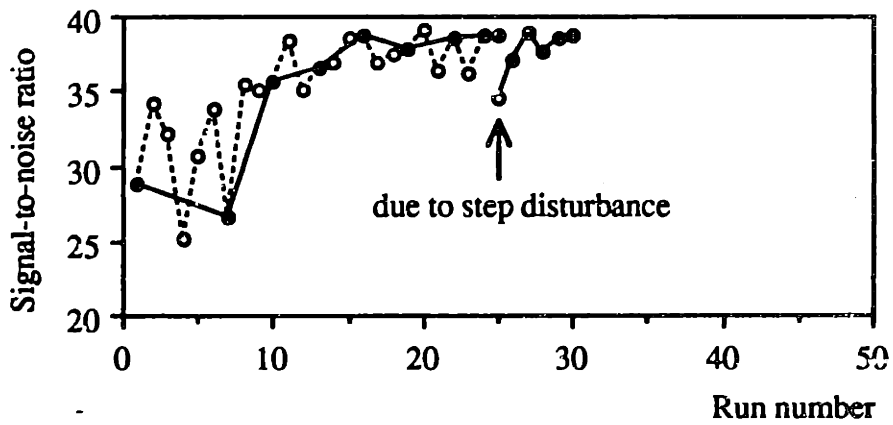

Fig. 2.6 Run by run control following optimization of Fig. 2.5.

2.4.5 Parameter Extraction

In the examples just discussed, the optimization and control action is based on post-process measurements. The Run by Run Controller can also utilize *in situ* measurements

for process optimization and control. In this case, however, the real time *in situ* measurements must be summarized into a relatively small number of parameters so that the Run by Run Controller can work with data which characterizes the process on a run by run basis. This summarization is accomplished by the Parameter Extraction module. As an example, the Parameter Extraction module might calculate an average value of an *in situ* measurement over the course of a run. Alternatively, the Parameter Extraction module might fit a first-order time response to the *in situ* data from a run and deliver the time constant and steady state value to the Run by Run Controller. In this manner, *in situ* measurements might be used as indicators of disturbances within the system which could be compensated by changes in the equipment settings. *In situ* measurements might also be used to replace post-process measurements when they are not available on a timely basis.

2.5 Real Time Controller

The Real Time Controller accepts *in situ* measurements as inputs and modifies the equipment settings during a process step in order to bring the result as close to target as possible. A feature that distinguishes the Real Time Controller from the Flexible Recipe Generator and the Run by Run Controller is that the Real Time Controller can utilize equipment models which include time response [13].

In principle, the Real Time Controller is compensating for small differences that exist between one product run and another. The differences might be due to incoming product, incoming raw materials, or equipment operation. When these differences can be characterized before the run starts, the Run by Run Controller can be used to compensate for them. When the differences can only be characterized during the run by *in situ* measurements, the Real Time Controller must be used to compensate for them.

2.6 Equipment Modeling

2.6.1 Definition

Equipment models play an important role in the process control system. They are constructed in the three core modules to serve as the basis of process control. Here we define an equipment model as a simulation of a manufacturing process and related equipment.

Fig. 2.7 illustrates a generic model for a manufacturing process and related equipment with two types of inputs : the inputs that we have control over, and the disturbances that we have no control over [21]. The inputs that we have control over include equipment settings and incoming work material. We can alter the output of a process by changing these controllable inputs. Disturbances are those inputs which are subject to unintended and undesired variations. They include variations in the properties of incoming work material, variations in the equipment settings, and variations in other factors affecting the process.

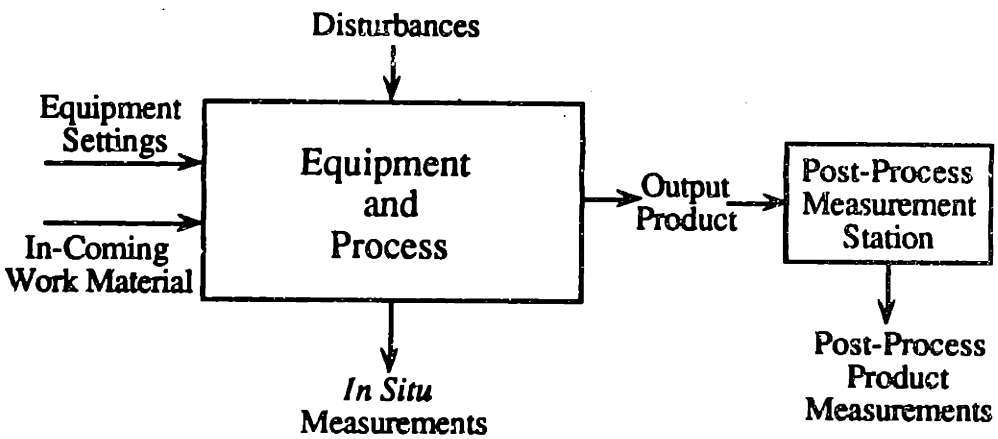

Fig. 2.7 Generic model for manufacturing process and related equipment.

There are also two types of outputs : the output product itself and the *in situ* state. The output product is often measured post-process at a separate station resulting in post-process product measurements. The *in situ* state is measured inside the equipment itself while the process is taking place resulting in *in situ* measurements.

The definition of equipment models used in this thesis mirrors the external structure of a process and related equipment as shown in Fig. 2.7. In this case, the process and equipment are treated as one unit with the inputs and outputs described previously. While this treatment is appropriate to the demands of process control, a more general equipment modeling framework can be developed for different applications including process representation, process simulation, process synthesis, and process control [22]. Such a general framework involves more detailed decompositions and state transformations. The definition of equipment models used in this thesis can be described as a subset of this general modeling framework.

2.6.2 Construction Approaches

The approaches to construct equipment models may be classified according to the amount of process physics included in the development of the model (Fig. 2.8). At one extreme are mechanistic models which are based on a thorough understanding of the underlying physics. At the other extreme are empirical models, where the relationships between variables are determined experimentally. Semi-empirical modeling methodologies tend to combine the above two approaches.

Mechanistic models derived from the underlying process physics may be either closed form (analytical function) or numerical in nature (differential equations solved by numerical techniques). Mechanistic models can often be transferred from one piece of equipment to

another and can often provide some insight into behavior beyond the range of experimental verification. However, because of frequent limitations in the understanding of the physics, the absolute accuracy of mechanistic models is limited, even when interpolating within the experimental range. Mechanistic models are usually time consuming to develop. They may also be too computationally intensive to be useful for on-line control applications.

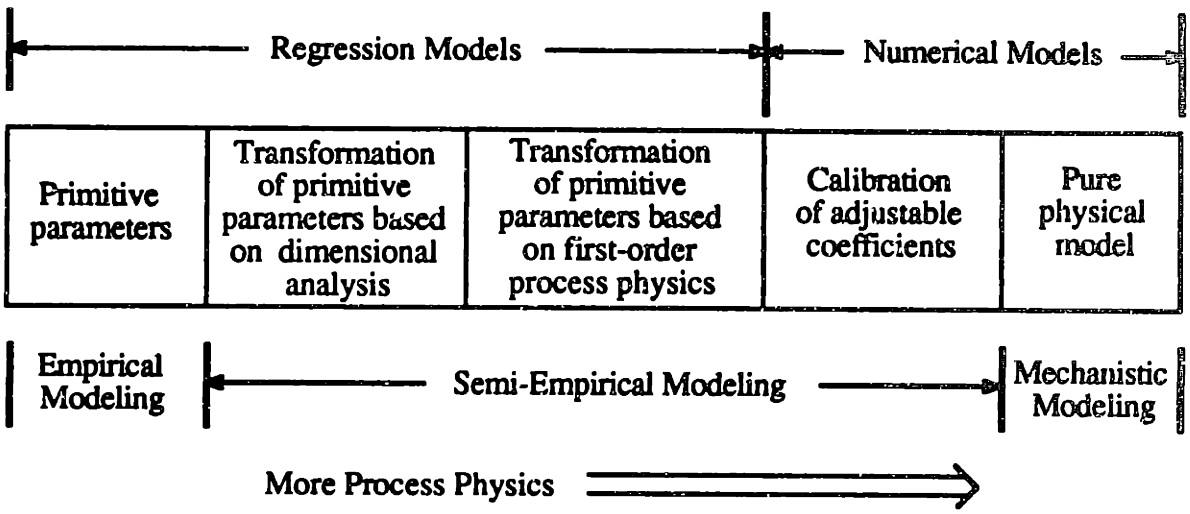

Fig. 2.8 Approaches to construction of equipment models.

Empirical models are usually polynomial regression models which are most effectively developed using methods of design of experiments [3][4]. In such methods, physical understanding is often used to decide which variables to include in the model. Physical understanding is sometimes used to decide the form of the relationships; however, the quantitative portion of these relationships is derived from a set of experiments. Empirical models have the advantage of rapid development and utility even when there is limited physical understanding of the system under study. The low-order polynomial expressions usually used in the modeling can provide great interpolative accuracy within a limited range of experimental space. However, such polynomial relationships can sometimes fail to

capture the true behavior over a large region of setting space. In addition, the accuracy and certainty of the expressions decreases rapidly as one extrapolates from the initial experimental space.

Semi-empirical modeling seeks to combine the advantages of mechanistic and empirical modeling in order to achieve good interpolative accuracy, good extrapolative accuracy, and the ability to create models even when the physics is not completely understood. One proposed semi-empirical modeling methodology is to incorporate one or more adjustable coefficients in the development of a mechanistic model [18]. These adjustable coefficients, which represent the uncertainty of the underlying process physics, are then calibrated using design of experiments. There are many other ways to construct semi-empirical models. For example, they can be developed using statistical regression techniques with physically-based transformations of the primitive parameters used in the regression. Models with transformations of the primitive parameters which are based on dimensional analysis might have better modeling accuracy compared to the primitive parameter models [23] - [25]. Collins [26] introduced a methodology for the development of a semi-empirical model in which a nonlinear, multi-layer regression technique combined with an analytical process model was used to develop a hybrid equipment / process model. Lin [27] reported another methodology in which physically-based models were first linearized and subsequently fitted using multi-stage D-Optimal experimental designs.

The three core modules all use equipment models which simulate the output of a manufacturing process and related equipment given information about the inputs. A common ingredient in the construction of these equipment models is the statistical design of experiments; however, each module uses design of experiments in a different way. In order to cover a wide range of setting space, the Flexible Recipe Generator combines

physical modeling with statistical modeling [13]. The Run by Run Controller utilizes the sequential design of experiments to adapt statistical models to a process while achieving on-line optimization and control. The Real Time Controller [13] uses time domain control theory to handle the dynamics of the process in combination with statistical models which characterize the steady state performance of the process.

CHAPTER THREE

MODELING OF SPATIAL UNIFORMITY

3.1 Empirical Models

As described in chapter two, models are developed to serve as a simulation of a manufacturing process and related equipment. They are the basis of process optimization and control. This thesis focuses on the modeling of spatial uniformity, which in most processes is difficult to model physically. We use empirical models as they have the advantage of rapid development and utility even if there is limited physical understanding of the system under study. Empirical models are usually polynomial regression models which are most effectively developed using methods of design of experiments.

3.2 Design of Experiments

Two methods of design of experiments are used to model spatial uniformity; parallel and sequential. They both share the common feature of varying many or all of the equipment settings simultaneously.

In parallel design of experiments, all experiments are designed at the beginning and then performed. Models are constructed after all data are collected and then used for the subsequent process optimization and control. Examples of parallel design of experiments include full and fractional factorial designs [3], central composite designs [4], and Taguchi's orthogonal array [6] - [10]. In this thesis, full factorial design is used to model spatial uniformity.

Parallel design of experiments is widely used for the characterization of a process at a design stage and in off-line optimization. Parallel design of experiments is the most appropriate approach when one must spend a great deal of time in either the preparation or running of experiments and the possibility exists to prepare or run the experiments in parallel. The classic application which spawned the development of parallel design of experiments is in agriculture where experiments usually require an entire growing season to complete, but many experiments may be run simultaneously. Another example would be in the design of a reactor where one of the experimental variables is the geometry of a susceptor, which might take eight weeks to fabricate. In this case, three or more susceptors could be fabricated in parallel before starting the experimental runs. However, in application to on-line optimization and control, parallel design of experiments presents a problem in that many of the design points produce scrap (material that is out of specification). Parallel design of experiments often makes scrap because of its nature of designing experiments uniformly in the entire setting space. This might be acceptable at a design stage when there is little concern about making scrap, but not at a manufacturing stage when each "experiment" represents daily production.

In sequential design of experiments, each new data point is used to help design the next experiment. As each new data point is obtained, models are updated and the new models are used to design the next run in order to seek improvement of the process. Examples of sequential design of experiments include Evolutionary Operation [28], the Simplex method [29], the Ultramax method [19][20], and our Run by Run Controller.

One major advantage of sequential design of experiments over parallel design of experiments is that it allows for the optimization and control of a process without making scrap. The protection against making scrap is the result of creating models which place

greater emphasis on accuracy in the immediate region of operation and less emphasis on global accuracy. In addition, scrap is avoided by limiting the magnitude of the changes between runs. The ability to avoid making scrap makes sequential design of experiments ideally suited to on-line use.

Another advantage of sequential design of experiments for on-line use is that a manufacturing operation is inherently sequential. Hence, no extra delay is incurred by the use of sequential design of experiments as compared with parallel design of experiments.

3.3 Single and Multiple Response Surfaces

Spatial uniformity is usually a function of many more primitive output characteristics. Table 3.1 shows an example of parallel design of experiments with two equipment settings and output characteristics measured at three sites. We will examine two alternative approaches to create empirical models from the same set of data. Procedurally, the distinction between the approaches is that different metrics are fitted with empirical models. In one approach ("Single Response Surface"), spatial uniformity is the fitted metric. In the alternative approach ("Multiple Response Surfaces"), the output characteristics are the fitted metric.

The first approach follows the procedure of first calculating the value of the spatial uniformity for each experimental run, and then fitting an equation to these values. With reference to Table 3.1, the uniformity is calculated for each row (experimental run) and the value is entered into the last column. A model is then fitted to the calculated values in the last column. In this "Single Response Surface" approach, a high-order expression is required to fit the spatial uniformity as the curvature of the response surface is usually high.

For example, the uniformity model fitted with a second-order polynomial has the following form :

$$\frac{\sigma}{\mu} = C_1 + C_2X_1 + C_3X_2 + C_4X_1^2 + C_5X_2^2 + C_6X_1X_2 \qquad (3.1)$$

Table 3.1 Parallel design of experiments to create uniformity model.

	Equipment settings		Output characteristics			Spatial uniformity
Run	X_1	X_2	Y_1	Y_2	Y_3	$\frac{\sigma}{\mu}$
1	x_{11}	x_{12}	y_{11}	y_{12}	y_{13}	$(\frac{\sigma}{\mu})_1$
2	x_{21}	x_{22}	y_{21}	y_{22}	y_{23}	$(\frac{\sigma}{\mu})_2$
3	x_{31}	x_{32}	y_{31}	y_{32}	y_{33}	$(\frac{\sigma}{\mu})_3$
⋮	⋮	⋮	⋮	⋮	⋮	⋮
n	x_{n1}	x_{n2}	y_{n1}	y_{n2}	y_{n3}	$(\frac{\sigma}{\mu})_n$
			Response surface of Y_1	Response surface of Y_2	Response surface of Y_3	Response surface of (σ / μ)

In this work, we suggest a new approach that is preferable : first fit a response surface to each primitive output characteristic and then combine these response surfaces to obtain the model of the spatial uniformity. With reference to Table 3.1, a separate model is fitted to each column (measurement site) of data for "output characteristics". The resulting response surfaces are entered in the last row of the table. The uniformity model is obtained by combining the multiple response surfaces of the last row. In this "Multiple Response Surfaces" approach, low-order response surfaces (usually first-order) are sufficient to

model each output characteristic. In the example of Table 3.1, the uniformity model is obtained by combining three fitted response surfaces as follows :

i) fit three output characteristics with first-order polynomials

$$Y_1 = C_{11} + C_{12}X_1 + C_{13}X_2 \tag{3.2}$$

$$Y_2 = C_{21} + C_{22}X_1 + C_{23}X_2 \tag{3.3}$$

$$Y_3 = C_{31} + C_{32}X_1 + C_{33}X_2 \tag{3.4}$$

ii) substitute (3.2), (3.3), and (3.4) into (3.5) and (3.6)

$$\mu = \frac{1}{3}(Y_1 + Y_2 + Y_3) \tag{3.5}$$

$$\frac{\sigma}{\mu} = \frac{\sqrt{\frac{1}{2}\left[(Y_1-\mu)^2+(Y_2-\mu)^2+(Y_3-\mu)^2\right]}}{\mu} \tag{3.6}$$

3.4 Related Work

The most common approach to modeling spatial uniformity is the Single Response Surface approach. In some cases, a full second-order model is used, while in other cases, only the statistically relevant terms are retained. For example, Lin [27] modeled the within-wafer deposition rate uniformity and residual stress uniformity in an LPCVD process. May [30] modeled the etch uniformity across one wafer in a plasma etching process. Riley [31] also modeled the etch uniformity across one wafer in another plasma etching process. In their works, second-order polynomials were used to fit uniformity directly; however, only the statistically relevant terms were retained.

Hunter [32] described an approach to modeling a process yield which is the product of two components. In his work, first-order models for the components were multiplied to obtain a second-order model for the process yield. The resulting composite model was compared to that obtained by directly fitting a second-order polynomial to the process yield. The proposed method is especially useful when the usual procedure of directly fitting the response interested fails to produce a satisfactory model. In some cases, instead of fitting all output components, it will be beneficial to combine some of them together in one or more subsets. Careful examination of such response relationships will usually lead to a better understanding of the overall system.

3.5 A Simple Example

A simple example is given to illustrate the procedures to create uniformity models. Table 3.2 shows a simulated process with two equipment settings and three output characteristics. A 3^2 design (three levels for each of the two equipment settings) is performed and the data are collected.

By using the Single Response Surface approach, we fit a second-order polynomial to the last column (uniformity) and obtain the uniformity model as follows :

$$\frac{\sigma}{\mu} = 55.9207 - 1.4528X_1 - 0.9196X_2 + 0.01094X_1^2 + 0.00867X_2^2 + 0.00658X_1X_2 \quad (3.7)$$

By using the Multiple Response Surfaces approach, we fit first-order polynomials to three output characteristics and obtained multiple models as follows :

$$Y_1 = 28.8449 + 0.2940X_1 + 0.1175X_2 \quad (3.8)$$

$$Y_2 = 34.0764 + 0.2048X_1 + 0.1378X_2 \quad (3.9)$$

$$Y_3 = 41.3942 + 0.1346X_1 + 0.0355X_2 \quad (3.10)$$

The uniformity model is obtained by substituting (3.8) - (3.10) into (3.5) and (3.6) :

$$\frac{\sigma}{\mu} = \frac{\sqrt{34.140 - 0.911X_1 - 0.537X_2 + 0.0064X_1^2 + 0.0029X_2^2 + 0.0062X_1X_2}}{0.01\,(35.105 + 0.211X_1 + 0.097X_2)} \quad (3.11)$$

Table 3.2 Simple example of parallel design of experiments.

	Equipment settings		Output characteristics			Spatial uniformity
Run	X_1	X_2	Y_1	Y_2	Y_3	$\frac{\sigma}{\mu}$ (%)
1	46	22	45.994	46.296	48.589	3.022
2	56	22	48.843	48.731	49.681	1.058
3	66	22	51.555	50.544	50.908	1.004
4	46	32	47.647	47.846	48.519	0.952
5	56	32	50.208	49.930	50.072	0.278
6	66	32	52.931	52.387	51.505	1.377
7	46	42	47.641	49.488	48.947	1.950
8	56	42	51.365	51.365	50.642	0.817
9	66	42	54.436	52.985	51.716	2.566

quations (3.8) - (3.11) are obtained by using all nine data points. Since first-order polynomials are being fitted, four data points at the corner of the 3^2 design (Fig. 3.1(c)) are enough to fit multiple models. The resulting output characteristic models and uniformity model are shown as follows :

$$Y_1 = 28.9857 + 0.3089X_1 + 0.1132X_2 \tag{3.12}$$

$$Y_2 = 34.4789 + 0.1936X_1 + 0.1408X_2 \tag{3.13}$$

$$Y_3 = 41.9840 + 0.1272X_1 + 0.0292X_2 \tag{3.14}$$

$$\frac{\sigma}{\mu} = \frac{\sqrt{42.576 - 1.165X_1 - 0.593X_2 + 0.0085X_1^2 + 0.0034X_2^2 + 0.0065X_1X_2}}{0.01\,(35.150 + 0.210X_1 + 0.094X_2)} \tag{3.15}$$

Fig. 3.1 shows the contour plots of the predicted (σ / μ) based on (3.7), (3.11), and (3.15). Solid circles represent the locations of the data points which are used to create the models. Notice that nine data points are needed in the Single Response Surface approach to create the uniformity model. In the Multiple Response Surfaces approach, the uniformity model can be obtained using four data points (Fig. 3.1(c)) as first-order polynomials are fitted to each output characteristic, and the result is similar to that obtained by using all nine data points (Fig. 3.1(b)). Such advantage of less number of data points to model spatial uniformity and other advantages by using Multiple Response Surfaces are further discussed in the next chapter.

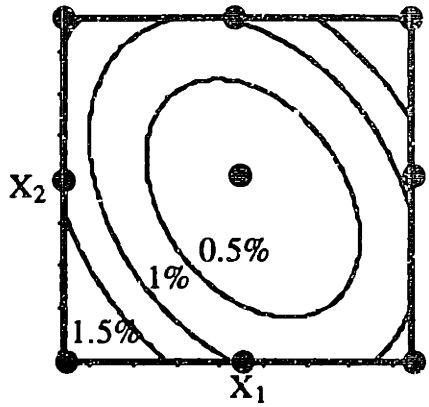

(a) Single Response Surface

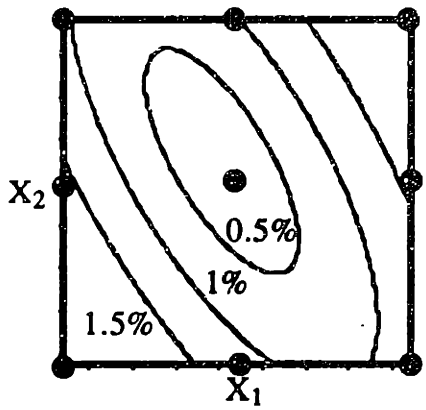

(b) Multiple Response Surfaces
based on nine data points

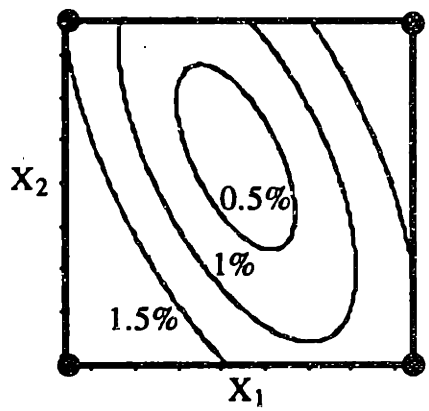

(c) Multiple Response Surfaces
based on four data points

Fig. 3.1 Predicted (σ / μ) using Single and Multiple Response Surfaces. Solid circles represent data points used to create models.

CHAPTER FOUR

SINGLE VERSUS MULTIPLE RESPONSE SURFACES

4.1 Advantages

The Multiple Response Surfaces approach has several characteristics which provide advantages over the Single Response Surface approach when modeling spatial uniformity. These characteristics are:

- Effective models from a small number of data.
- Rapid adaptation of models after a process disturbance.
- Immunity of models to the presence of noise.
- Model forms which are compatible with process knowledge.

These advantages will be discussed in the subsequent sections.

4.1.1 Effective Models from a Small Number of Data

The Multiple Response Surfaces approach requires fewer data than the Single Response Surface approach in order to create models of the same or better accuracy. This translates into more rapid modeling and optimization when using either parallel or sequential design of experiments.

By way of illustration, Fig. 4.1 shows a process with one input (equipment setting) and two sites within a batch where thickness measurements are taken (left and right). In Fig. 4.1(a) we see that as the input is increased, the thickness at the left site decreases

linearly and the thickness at the right site increases linearly[3]. In Fig. 4.1(b) we see the result of calculating the uniformity from these two responses[4]. As expected, the uniformity has a minimum at the value of input where the thickness at the left and right sites are equal and has positive values at higher and lower values of the input. As a result, the uniformity has a significantly more complex shape and would have to be modeled with at least a second-order polynomial to capture the basic behavior. This higher-order model would have to be fitted to experiments performed at three levels of the input (low, medium, and high). By contrast, the individual site response surfaces of Fig. 4.1(a) could be captured with first-order models based on experiments at only two levels of the input (low and high).

Note that in this simple example, Multiple Response Surfaces requires a minimum of two experiments, while Single Response Surface requires a minimum of three experiments. In more realistic examples with multiple inputs (equipment settings), the savings in the number of experiments is greater. For example, a second-order model for uniformity as a function of five inputs would have 21 coefficients, and therefore would need a minimum of 21 experiments. However, the first-order models for individual site behavior as a function of five inputs would each have only six coefficients, and therefore would need only six experiments.

---

[3] As an example, such a situation might be realized in a CVD process where the input represented an adjustment to a balance of gas flows between two injectors.

[4] In this simple example with two measurement sites, the uniformity actually has a lowest value of zero and has the "V" shape shown in Fig. 2(b). In a more realistic case of three or more measurement sites, the uniformity would have a non-zero minimum and would have a smoother shape.

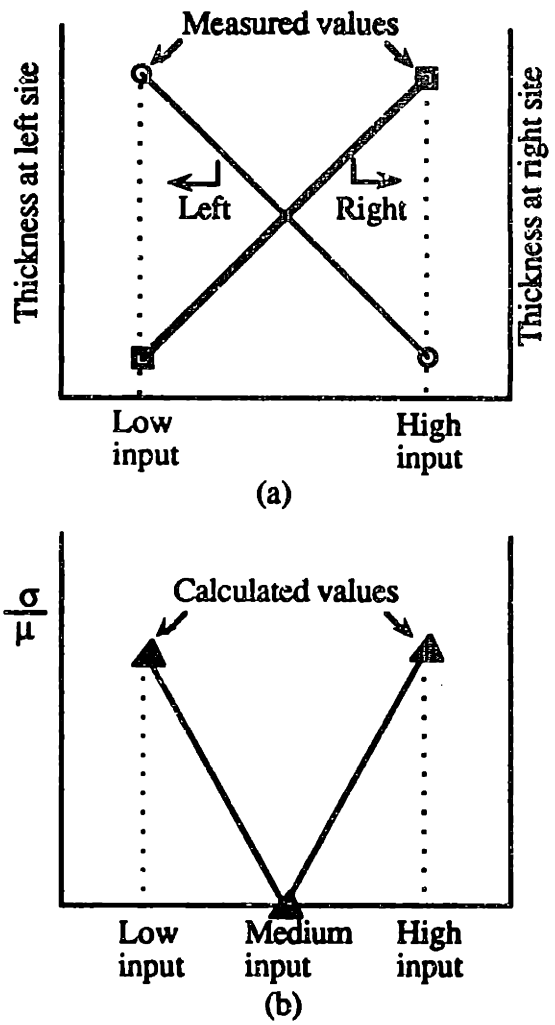

Fig. 4.1 Simple example to show complexity of uniformity.

Further insight into the difference between Single and Multiple Response Surfaces can be gained by noting that when we calculate the uniformity, we lose information about directionality. Thus, in Fig. 4.1(b), the uniformity at the low level of input is not distinguishable from the uniformity at the high level of input. However, in Fig. 4.1(a) we see that the responses at low and high levels of input are distinguishable. At the low level of input, the left site is thicker than the right, while at the high level of input, the right site is thicker than the left. The reason that information is lost when we calculate the uniformity is

that the calculation involves squaring the difference between measurement sites (or each site and the mean of all sites). Thus, a negative difference is equivalent to a positive difference in the calculation of uniformity[5]. This loss of directional information is the basic reason that higher-order models are needed for modeling the uniformity as compared with the individual site responses.

4.1.2 Rapid Adaptation of Models after a Process Disturbance

A key advantage of Multiple Response Surfaces is that this approach can rapidly adapt to a process that has changed as the result of a step disturbance such as a shift due to a maintenance operation. When we use Multiple Response Surfaces to model a shift in the process behavior we will be able to predict both the direction and magnitude of an adjustment needed to bring the process back to target after only one run. If we use the Single Response Surface approach to model spatial uniformity we will not even know the proper direction of adjustment to the process input after one run.

By way of illustration, let us consider that as the result of a maintenance operation, the input knob on the process of Fig. 4.1 has been recalibrated such that the same setting number delivers a different value of the input (however, we are unaware of this change). The situation is illustrated in Fig. 4.2 where we see both the intended input and two cases showing the actual input. In case one, the input is lower than expected and in case two the input is higher than expected. In Fig. 4.2(a) we see the measured values of left and right thickness corresponding to the two cases and in Fig. 4.2(b) we see the calculated value of uniformity corresponding to the two cases. Note that by the uniformity value we would be

---

[5] Occasionally, uniformity is calculated using the absolute values of differences, rather the square of differences. The same information loss results in this case.

unable to distinguish between the two cases, and hence we would not know whether to take a corrective action by increasing or decreasing the input. However, we could distinguish the two cases by looking at the individual site responses as one case has left thicker than right and the other has right thicker than left. For example, if we observe that the left is thicker than the right, our individual site models would indicate that we should increase the input in order to drive the sites toward equal thickness.

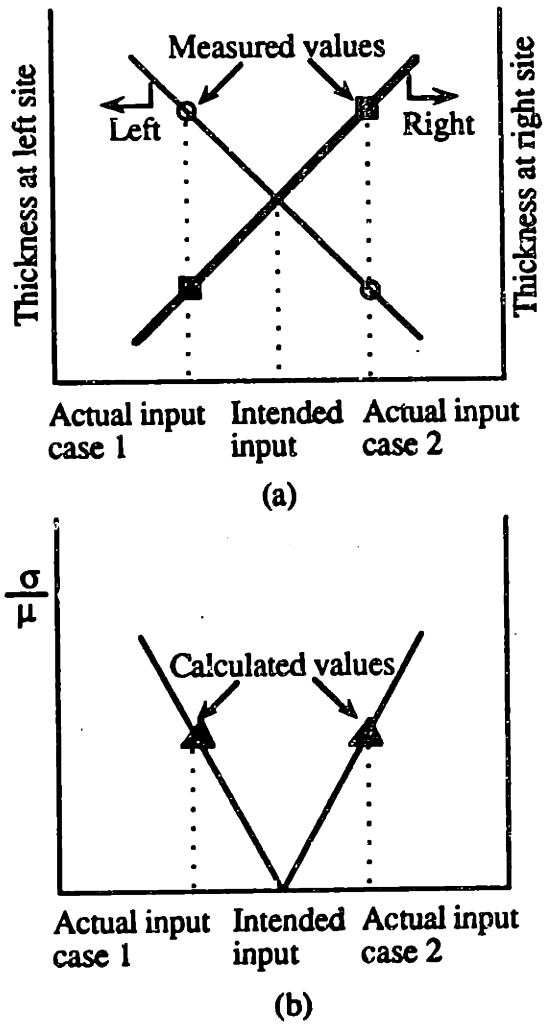

Fig. 4.2 Simple example to show two process shifts.

4.1.3 Immunity of Models to the Presence of Noise

A critical issue concerns the ability of a modeling method to distinguish the signal from the noise. Indeed, at first glance, there is cause for concern on this issue due to the total number of coefficients that must be estimated with Multiple Response Surfaces. If we return to the example discussed above in which there are five equipment settings, we found that the second-order model had 21 coefficients to estimate (and therefore needed at least 21 experiments to estimate the model). At the same time, we found that the first-order models for each site had six coefficients (and therefore needed at least six experiments to estimate the model). However, it is also true that there are multiple first-order models, one for each site. Therefore, if there are 11 sites being measured, 66 coefficients have to be estimated. Note that this is possible to do from just six experiments as each experiment yields 11 pieces of data for a total of 66 data. The possibility now exists that since many coefficients are being estimated, the estimates will be sensitive to noise.

Fortunately, it seems from experience including simulations and experiments on real equipment, that Multiple Response Surfaces often provides better immunity to noise than Single Response Surface. Indeed, the individual models can be affected by noise; however, the spatial uniformity obtained by the combined action of the multiple models seems to be quite immune to noise. Examples to substantiate this point are presented later in this thesis, including the simulation of polysilicon LPCVD and epitaxy experiment.

4.1.4 Model Forms Which are Compatible with Process Knowledge

The low-order models used in the Multiple Response Surfaces approach are easy to interpret in the light of physical understanding. Thus, when the behavior of an individual site is expressed as a first-order function of equipment settings, we can easily deduce the

effect of various settings on the site behavior. Further, the forms of the models used in Multiple Response Surfaces are often motivated by physical understanding of the process. For example, at times it will be advantageous to model the difference between two sites as a low-order function of the equipment settings when the difference captures the dominant contribution to the spatial uniformity (an example of this type of modeling is discussed in the chapter seven with reference to the silicon epitaxy experiment).

4.2 Illustration : Simulation of LPCVD of Polysilicon

Many of the features of the Multiple Response Surfaces approach can be illustrated using the LPCVD example as described previously. Comparisons of the performance of Single and Multiple Response Surfaces are presented for four cases:

- Parallel design of experiments : no noise superimposed.
- Parallel design of experiments : noise superimposed.
- Sequential design of experiments : run by run optimization and control.
- Sequential design of experiments : rapid response to a step disturbance.

4.2.1 Parallel Design of Experiments : No Noise Superimposed

In order to be able to visualize the response surface in three dimensions, we used only two equipment settings, the flow rates of the load and center injectors, to adjust the uniformity. Fig. 4.3(a) shows the response surface of the spatial uniformity (SN Ratio) which was obtained by running the equipment simulator at many flow rate settings and then fitting a third-order polynomial to $(\sigma / \mu)^2$. Fig. 4.3(c) and Fig. 4.3(d) show the response surfaces of the deposition rates of two monitor wafers obtained by fitting second-order

models to the deposition rate data. As can be seen, the response surface of the spatial uniformity is more complicated than the response surface of each output characteristic. The SN Ratio must be fitted using a high-order polynomial while each deposition rate could be approximated very well by a first-order polynomial. Fig. 4.3(b) also shows the response surface of the SN Ratio using a contour plot.

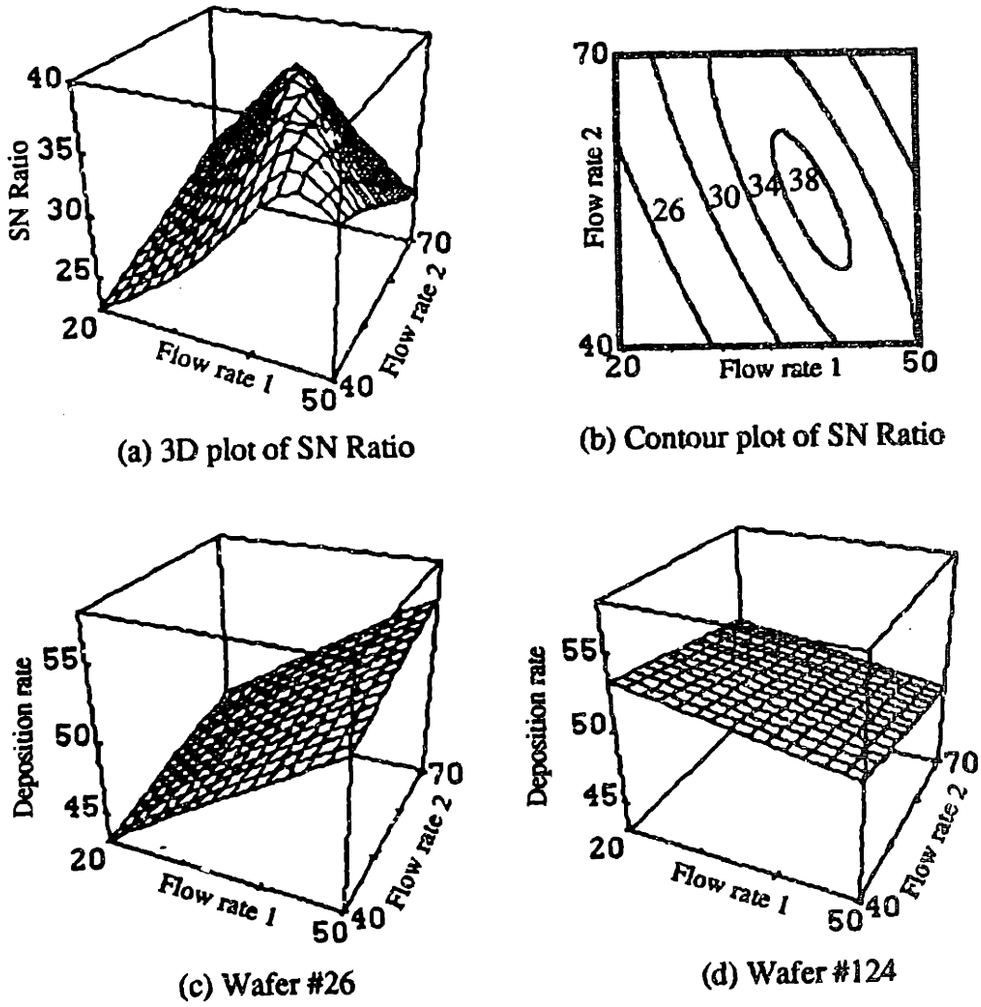

(a) 3D plot of SN Ratio

(b) Contour plot of SN Ratio

(c) Wafer #26

(d) Wafer #124

Fig. 4.3 Three dimensional plots and contour plot showing complicated dependence of SN Ratio and simple dependence of deposition rates on two silane flow rates.

A 3^2 design was run on the simulator and the data were collected (appendix C). By using the Single Response Surface approach, we fit a second-order polynomial with six coefficients to the SN Ratio and plot the fitted model in Fig. 4.4(a). Solid circles in the contour plot represent the locations of the nine data points used to construct the Single Response Surface model. Fig. 4.4(b) shows the prediction of SN Ratio based on the Multiple Response Surfaces approach. In this case, only the four corner data points were used since the eleven site models (one for each of the eleven monitor wafers) are first-order polynomials with only three coefficients. By comparing the response surface of Fig. 4.3(b) with the model predictions of Fig. 4.4(a) and Fig. 4.4(b), we conclude that the Multiple Response Surfaces approach results in a more accurate model with a smaller number of data points required.

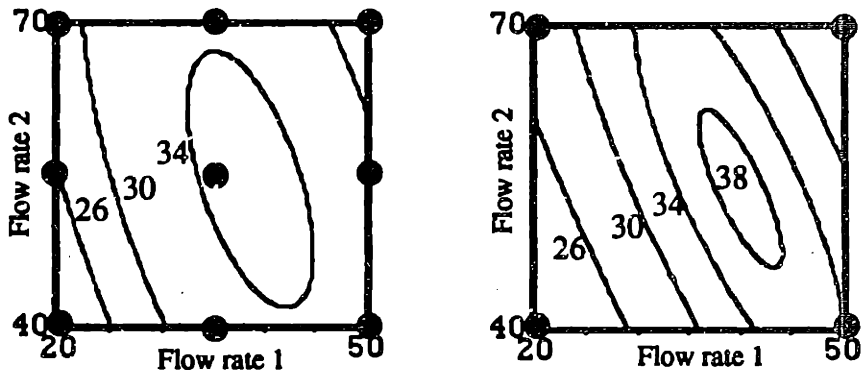

(a) Single Response Surface (b) Multiple Response Surfaces

Fig. 4.4 Predicted SN Ratio. Solid circles represent data points used to create models.

4.2.2 Parallel Design of Experiments : Noise Superimposed

Since all processes contain noise, a series of simulations were also performed with random noises superimposed onto the flow rates settings (X_i) and the output deposition rates (Y_i). The magnitude of the noises was chosen to be representative of equipment and

measurement noise that might be realistically expected. These noises were generated by the following equations :

$$X_i' = X_i\,(1 + 0.01\,R_i) \quad i = 1, 2 \tag{4.1}$$

$$Y_i' = Y_i\,(1 + 0.0075\,R_i) \quad i = 1, 2, \cdots, 11 \tag{4.2}$$

where R_i is a random number generated from a standard normal distribution N(0, 1).

The 3^2 design previously run with no noise was now run with random noises superimposed. The design was repeated 24 times and both Single and Multiple Response Surfaces were used to fit the data from each design. Since noises were added to the equipment settings and deposition rates, the resulting data were different for each of the 24 repeats of the design (appendix C). In each design, all nine data points were used in the Single Response Surface approach and four data points were used in the Multiple Response Surfaces approach. Single and Multiple Response Surfaces were compared based on their sensitivity to noises and accuracy of predictions. Fig. 4.5 shows the contour plots of uniformity models based on fitting second-order polynomials for each of the 24 designs. Model predictions based on Multiple Response Surfaces from the corresponding 24 designs are also plotted in Fig. 4.6 for comparison. As can be seen, models created based on Multiple Response Surfaces are more consistent, meaning that the noise immunity is better. Since the derived models are used for subsequent process optimization and control, it might be useful to compare the consistency of the predicted optimum settings. Fig. 4.7 shows the 24 predicted optimum settings within the experimental space. Again, the predictions based on Multiple Response Surfaces are more consistent, while three of the predicted optimum settings based on Single Response Surface tend to go beyond the experimental space and are shown on the boundary of the experimental space (Fig. 4.7).

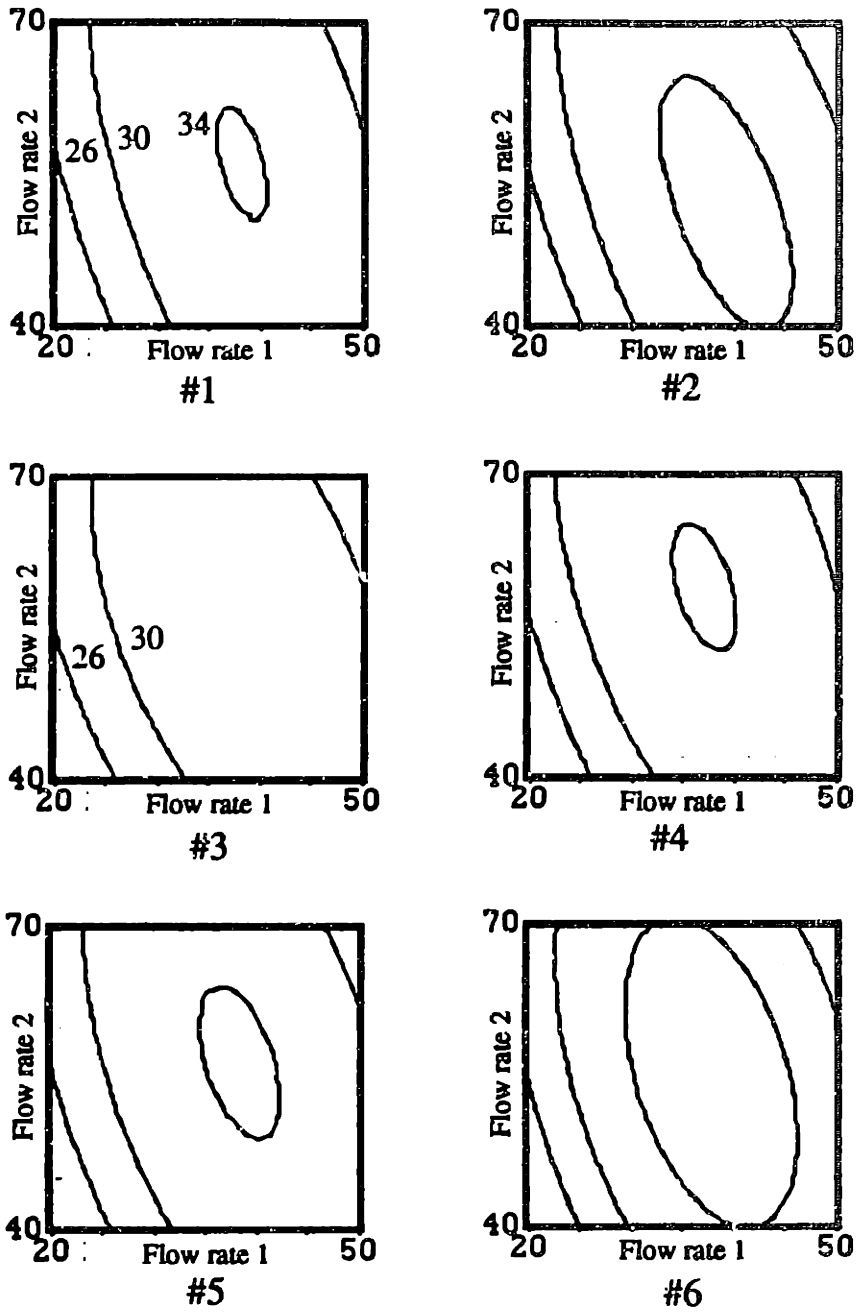

Fig. 4.5(a) Predicted SN Ratio based on Single Response Surface.

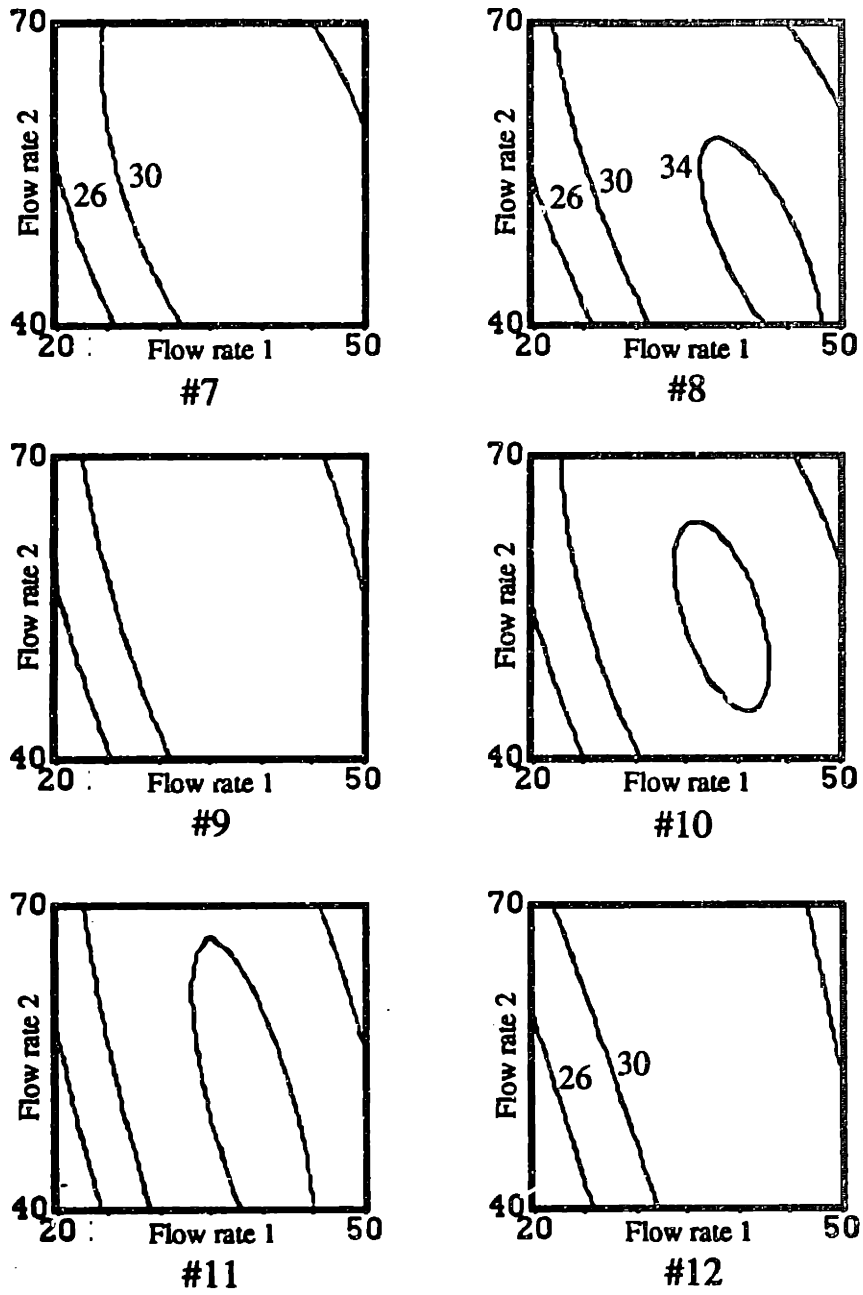

Fig. 4.5(b) Predicted SN Ratio based on Single Response Surface. #12 has saddle point.

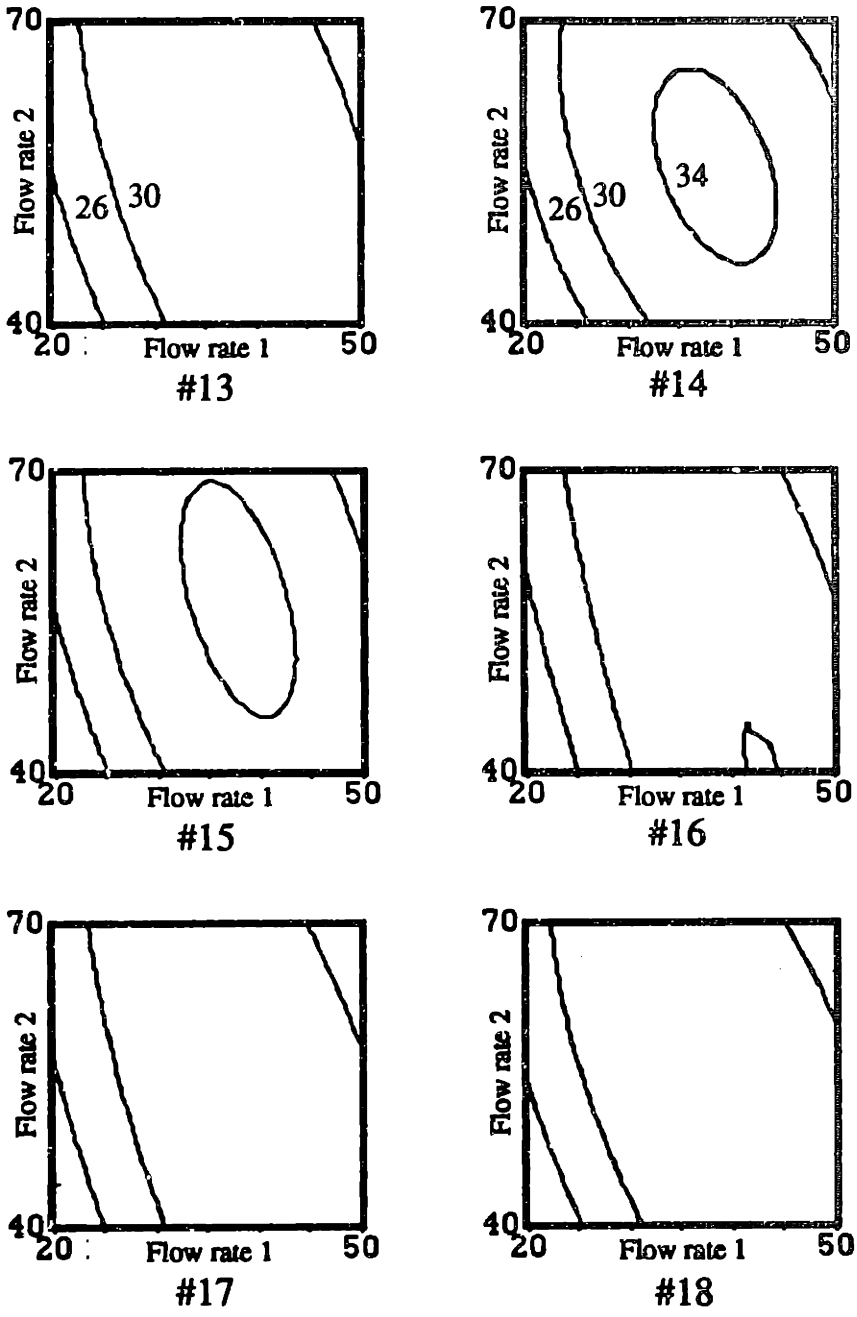

Fig. 4.5(c) Predicted SN Ratio based on Single Response Surface. #16 has optimum settings outside experimental sapce.

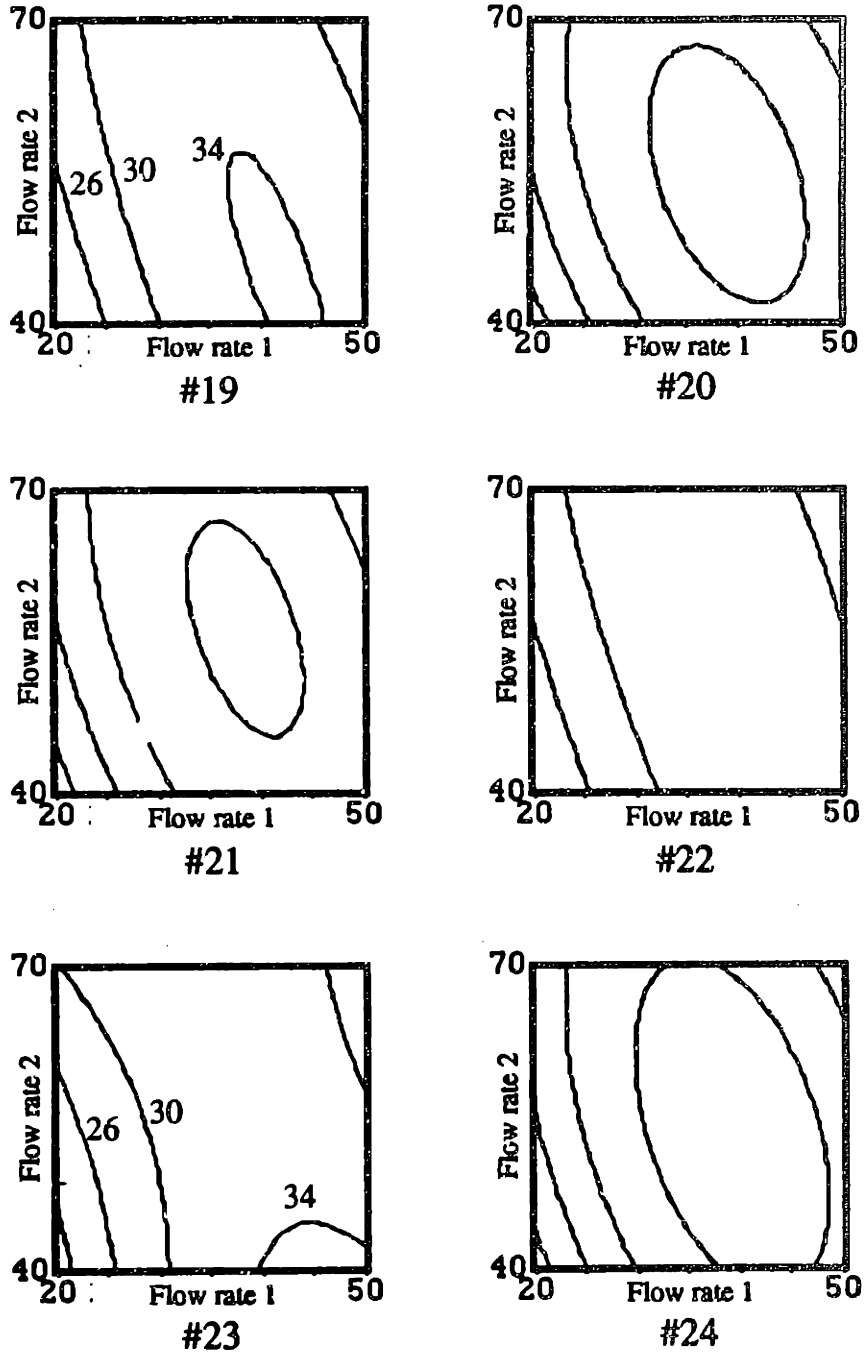

Fig. 4.5(d) Predicted SN Ratio based on Single Response Surface. #23 has saddle point.

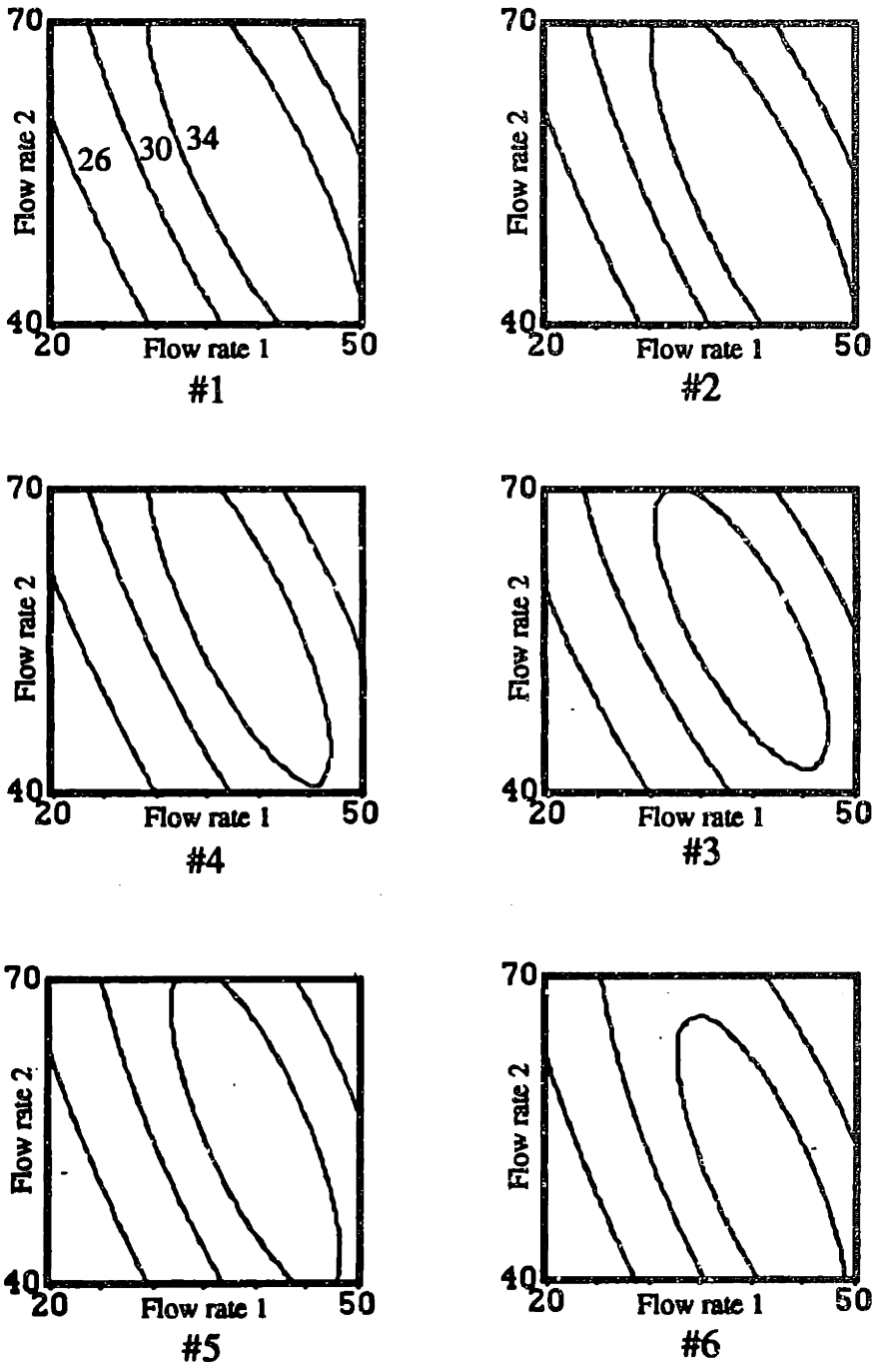

Fig. 4.6(a) Predicted SN Ratio based on Multiple Response Surfaces.

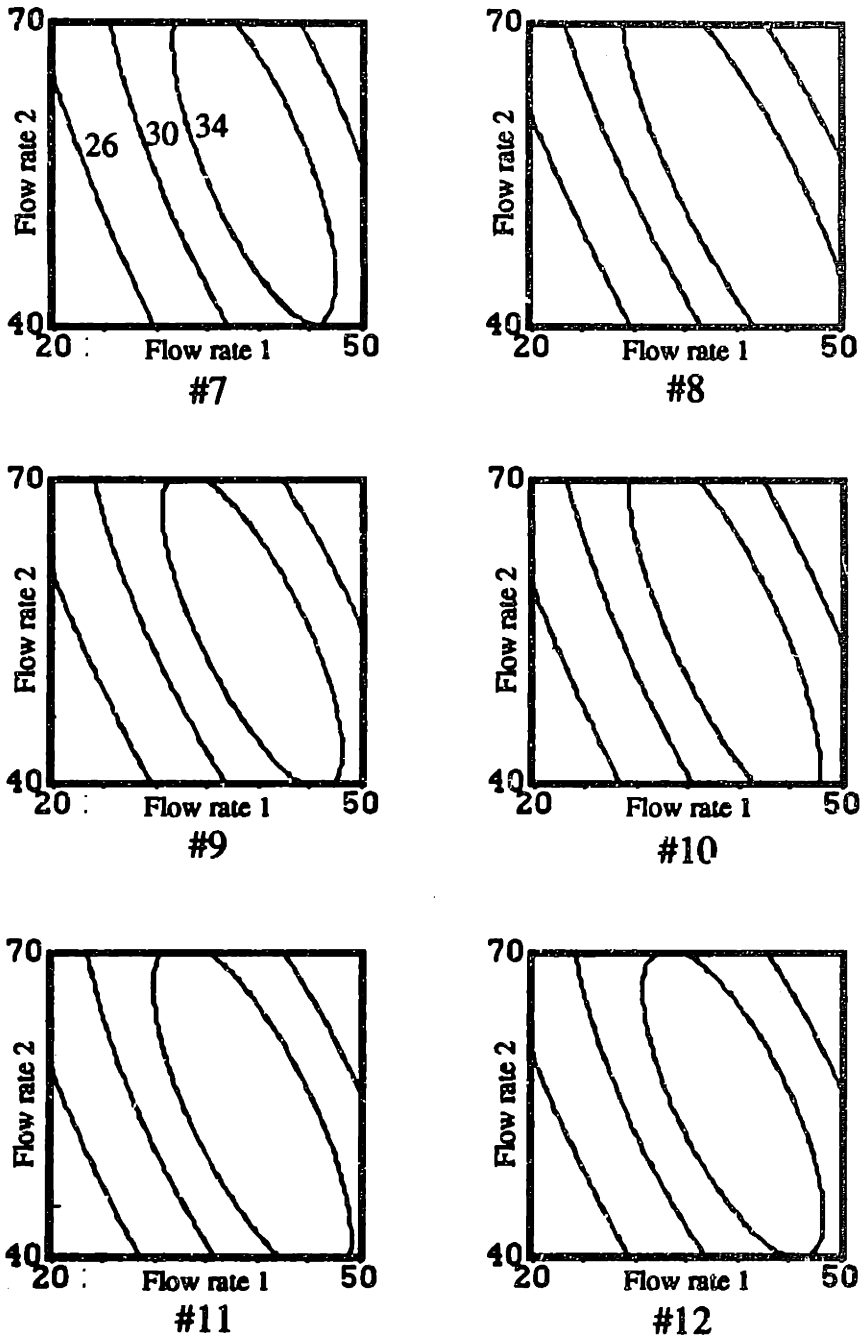

Fig. 4.6(b) Predicted SN Ratio based on Multiple Response Surfaces.

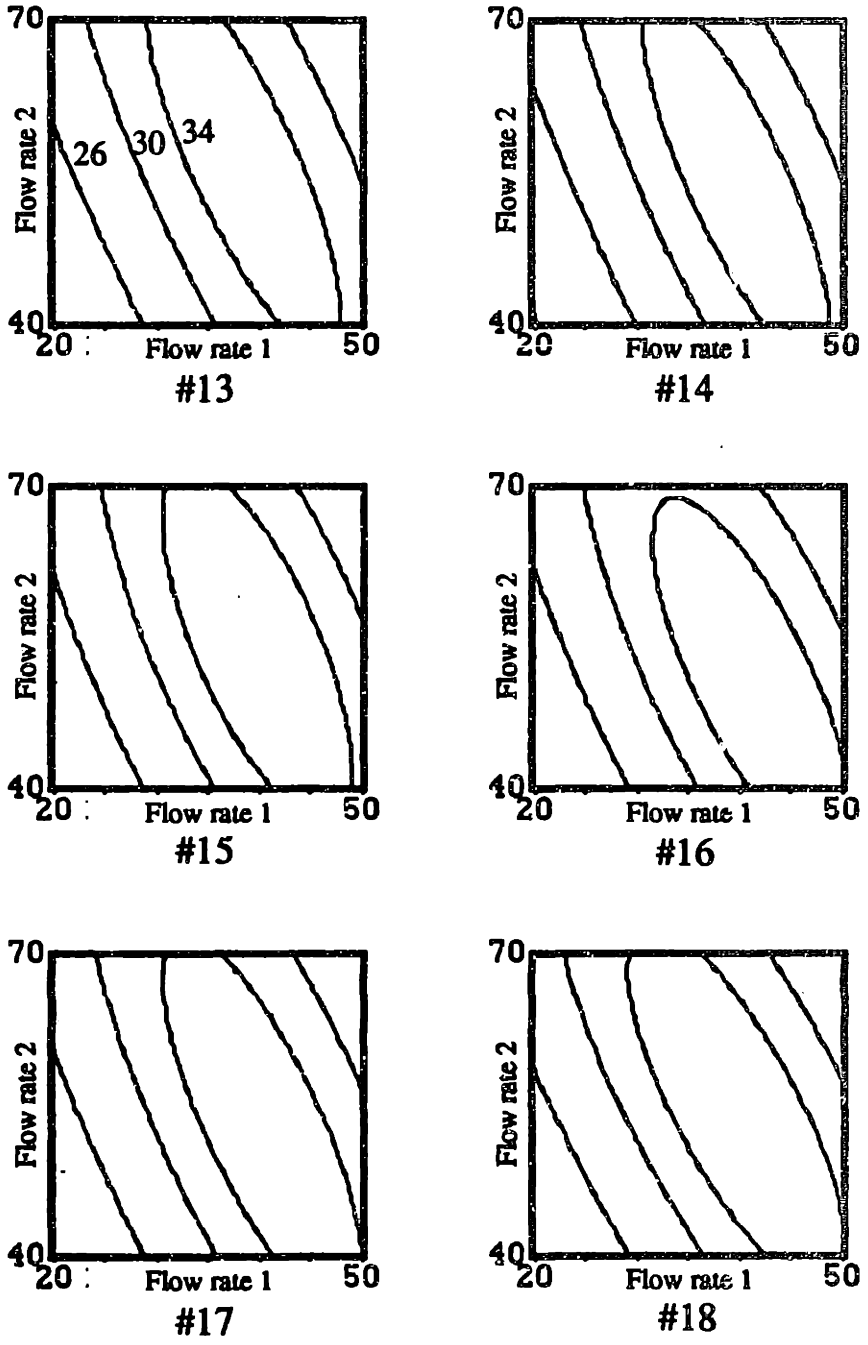

Fig. 4.6(c) Predicted SN Ratio based on Multiple Response Surfaces.

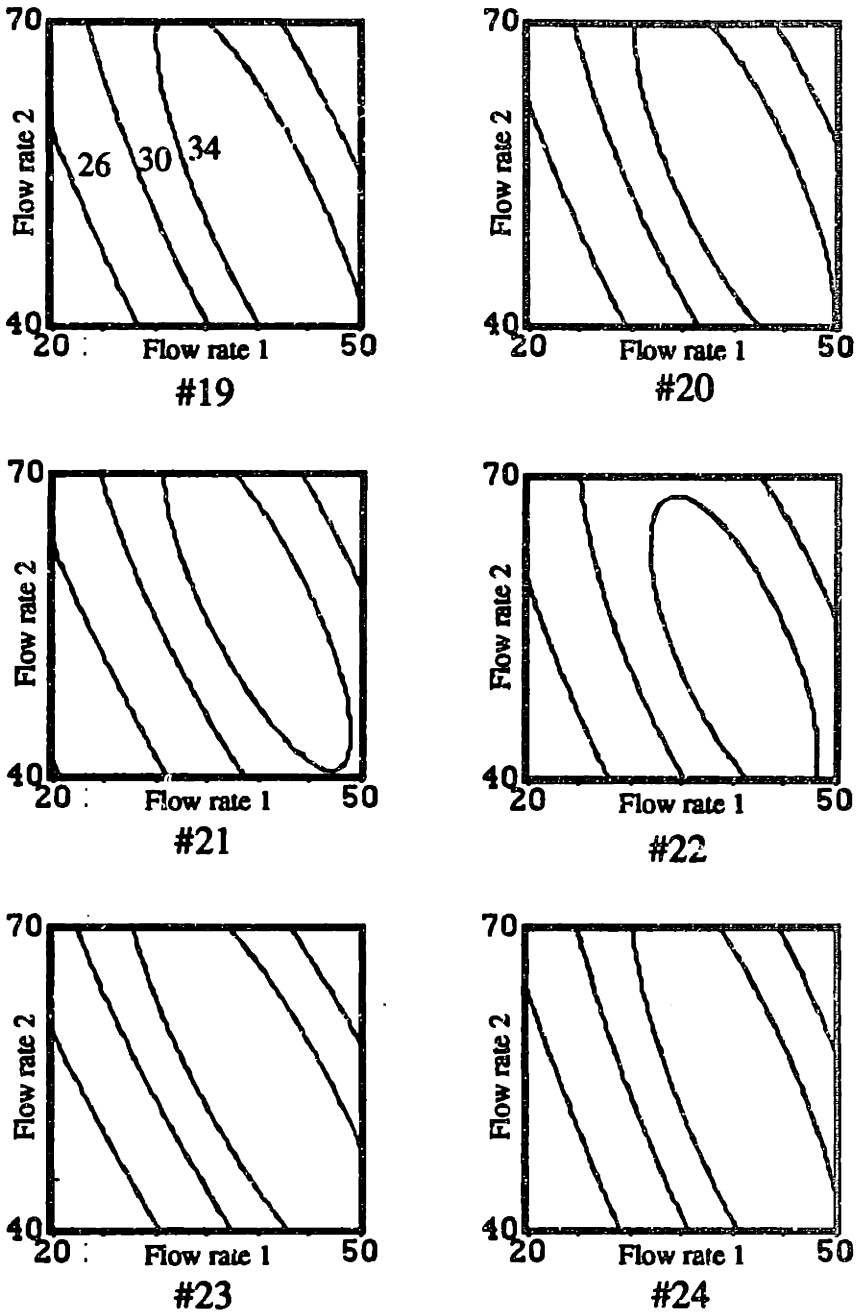

Fig. 4.6(d) Predicted SN Ratio based on Multiple Response Surfaces.

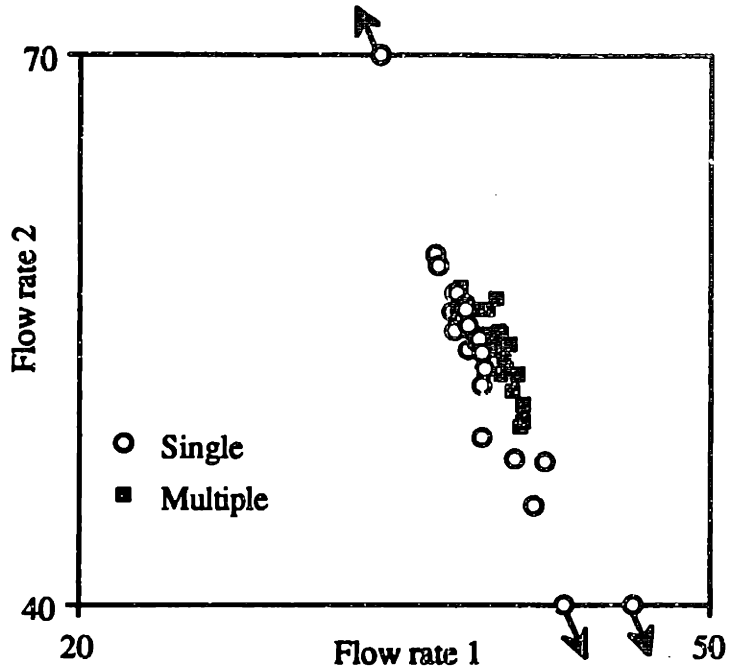

Fig. 4.7 Predicted optimum settings from 24 designs.

The fact that the Single Response Surface approach can sometimes lead to a predicted optimum point which is far off the mark is an important observation as it indicates that this approach is subject to overfitting the data. In an extreme case such as #23 in Fig. 4.5, the model has a saddle point and hence optimum settings can not be found (in the global setting space). Saddle points occurred in two of the 24 designs when using the Single Response Surface approach, but did not occur when using the Multiple Response Surfaces approach (see also chapter six and appendix A).

A further comparison of the two approaches can be made by comparing the predictions at the center point of the 3^2 design, which is close to the optimum settings. Fig. 4.8(a) shows the histogram of the measured SN Ratio with a total number of 24 replicates. As can be seen, the resulting distribution is similar to a normal distribution and the information can be plotted using a box plot which is shown in Fig. 4.8(b). The box plots of the fitted

SN Ratio obtained by using Single and Multiple Response Surfaces from the 24 designs are also plotted in Fig. 4.8(b) for comparison. As can be seen, models based on Multiple Response Surface are more accurate (by comparing the median of the distributions) and more immune from noise (by comparing the variation).

Similar conclusions can be made at the other design setting points. For example, Fig. 4.9 shows the comparison at another design setting point which is at the right upper corner of the experimental setting space.

4.2.3 Sequential Design of Experiments : Run by Run Optimization and Control

Single and Multiple Response Surfaces were also compared in the sequential optimization and control of the equipment simulator of LPCVD of polysilicon. The same problem as described in chapter two to demonstrate the functions of the Run by Run Controller was considered. All five equipment settings were used to tune the spatial uniformity, SN Ratio.

The commercial software package Ultramax was used as the basis of the sequential design of experiments. It uses the Single Response Surface approach and sequentially updates a second-order model relating the SN Ratio to five equipment settings. Results of the optimization test are shown in Fig. 4.10. Fig. 4.10(a) shows the run by run history of SN Ratio, and demonstrates an overall trend of improvement (solid line connecting the solid circles). Fig. 4.10(b) shows the deposition rate profile down the length of the tube corresponding to runs #1 and #64. As can be seen, run #64 has a lower mean deposition rate, but a substantially better uniformity, leading to a higher SN Ratio.

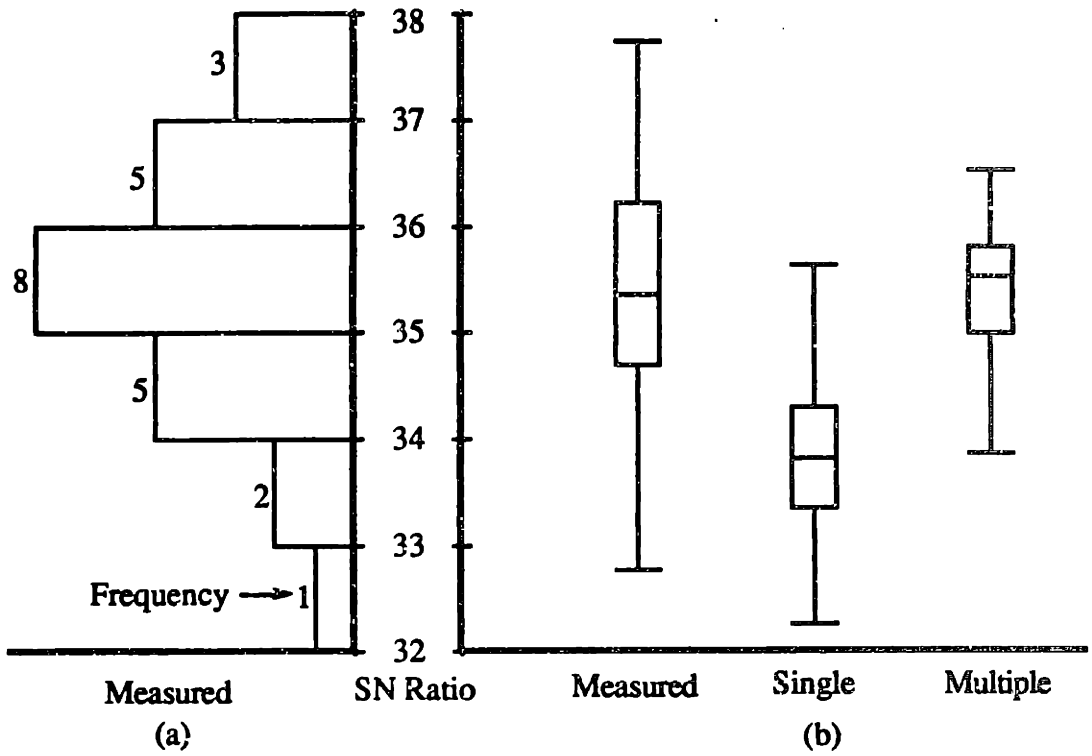

Fig. 4.8 Measured versus predicted SN Ratio from 24 designs at the center of the 3^2 design which is close to the optimum settings.

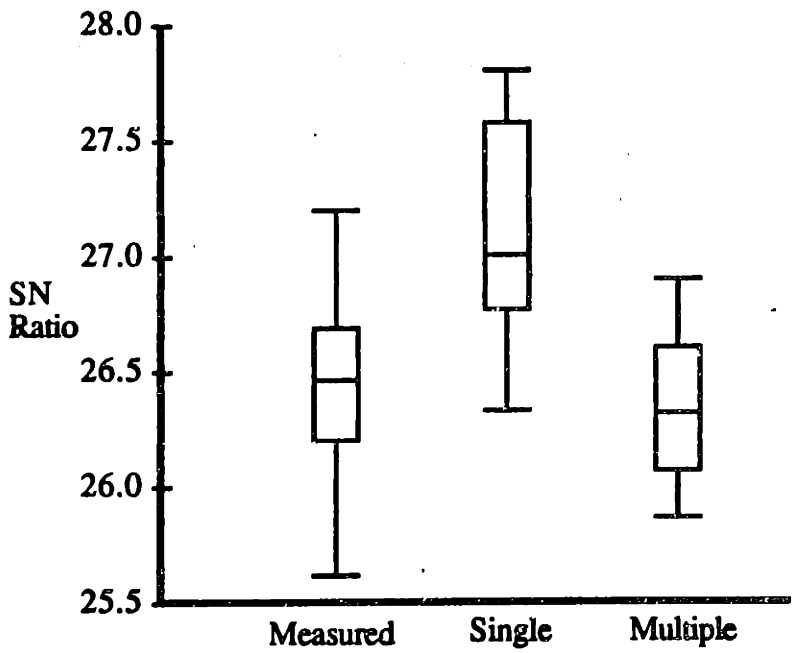

Fig. 4.9 Measured versus predicted SN Ratio from 24 designs at another setting point.

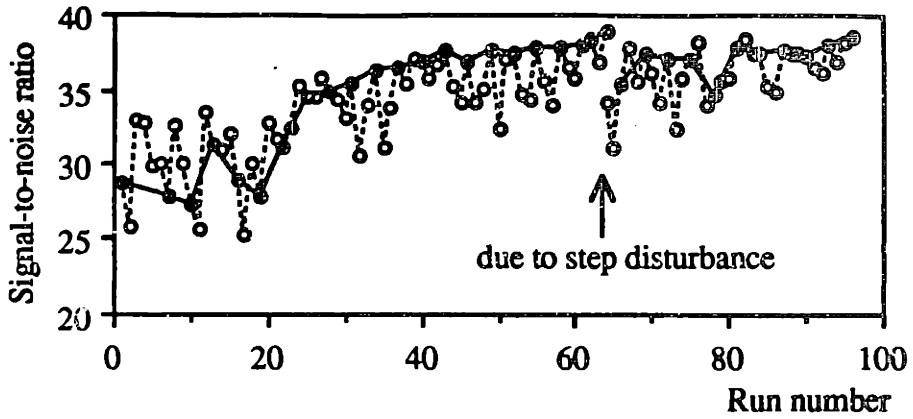

(a) Improvement of SN Ratio

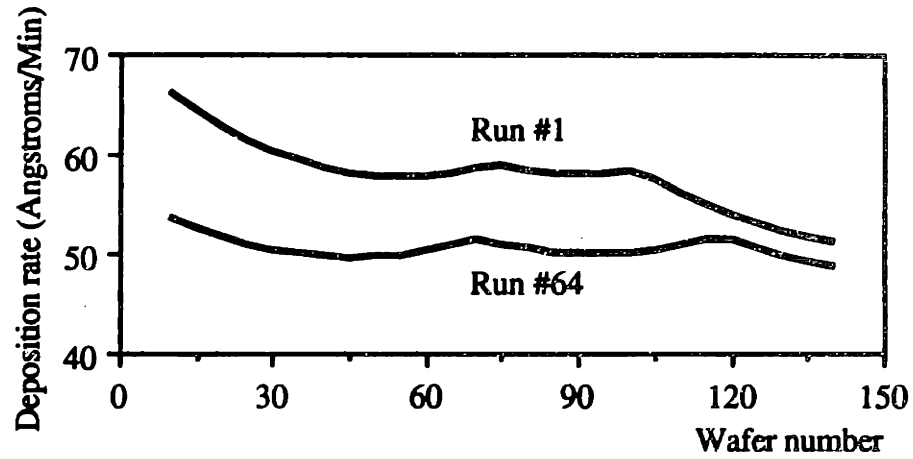

(b) Deposition rate profiles

Fig. 4.10 Run by run optimization and control using Single Response Surface.

In the case of control, the simulated step disturbance (a shift in injector positions) was applied between runs #64 and #65, immediately following an optimization sequence. Fig. 4.10(a) shows that the step disturbance resulted in a process that was less well tuned, and that Ultramax was then able to respond and effect a recovery of deposition rate uniformity.

While Ultramax was successful at optimizing a process and responding to a step disturbance, it was too slow at doing so. The speed is limited by the fact that the second-order model of the SN Ratio in five equipment settings has 21 coefficients and therefore requires a minimum of 21 runs to fit.

The Multiple Response Surfaces approach was used to enhance the performance of sequential optimization and control using Ultramax. In this case, 11 first-order deposition rate models were updated after each run. Since there are five equipment settings, the number of coefficients for each model is six. This small number of coefficients allows for rapid optimization and control. Results of using the new modeling approach are shown in Fig. 4.11. As can be seen, the number of runs to reach the optimum by using the Multiple Response Surfaces approach is reduced to one third of the number required by using the Single Response Surface approach, roughly in proportion to the number of coefficients in an individual site model versus the number in a Single Response Surface model. In the case of control, it takes only six runs to recover back from a step disturbance, exactly the same as the number of coefficients of each deposition rate model.

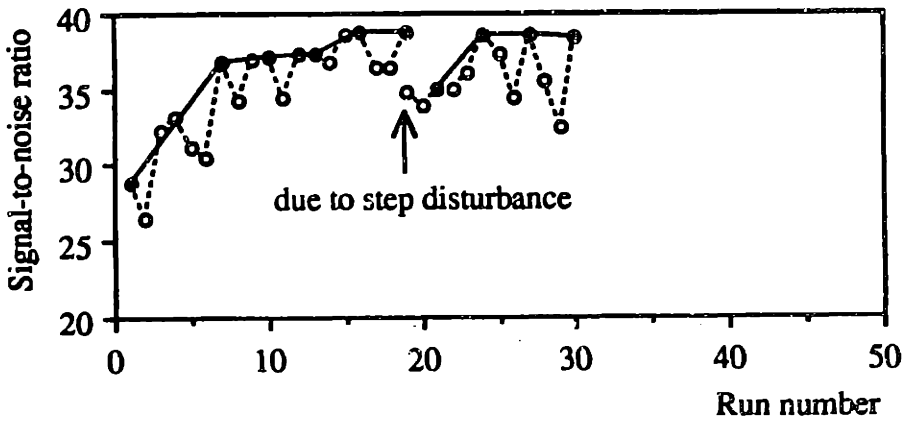

Fig. 4.11 Run by run optimization and control using Multiple Response Surfaces. All terms are refitted after the step disturbance.

4.2.4 Sequential Design of Experiments : Rapid Response to a Step Disturbance

One strategy to enhance the speed of recovery after a step disturbance is to update the constant term of each site model while keeping the first-order coefficients constant after the

step disturbance. In this ase, we are assuming that the effect of a step disturbance can be characterized by the change of the constant terms (each response surface is shifting by a different constant value) but no change in the sensitivity of the process to the equipment settings. This approach to adapting the constant terms after a step disturbance is implemented in the "Run by Run Controoler" [14] as described in chapter two. An experiment on silicon epitaxy in a barrel reactor has been performed to verify this assumption [33].

Rapid model adaptation using Multiple Response Surfaces with adaptation of the constant terms only was applied to the equipment simulator of LPCVD of polysilicon. As shown in Fig. 4.12, rapid recovery was achieved within one run since only the constant terms of each deposition rate model were modified after the step disturbance.

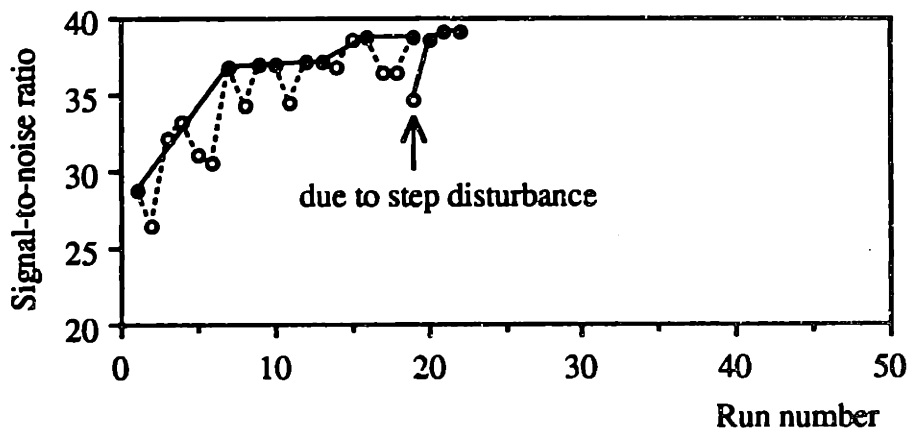

Fig. 4.12 Rapid response to step disturbance by updating constant terms only.

In order to simulate the real process, the above sequential optimization and control has been repeated with reasonable random noises superimposed onto the equipment settings and output deposition rates in each run. The best result obtained by using the Multiple Response Surfaces approach and the rapid adaptation of the constant terms after a step

disturbance is shown in Fig. 4.13. As can be seen, the optimization and control speed is a little slower due to the adding of noises; however, it is still very fast. Notice that Fig. 4.13 was previously used in chapter 2 (Fig. 2.6) as an illustration of the use of the Run by Run Controller.

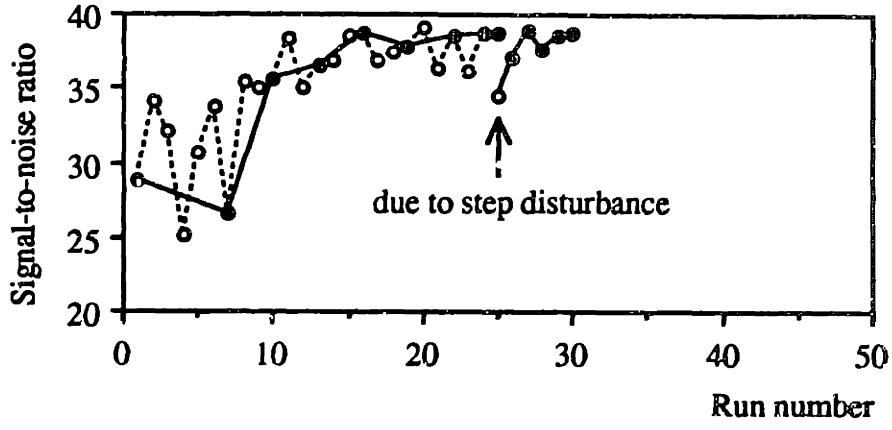

Fig. 4.13 Run by run optimization and control with noise superimposed.

CHAPTER FIVE

EXPERIMENTAL RESULTS

5.1 Silicon Epitaxy

A series of experiments were performed on an Applied Materials 7800 epitaxy barrel reactor (Fig. 5.1). Thickness uniformity across 15 measurement sites on one susceptor face was tuned by adjusting two equipment settings : horizontal jet angle (the horizontal angles of the two injectors are constrained to be the same), and nozzle flow balance (distribution of flow rates between the two injector nozzles).

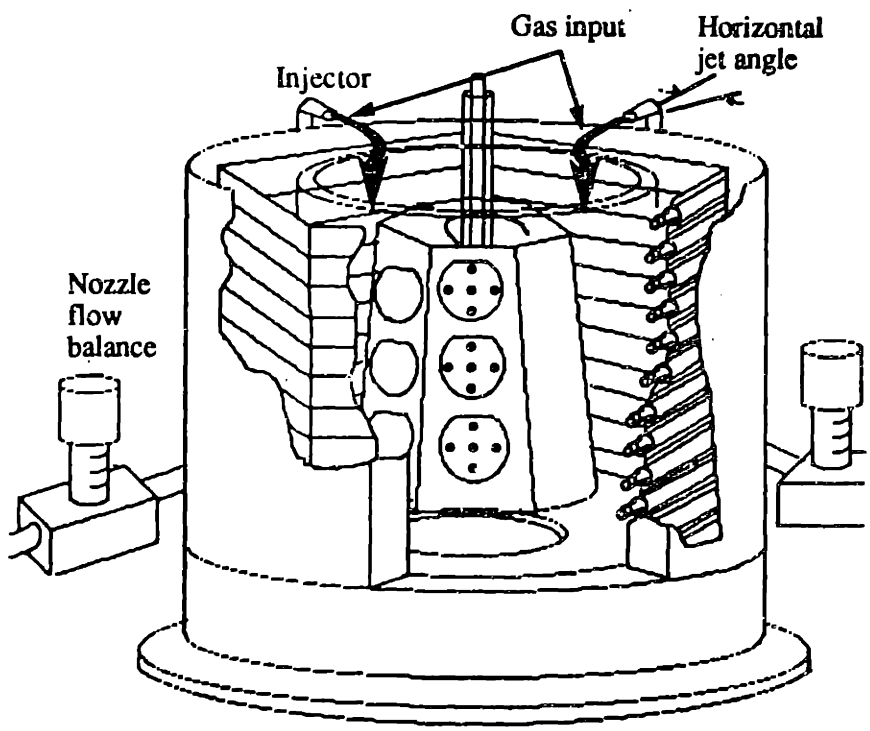

Fig. 5.1 Schematic of epitaxy reactor.

A 3^2 design was performed and the data were collected (appendix D). Nine data points were used in the Single Response Surface approach to create a second-order (σ / μ) model. Four data points were used in the Multiple Response Surfaces approach to create 15 first-order thickness models. Results of experimental uniformity versus predicted uniformity are plotted in Fig. 5.2. Here we use a straight line to represents a perfect fit, and define an average error as follows :

$$\text{Average error} = \frac{1}{9}\sum_{i=1}^{9} |\,\text{experimental value} - \text{predicted value}\,|_i \qquad (5.1)$$

As can be seen, Single Response Surfaces has a slightly better fit than Multiple Response Surfaces. The average error for Single Response Surface is 0.47% while the average error for Multiple Response Surfaces is 0.62%. Fig. 5.3 also shows the predicted uniformity within the experimental space. As can be seen, both approaches have roughly the same optimum settings; however, the Multiple Response Surfaces approach uses a smaller number of experimental data.

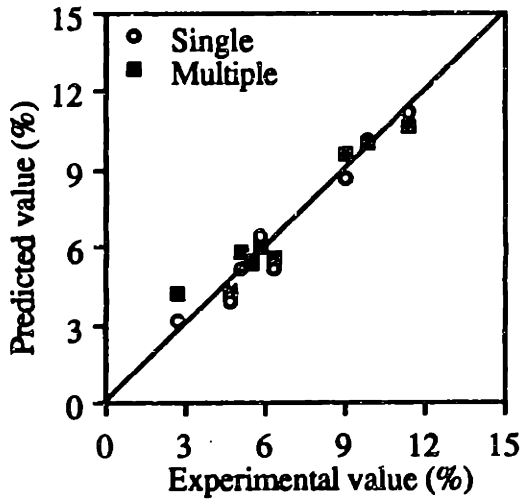

Fig. 5.2 Experimental versus predicted uniformity.

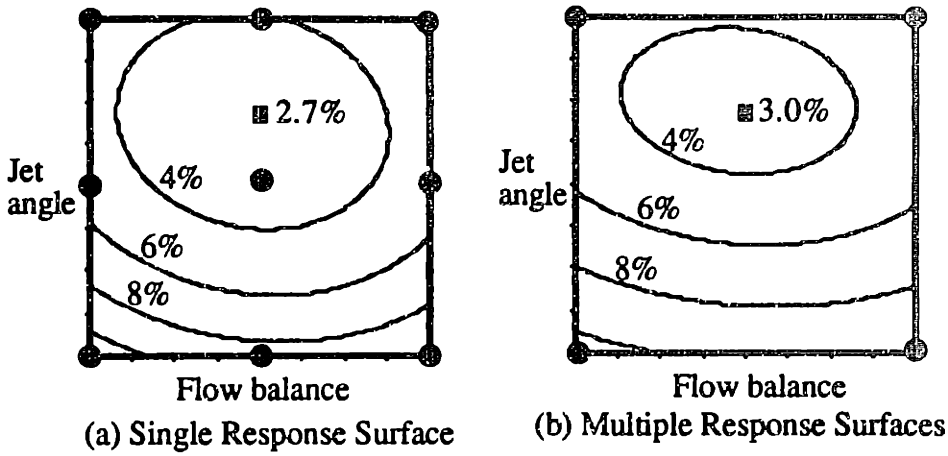

(a) Single Response Surface (b) Multiple Response Surfaces

Fig. 5.3 Predicted uniformity using two approaches. Solid circles represent experimental data used to create models, while solid squares represent predicted optimum settings and corresponding optimum uniformity.

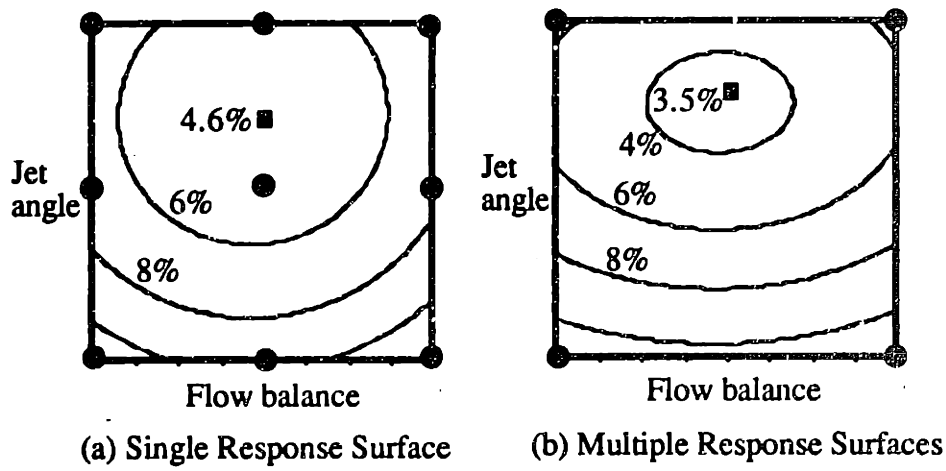

(a) Single Response Surface (b) Multiple Response Surfaces

Fig. 5.4 New predicted uniformity using two approaches. Solid circles represent simulated experimental data to create models, which were obtained by adding noises to original experiment data. Solid squares represent predicted optimum settings.

In order to characterize the sensitivity of the two approaches to noise, we superimposed 5% random noises onto the measured thickness data, as shown in (5.2)

$$Y_i' = Y_i (1 + 0.05\ R_i) \quad i = 1, 2, \cdots, 15 \tag{5.2}$$

where R_i is a random number generated from a standard normal distribution N(0,1).

The simulated experimental data were then used to create uniformity models using Single and Multiple Response Surfaces, and the new predictions were compared to those obtained by fitting original experimental data. Fig. 5.4 shows the new predicted uniformity within the experimental space. By comparing Fig. 5.3 and Fig. 5.4, we can see that model predictions based on Multiple Response Surfaces are more consistent. For example, the optimum uniformity changes from 2.7% to 4.6% in the Single Response Surface case, and it changes from 3.0% to 3.5% in the Multiple Response Surfaces case.

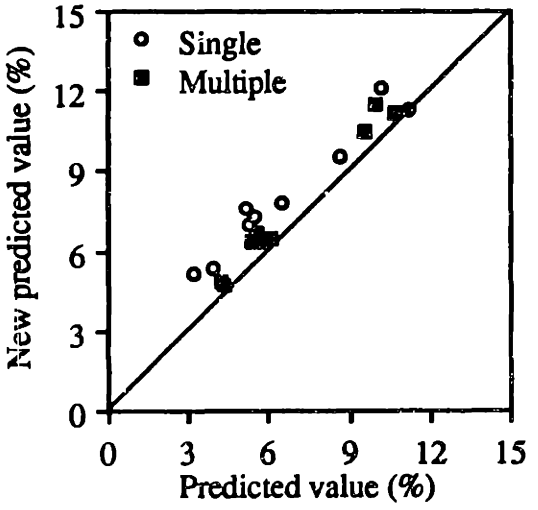

Fig. 5.5 Predicted versus new predicted uniformity.

Fig. 5.5 plots the difference between the predicted uniformity (obtained by fitting original experimental data) and the new predicted uniformity (obtained by fitting simulated

experimental data) at the nine design setting points. As can be seen, the average difference is smaller for Multiple Response Surfaces. Here the average difference is defined in (5.3) and is a metric used to characterize the sensitivity to noise. A smaller value represents a smaller change in the predicted values and a better noise immunity. In this example, the average difference for Single Response Surface is 1.61%, while the average difference for Multiple Response Surfaces is 0.84%, meaning that Multiple Response Surfaces is more immune from noise.

$$\text{Average difference} = \frac{1}{9}\sum_{i=1}^{9} |\,\text{predicted value - new predicted value}\,|_i \qquad (5.3)$$

In the LPCVD and silicon epitaxy examples, we have superimposed simulated random noises onto the data and the results did indicate that Multiple Response Surfaces has a better noise immunity than Single Response Surface. Fig. 5.6 compares the fit of each site model (using adjusted R^2) before and after the addition of simulated noise. As can be seen, the individual site models can be affected by noise and the fits might not be very good; however, the spatial uniformity obtained by the combined action of multiple models is quite immune from noise. In the Single Response Surface case, the adjusted R^2 for the fitted uniformity model has changed from 94% to 76%.

5.2 Tungsten CVD

Processes for forming W-CVD films both in selective and blanket deposition have been successfully pursued. These films have found applications as low resistance gate interconnections, ohmic contacts, planarized low resistance vias, and contact barrier materials [2][34]. In this work, the experiments were performed on a Spectrum 202 reactor (Fig. 5.7). Selective deposition was used to deposit W films on blanket Si wafers.

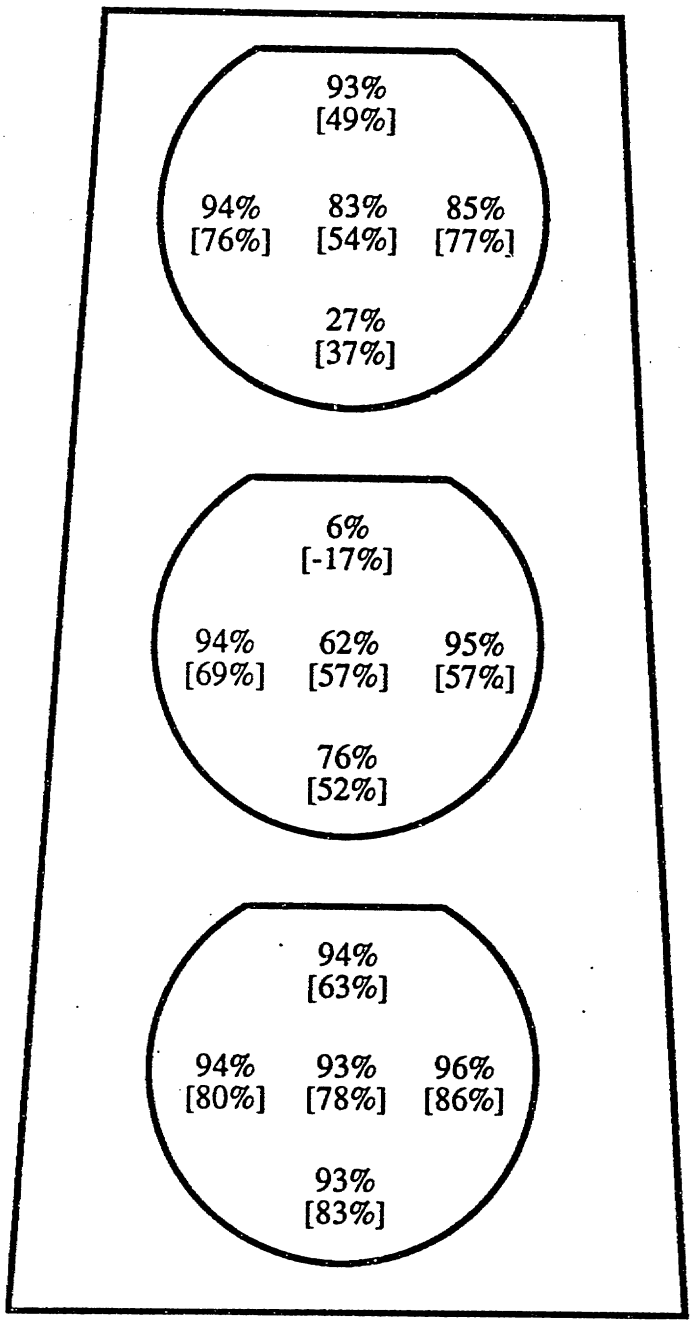

Fig. 5.6 Adjusted R^2 of each site model. Numbers in the brackets represent the adjusted R^2 after adding noises to the experimental data.

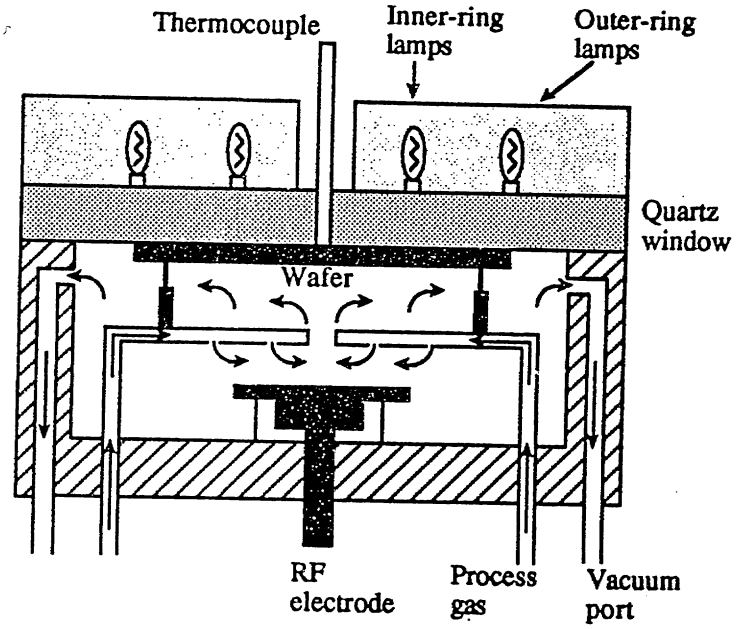

Fig. 5.7 Schematic of tungsten CVD reactor.

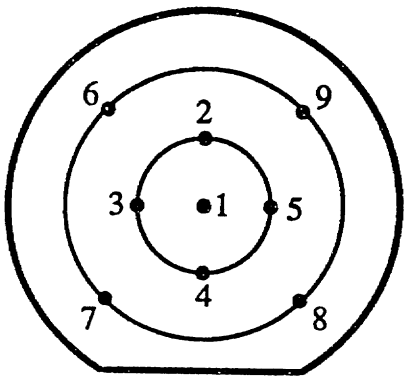

Fig. 5.8 Nine measurement sites on single wafer which are used in tungsten CVD and plasma etching experiments.

Resistivity uniformity across nine measurement sites on each wafer (Fig. 5.8) was tuned by adjusting two equipment settings: temperature and voltage ratio (the ratio of

voltages applied to two rings of lamps). A series of screening experiments were performed and the result indicated that these two equipment settings have the largest effect on the resistivity uniformity. This is consistent with the result found in the literature: resistivity decreases as temperature increases [35] and the radial uniformity can be controlled by a temperature gradient [36] along the radial direction.

A 3^2 design was performed and the data were collected (appendix E). Nine data points (nine combinations of equipment settings) were used in the Single Response Surface approach to create a second-order (σ / μ) model. Four data points were used in the Multiple Response Surfaces approach to create nine first-order resistivity models, one for each of the nine measurement sites.

Fig. 5.9 shows the contour and three-dimensional plots of the predicted (σ / μ) within a setting space which is larger than the experimental space. As can be seen, the shapes of the two response surfaces are quite different, especially for the prediction of the optimum settings. In the Single Response Surface case, (σ / μ) has no minimum value and decreases as temperature decreases since the model has a saddle point. The predicted (σ / μ) passes through zero at a temperature of 260 °C and a voltage ratio of 2. In the Multiple Response Surfaces case, the predicted minimum value of (σ / μ) is 3.1% at a temperature of 296 °C and a voltage ratio of 2.8. Confirmation runs around the above two setting points were performed to test the accuracy of the predictions and the results are shown in Table 5.1. Although both test points are somewhat outside the experimental space for the models, the results do indicate that the predictions based on Multiple Response Surfaces are more accurate than those made using the Single Response Surface approach.

Fig. 5.10 also shows the results of experimental uniformity versus predicted uniformity. As can be seen, Single Response Surface has a slightly better fit than Multiple

Response Surfaces. However, based on the discussion above, it is possible that the small error of the Single Response Surface is actually the result of overfitting the data.

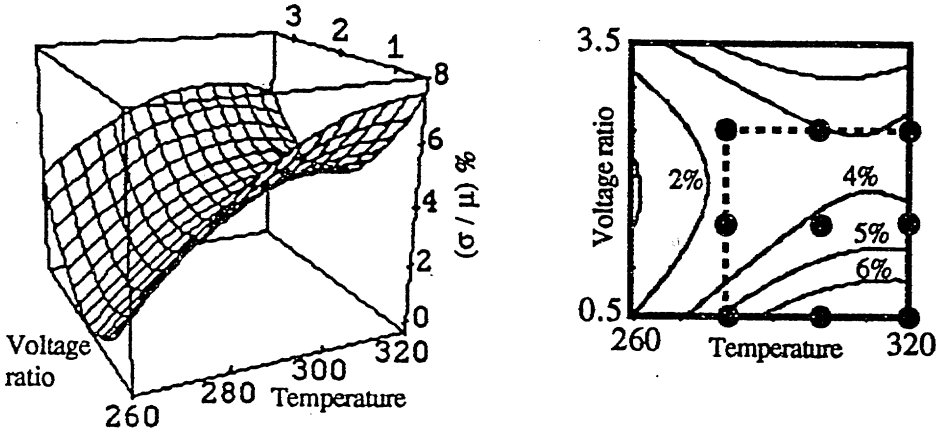

(a) Single Response Surface

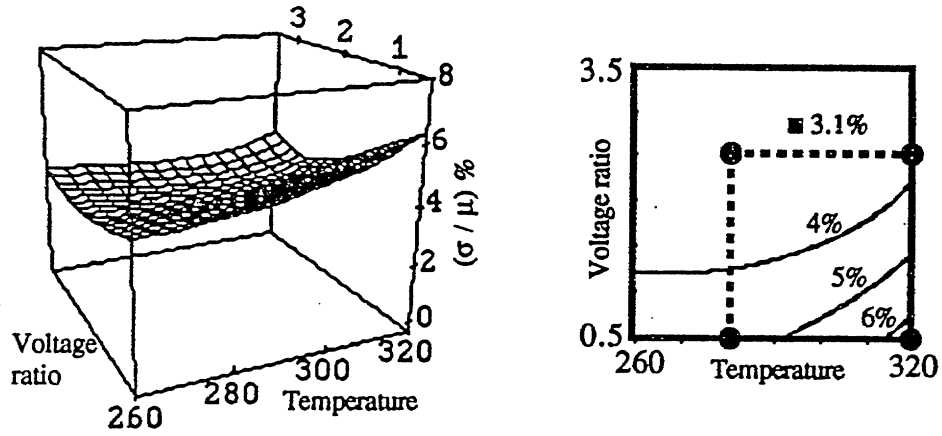

(b) Multiple Response Surfaces

Fig. 5.9 Predicted uniformity using two approaches. Solid circles represent experimental data used to create models, while solid squares represent predicted optimum settings and corresponding optimum uniformity. The dotted lines represent experimental space.

Table 5.1 Confirmation runs for tungsten CVD.

	Temperature = 295 Voltage ratio = 3	Temperature = 260 Voltage ratio = 2
Measured $\frac{\sigma}{\mu}$ (%)	3.54%	4.59%
Predicted $\frac{\sigma}{\mu}$ (%) Single response	4.62%	-0.1%
Predicted $\frac{\sigma}{\mu}$ (%) Multiple reponses	3.12%	3.59%

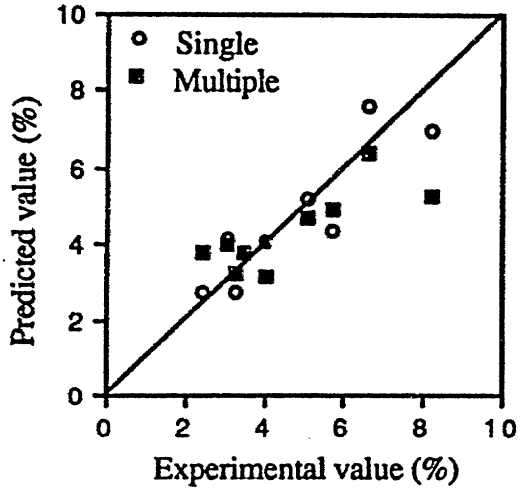

Fig. 5.10 Experimental versus predicted uniformity.

5.3 Plasma Etching

A series of experiments were performed on a Lam AutoEtch 590 single wafer plasma etcher (Fig. 5.11) to etch BPSG. Etch rate uniformity across nine measurement sites on

each wafer (Fig. 5.8) was optimized using the sequential design of experiments as implemented by Ultramax by adjusting five equipment settings, which include RF power, gap spacing, and three gas flow rates (He, CHF_3, and CF_4).

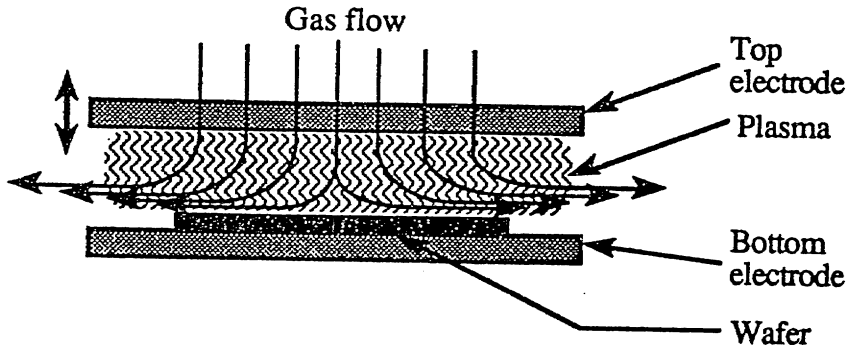

Fig. 5.11 Schematic of plasma etcher.

Screening experiments were first performed. It was found that when multiple models were fitted to each of the nine measurement sites, the fit of each model was relatively poor (see appendix F), which is consistent with the observation that plasma etching is a relatively noisy process. Noting that the typical etch rate pattern resembles a "bulls-eye", advantage was taken of the axial symmetry of the plasma etcher and models were created for each of the three radii at which measurements were made. The average of sites 6,7,8, and 9 (Fig. 5.8) was used to create one model, the average of sites 2,3,4, and 5 was used to create a second model, and site 1 was used for the third model[6]. Further noise immunity was gained by fitting a normalized metric which filters out noises that act as a multiplicative shift over the entire wafer (see also appendix F). The fitted metric was :

[6] Simulations have shown that even in cases where the individual models have poor fit, combining the site models can still achieve accurate predictions of uniformity. Nonetheless, in a case such where symmetry is evident, it may be advantageous to average measurement sites.

$$\frac{Y - \mu}{\mu} \tag{5.4}$$

where Y is the etch rate and μ is the mean etch rate of a batch. After fitting the three response surfaces for the normalized metrics, a radial uniformity model was obtained as follows :

$$\left(\frac{\sigma}{\mu}\right)_r = \sqrt{\frac{1}{8}\left[\left(\frac{Y_1-\mu}{\mu}\right)^2 + 4\left(\frac{\overline{Y}_2-\mu}{\mu}\right)^2 + 4\left(\frac{\overline{Y}_3-\mu}{\mu}\right)^2\right]} \tag{5.5}$$

where $\overline{Y}_2$ represents the average value of sites 2, 3, 4, and 5 and $\overline{Y}_3$ represents the average value of sites 6, 7, 8, and 9. The result of the run by run optimization is shown in Fig. 5.12. As can be seen, the radial variation was reduced below 2% in ten runs. By run #10 of Fig. 5.12, the radial variation has been reduced to the point where it is comparable to the circumferential variation and account must now be taken of both types of variation [37].

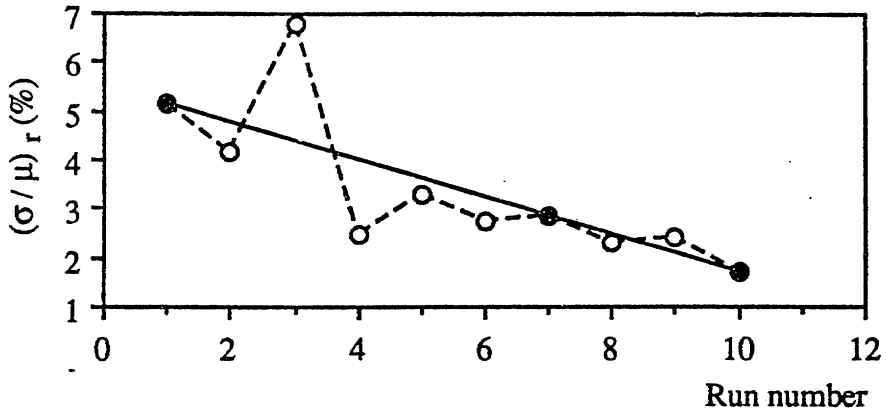

Fig. 5.12 Run by run optimization of etch rate uniformity.

CHAPTER SIX

BASIC CHARACTERISTICS OF MULTIPLE RESPONSE SURFACES

6.1 Robustness and Tuning

Multiple Response Surfaces can be used to model, optimize and control the uniformity within a batch of product. However, not all the variation within a batch can be addressed by this approach. Multiple Response Surfaces is useful when applied to modeling those components of uniformity that manifest themselves as a repeatable underlying pattern which is directly influenced by changes in equipment settings. As an example, let us consider the LPCVD process discussed earlier. If we consider the mean of each wafer as a function of position down the length of the tube (Fig. 6.1), we see that there is a repeatable underlying pattern which can be influenced by changing equipment settings such as the gas flow rates. This aspect of batch uniformity can be modeled and tuned using Multiple Response Surfaces, as has been demonstrated above. Superimposed on this tunable pattern is the variation of individual site measurements (error bar in Fig. 6.1) that takes place from run to run due to process disturbances. This variation is an example of a component of uniformity which cannot be tuned by changes in the equipment settings. This component of uniformity can be addressed by making the process less sensitive to the disturbances, that is, by making the process robust.

Another example is that of plasma etching. In this case, the radial component of uniformity can be tuned by changes in the equipment settings and hence is a good candidate for Multiple Response Surfaces. However, the circumferential uniformity cannot be tuned and must be addressed by techniques designed to optimize robustness [37].

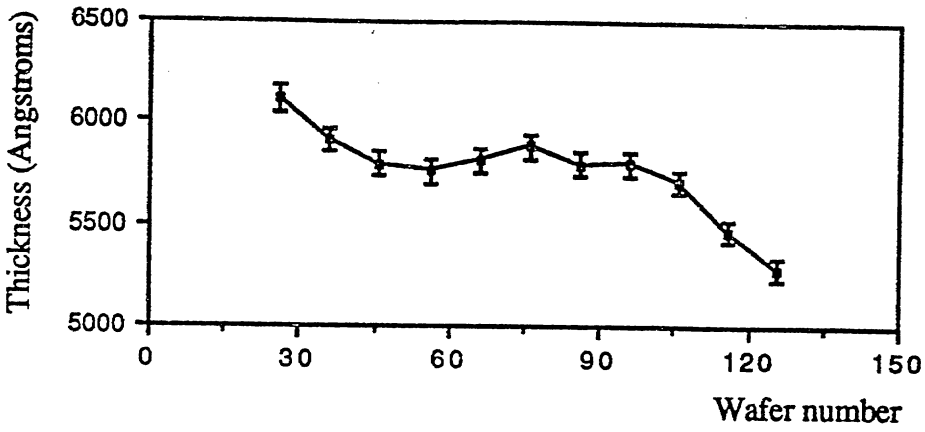

Fig. 6.1 Thickness profile of LPCVD process.

Robustness can be achieved using methods of experimental design when the proper objective function is used. Taguchi [6] discusses a two-step optimization procedure called parameter design which allows for the optimization of robustness and the adjustment of the mean value. Ha [37] discusses a three-step optimization procedure which allows for the optimization of robustness using robustness factors, tuning of the tunable components of batch uniformity using tuning factors, and adjustment of the mean using an adjustment factor. In the first step, a series of experiments are performed and the results are used to find the best tuning factors and adjustment factor and to set the levels of the robustness factors. In the second step, the tuning factors and Multiple Response Surfaces are used to tune the batch uniformity. In the third step, the adjustment factor is used to adjust the batch mean to a target value.

6.2 Curvature Effect of Uniformity

The advantage of Multiple Response Surfaces over Single Response Surface in creating a uniformity model with a smaller number of data is more significant when the curvature of

the underlying uniformity is high. In the LPCVD example where the curvature of the underlying uniformity is high, Multiple Response Surfaces used fewer data points and resulted in a more accurate uniformity model. By contrast, in the epitaxy case, where the curvature of the underlying uniformity is somewhat lower, Multiple Response Surfaces still used fewer data points but resulted in a uniformity model of accuracy comparable to that obtained by a Single Response Surface.

In order to characterize the effect of curvature of the underlying uniformity, a simulated process with three output characteristics and two equipment settings (X_1 and X_2) has been optimized using sequential design of experiments. The true response surfaces of the three outputs were taken to be first-order and the resulting uniformity model is plotted in Fig. 6.2.

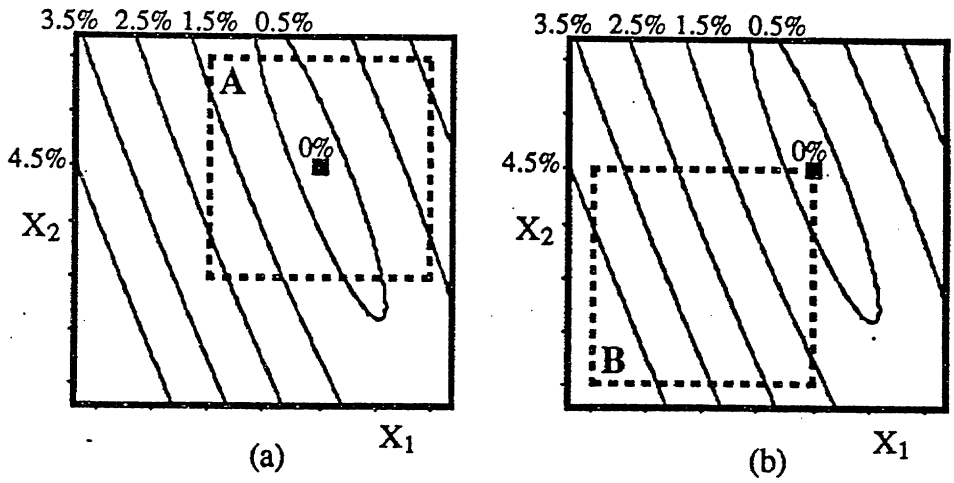

Fig. 6.2 Two setting space corresponding to high and low curvatures of uniformity.

Run by run optimization was performed by using Single and Multiple Response Surfaces. In region A (Fig. 6.2(a)), where the optimum setting point is inside the setting

space, the curvature of the uniformity is high and the optimization by Multiple Response Surfaces is much faster (Fig. 6.3).

In region B (Fig. 6.2(b)), where the optimum setting point is at the corner of the setting space, the curvature of the uniformity is very low. The result is that the optimization speed by the Single Response Surface approach is approximately the same as that by the Multiple Response Surfaces approach (Fig. 6.4), although the Multiple Response Surfaces approach does converge the optimum in a more nearly monotonic fashion.

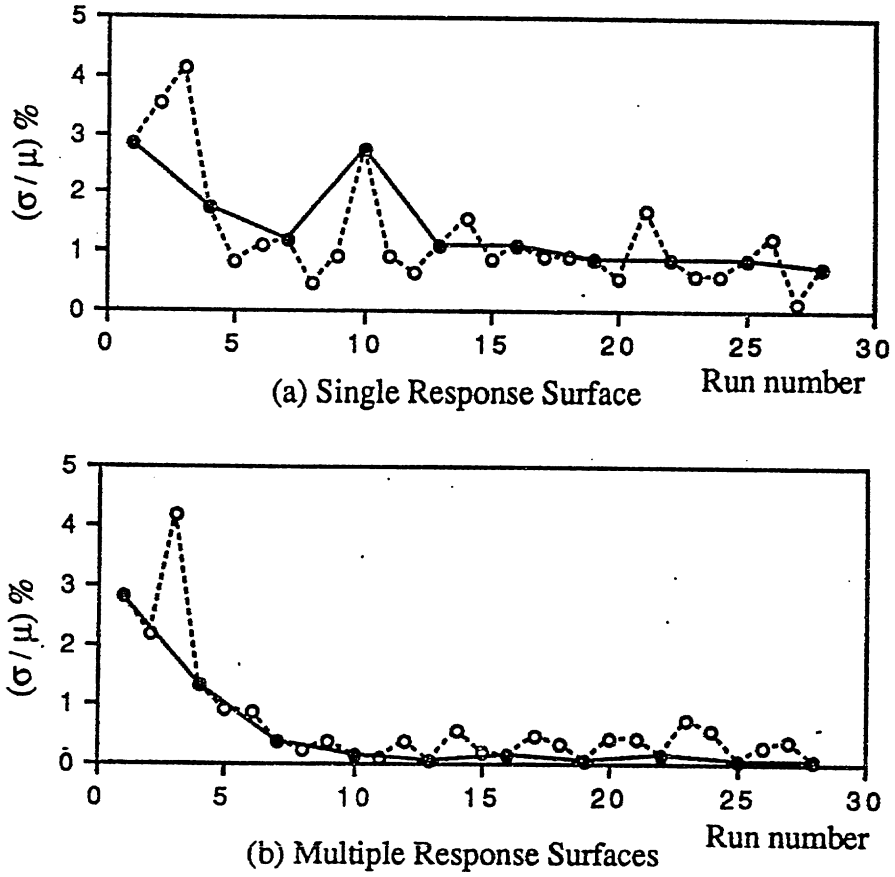

Fig. 6.3 Run by run optimization in region where uniformity curvature is high. Solid circles connected by solid line represent optimum runs, while open circles represent exploration runs.

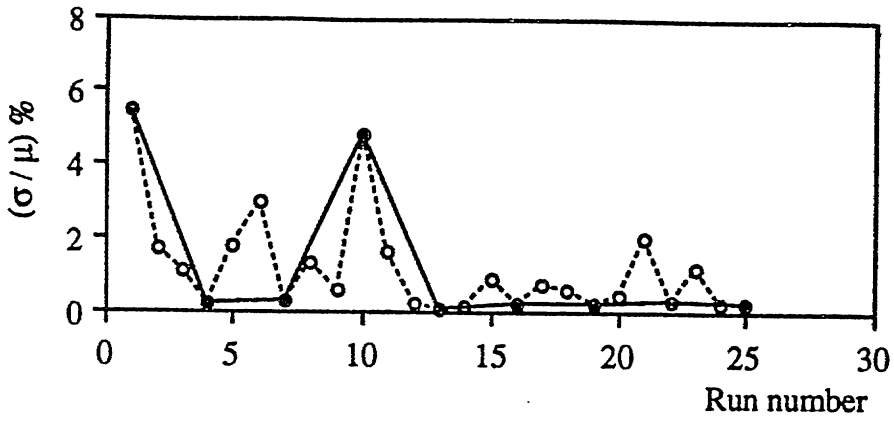

(a) Single Response Surface

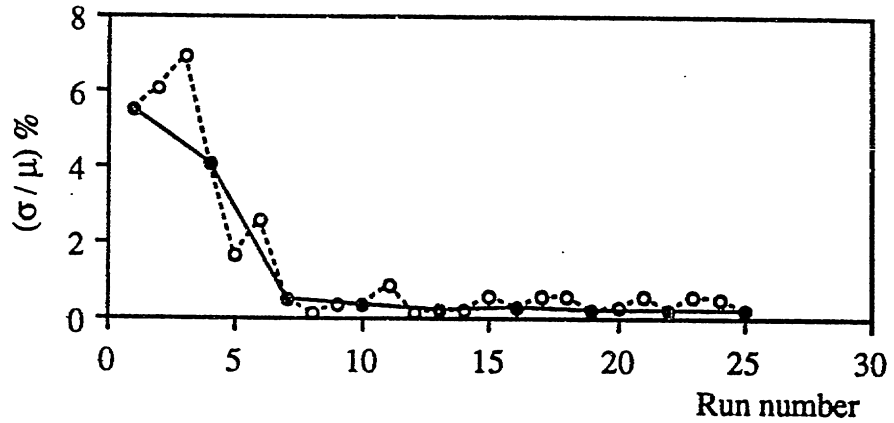

(b) Multiple Response Surfaces

Fig. 6.4 Run by run optimization in region where uniformity curvature is low.

In practice, the curvature of the uniformity will be higher if the slope coefficients of individual site models have opposite signs. Physically, this means some of the responses increase with the increase of the equipment settings, while the other responses decrease with the increase of the equipment settings. This might occur for situations like a distribution of flow rates of lamp power. This is illustrated in Fig. 4.3 where the deposition rate of wafer 26 increases when flow rate 1 increases, while that of wafer 124 decreases when flow rate 1 increases (because the total flow rates were fixed). The result is that the optimum settings are inside the setting space interested and the curvature of the uniformity is high.

6.3 Saddle Point

In the LPCVD and tungsten CVD examples, saddle points were found in some of the models created by the Single Response Surface approach. In principle it is possible that the uniformity might actually have saddle point behavior. However, it should be noted that over any reasonable range, a model with a saddle point will predict that (σ / μ) passes through zero and becomes negative. As this is not possible, it is clear that a model with a saddle point can be appropriate over only a very small setting space.

It is of interest to note that no application of Multiple Response Surfaces has resulted in saddle point behavior for the uniformity. This can be intuitively understood by noting that the combination of individual site responses can never result in a uniformity which is less than zero. Appendix A provides a mathematical proof which shows that at least for a special class, Multiple Response Surfaces cannot result in a uniformity model that has a saddle point[7]. This behavior of Multiple Response Surfaces has some clear advantages for modeling spatial uniformity as it eliminates a class of responses that is physically unlikely (or impossible) and thus renders this approach more immune to noises.

6.4 Confidence Interval

In the LPCVD example, the noise immunity is characterized by plotting the distribution of the predicted values taken from 24 designs. However, in practice, we must be able to estimate a probable range of values from just one design. In the Single Response Surface

---

[7] Hunter [32] examined a parallel question for the case of models which are the result of multiplying two first-order models together. In that case, it was found that the composite model could not assume the form of a minimum or maximum, but could take on a saddle point.

approach, the estimation of a confidence interval for the predicted value is well established in the literature [38], and is summarized in appendix B.

The confidence interval for the predicted uniformity based on Multiple Response Surfaces can be developed from the confidence intervals of the constituent models. In the applications described above, each site model was fitted by a separate regression and therefore the confidence intervals for the models do not take into account the correlation between site responses. However, when sufficient data is available[8], multivariate regression can be used [38] (appendix B). The models derived from multivariate regression will be the same as those derived from separate regressions; however, proper accounting will be made of the correlation between site responses, resulting in confidence regions that are hyperellipsoids in the output characteristic space. For example, in a process with only two output characteristics, the confidence region is an ellipse centered at the predicted value of the two outputs Y_1 and Y_2. By choosing different values of α[9], we can obtain ellipses corresponding to confidence levels of 99.9%, 90%, ...,10% (Fig. 6.5(a)). Recognizing that each area bounded by two ellipses has an equal probability of occurrence, a histogram of uniformity values can be obtained by calculating uniformity for an equal number of sample points within each area (Fig. 6.5(b)). Fig. 6.5(c) shows such a histogram. At many points in equipment setting space, the distribution of (σ / μ) is similar to a normal distribution and the $100(1-\alpha)\%$ confidence interval of (σ / μ) is estimated using (6.1) as follows :

$$\hat{u} \pm z\left(\frac{\alpha}{2}\right) \hat{\sigma}_u \qquad (6.1)$$

---

[8] The number of data points must be larger than the total number of output characteristics and equipment settings (for first-order models) in order to create confidence ellipsoids. See (B.9) for details.

[9] α is the probability of a value lying outside a confidence interval. Thus, a value of 10% correspond to a $(1-\alpha) = 90\%$ confidence interval.

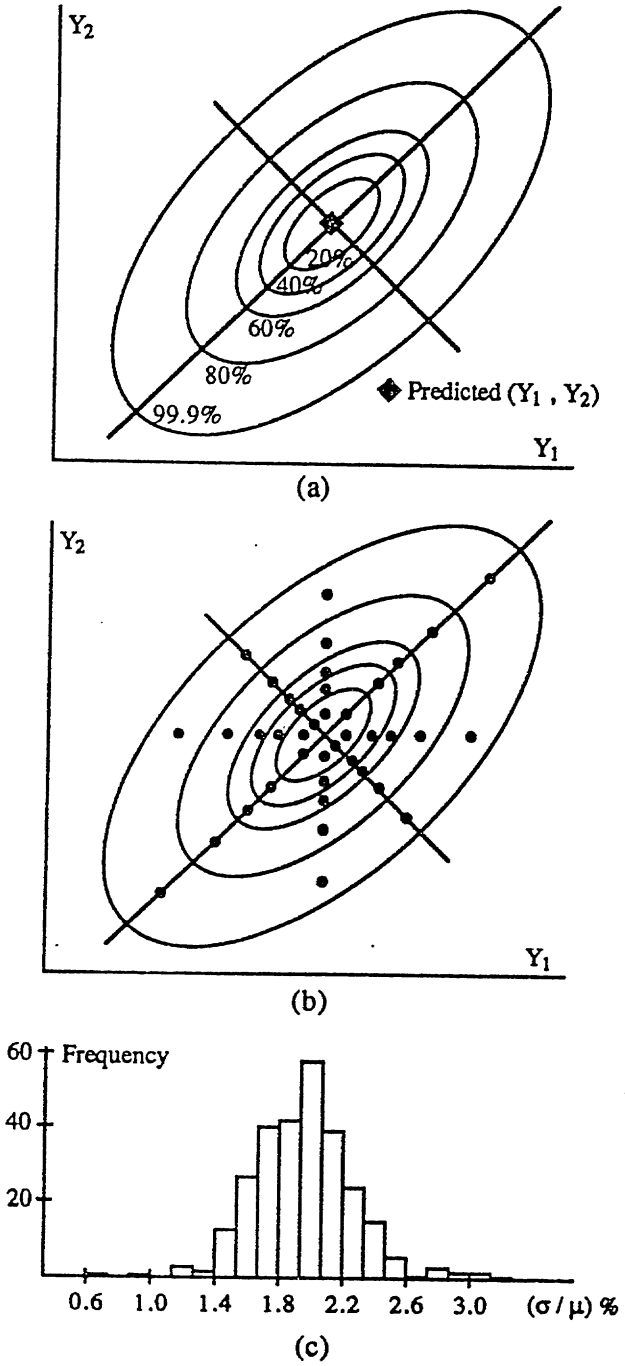

Fig. 6.5 Sequences to find distribution of uniformity.

where $\hat{u}$ and $\hat{\sigma}_u$ are the observed mean and standard deviation of the distribution of (σ / μ), and $z(\alpha/2)$ is the upper percentage point of a normal distribution.

Near the optimum in equipment setting space, the mean of the distribution of uniformity values is close to zero and the distribution resembles that of a Chi-squared statistic (Fig. 6.6(a)). This case may be treated by applying a logarithmic transformation to (σ / μ) which results in a distribution that is more like a normal distribution (Fig. 6.6(b)). We then estimate a confidence interval for the transformed variable, which can be transformed back into a confidence interval for (σ / μ).

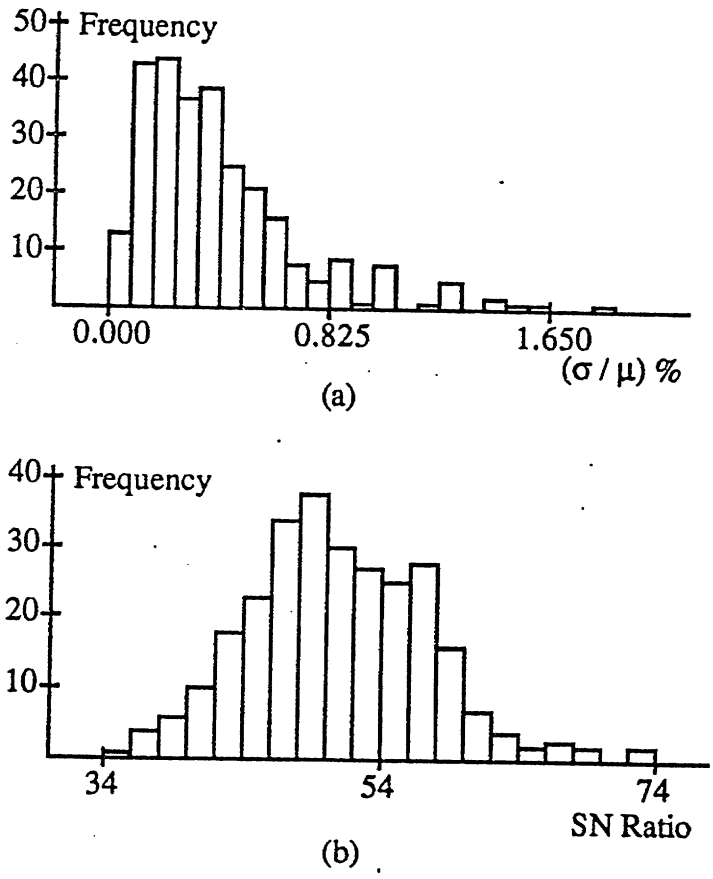

Fig. 6.6 Transformation of uniformity metric to resemble normal distribution.

In order to test the accuracy of the estimated confidence interval by the above approaches, a simulated process with two equipment settings and three output characteristics was used. The true response surfaces of three output characteristics were assumed to be first-order and random noises were superimposed onto the equipment settings and output characteristics to generate the data, which are similar to (4.1) and (4.2).

The 3^2 design was repeated 24 times and models were created for each design. In each design, all nine data points were used in the Single Response Surface approach and in the Multiple Response Surfaces approach. Nine data points were also used in the Multiple Response Surfaces approach in order to create the simultaneous confidence ellipsoid for all output characteristics. Fig. 6.7(a) plots the resulting 95% confidence intervals of the predicted (σ / μ) by using the Single Response Surface approach at one of the design setting points. The first confidence interval was taken as the "true" confidence interval as it was obtained based on the distribution of 24 predicted (σ / μ) (one from each of the 3^2 designs). By plotting the histogram of the 24 predicted (σ / μ), the distribution was found similar to a normal distribution and the confidence interval was estimated by using (6.1). Solid square represents the mean of the distribution. The next four intervals are the "estimated" confidence intervals of the predicted (σ / μ) from designs 1, 2, 3, and 4 respectively by using (B.4). Fig. 6.7(b) plots the resulting 95% confidence intervals of the predicted (σ / μ) by using the Multiple Response Surfaces approach at the same setting point. Again, the first one is the "true" confidence interval and the next four are the "estimated" confidence intervals from designs 1, 2, 3, and 4 respectively. As can be seen in Fig. 6.7, the estimated confidence intervals based on Multiple Response Surfaces correlate well with the true one, meaning that our method as illustrated in Fig. 6.5 works well. Similar conclusions can be made if we plot the estimated confidence intervals from design 5 to 24. Notice that the estimated confidence intervals based on Single Response

Surface are not very consistent. This might be due to the sensitivity of this approach to noise.

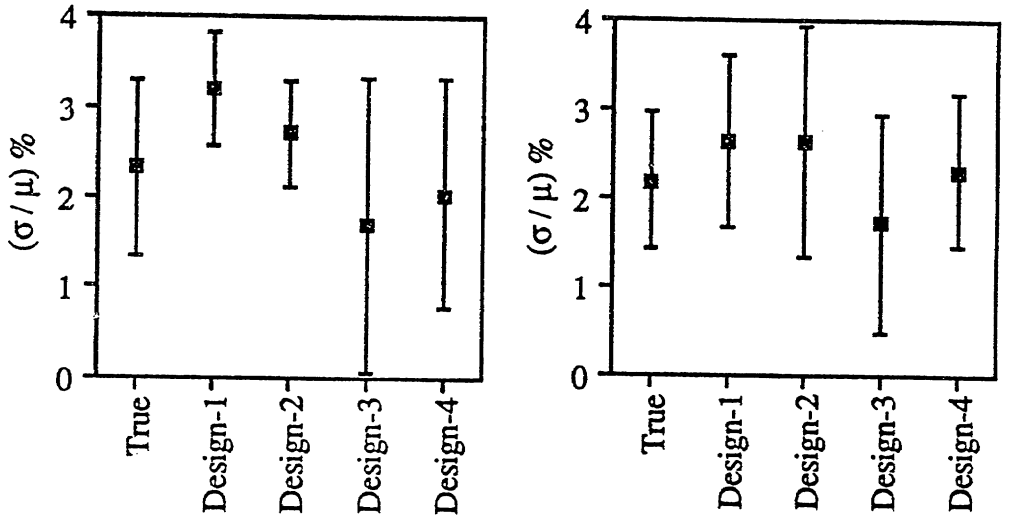

(a) Single Response Surface (b) Multiple Response Surfaces

Fig. 6.7 Confidence intervals based on 24 replicates and based on estimations from each design at one setting point.

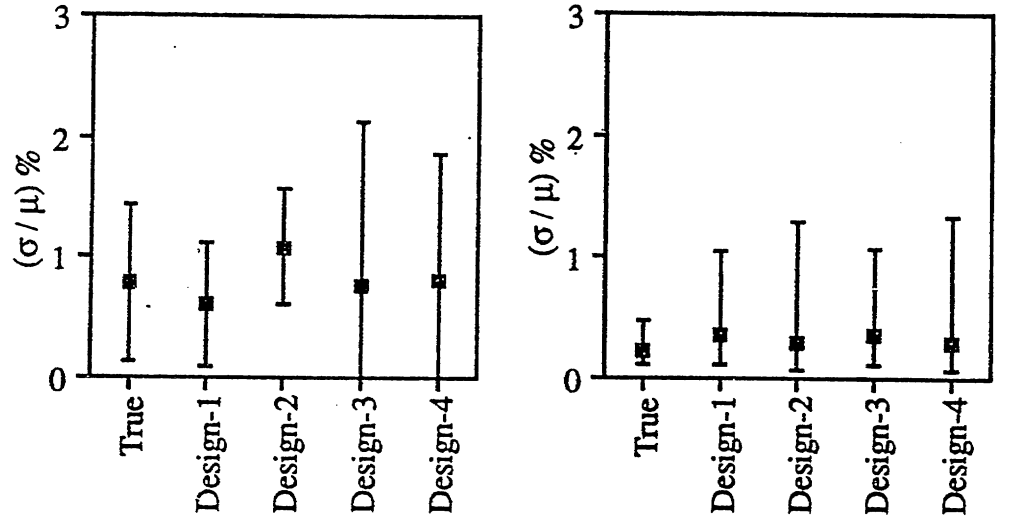

(a) Single Response Surface (b) Multiple Response Surfaces

Fig. 6.8 Confidence intervals based on 24 replicates and based on estimations from each design at optimum setting point.

The same comparison was repeated at another setting point (optimum settings) and the result is shown in Fig. 6.8. In this case, the estimated confidence intervals based on Multiple Response Surfaces overestimate the true one; however, they are still very consistent. Notice that a transformation from (σ / μ) to SN Ratio as illustrated in Fig. 6.6 was performed in order to obtain the confidence intervals.

CHAPTER SEVEN

ALTERNATIVE IMPLEMENTATIONS OF MULTIPLE RESPONSE SURFACES

7.1 Mixed Model

In the Multiple Response Surfaces approach, the output characteristics are the fitted metric. Each output characteristic can be assumed independent and the models obtained separately. In the example of Table 3.1, this approach is taken in (3.2) - (3.4). Alternatively, all the output characteristics can be assumed to be correlated and the models are obtained at the same time using multivariate regression. For the example of Table 3.1, multivariate regression would be represented as follows :

$$\begin{bmatrix} Y_1 \\ Y_2 \\ Y_3 \end{bmatrix} = \begin{bmatrix} C_{11} & C_{12} & C_{13} \\ C_{21} & C_{22} & C_{23} \\ C_{31} & C_{32} & C_{33} \end{bmatrix} \begin{bmatrix} 1 \\ X_1 \\ X_2 \end{bmatrix} \tag{7.1}$$

The correlation between the output characteristics at different measurement sties is at least partly related to the relative positions of the measurement sites. An extension of the Multiple Response Surfaces approach which takes such relative positions into account is the mixed model [39]. A mixed model may be thought to function in two stages. In the first stage, the coefficients C_{ij} relating the equipment settings to the measured output characteristics for the different sites are fitted as in (3.2) - (3.4) or (7.1) above. In the second stage, the coefficients C_{ij} are represented as polynomial functions of a spatial dimension.

In the example of Table 3.1, which has three measured output characteristics and two equipment settings, a mixed model can be implemented by using a first-order polynomial in the spatial dimension, Z. The resulting mixed model has the form :

$$Y = (\beta_1+\beta_2 Z) + (\beta_3+\beta_4 Z)X_1 + (\beta_5+\beta_6 Z)X_2 \qquad (7.2)$$

Although the model (7.2) can be fitted directly as a regression, we can better understand the meaning of the model by considering the fitting in the two stages described above and illustrated in Fig. 7.1(a). The solid squares show the coefficients C_{i1} (the constant terms of the models at the different measurement sites) that result from applying (3.2) - (3.4) or (7.1). The straight line represents the first-order polynomial in spatial dimension Z which is fitted to these coefficients C_{i1}. The coefficients $\hat{C}_{i1}$ (open squares) represent the smoothed coefficients that will be used to predict the output characteristics as in (7.2).

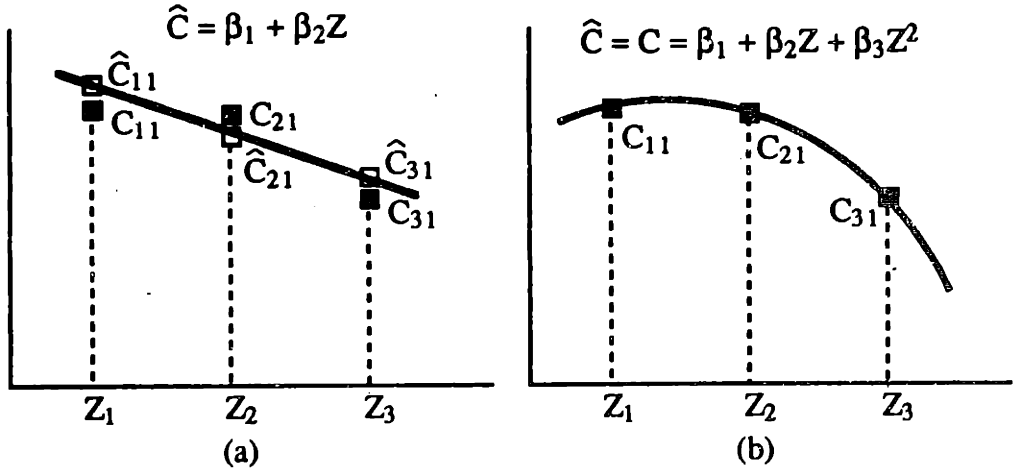

Fig. 7.1 Mixed model implementation of Multiple Response Surfaces.

If the polynomial in Z has the same number of coefficients as there are measurement sites, there is no smoothing of the coefficients C_{ij}. This situation is illustrated in Fig. 7.1(b) for the case of Table 3.1 where a second-order polynomial in Z (see also (7.3)) is used. In such a case, the mixed model may have utility in predicting output characteristics at sites between those where measurements were actually taken.

$$Y = (\beta_1+\beta_2 Z \beta_3 Z^2) + (\beta_4+\beta_5 Z+\beta_6 Z^2)X_1 + (\beta_7+\beta_8 Z+\beta_9 Z^2)X_2 \qquad (7.3)$$

The mixed model approach has been tested in application to the LPCVD simulator discussed previously with two equipment settings. In this application, measurements were taken at 11 sites and a second-order polynomial in Z was used (as shown in (7.3)). Random noises were superimposed onto equipment settings and deposition rates as before.

In the first case study, it was found that this method did indeed smooth the coefficients C_{ij}, resulting in estimates that were closer to the true values which were assumed to be close to the values estimated using Multiple Response Surfaces without noises superimposed. This is shown in Fig. 7.2. However, when the multiple models were combined, it was found that the prediction of uniformity was not better than that obtained using Multiple Response Surfaces as in (3.2) - (3.4) or (7.1), especially around the optimum settings (Fig. 7.3). This might be due to the fact that the predicted deposition rates based on Multiple Response Surfaces are also very accurate. This can be understood by looking at the estimated coefficients altogether (solid squares in Fig. 7.2). If one of the estimated coefficient is larger than the "true value", the other coefficients will be lower than the true values to compensate the error. As a result, when the coefficients are combined together to predict a deposition rate, the error will be small. A good example is wafer five, where C_{51} and C_{52} are lower than the true values, while C_{53} is larger than the true value.

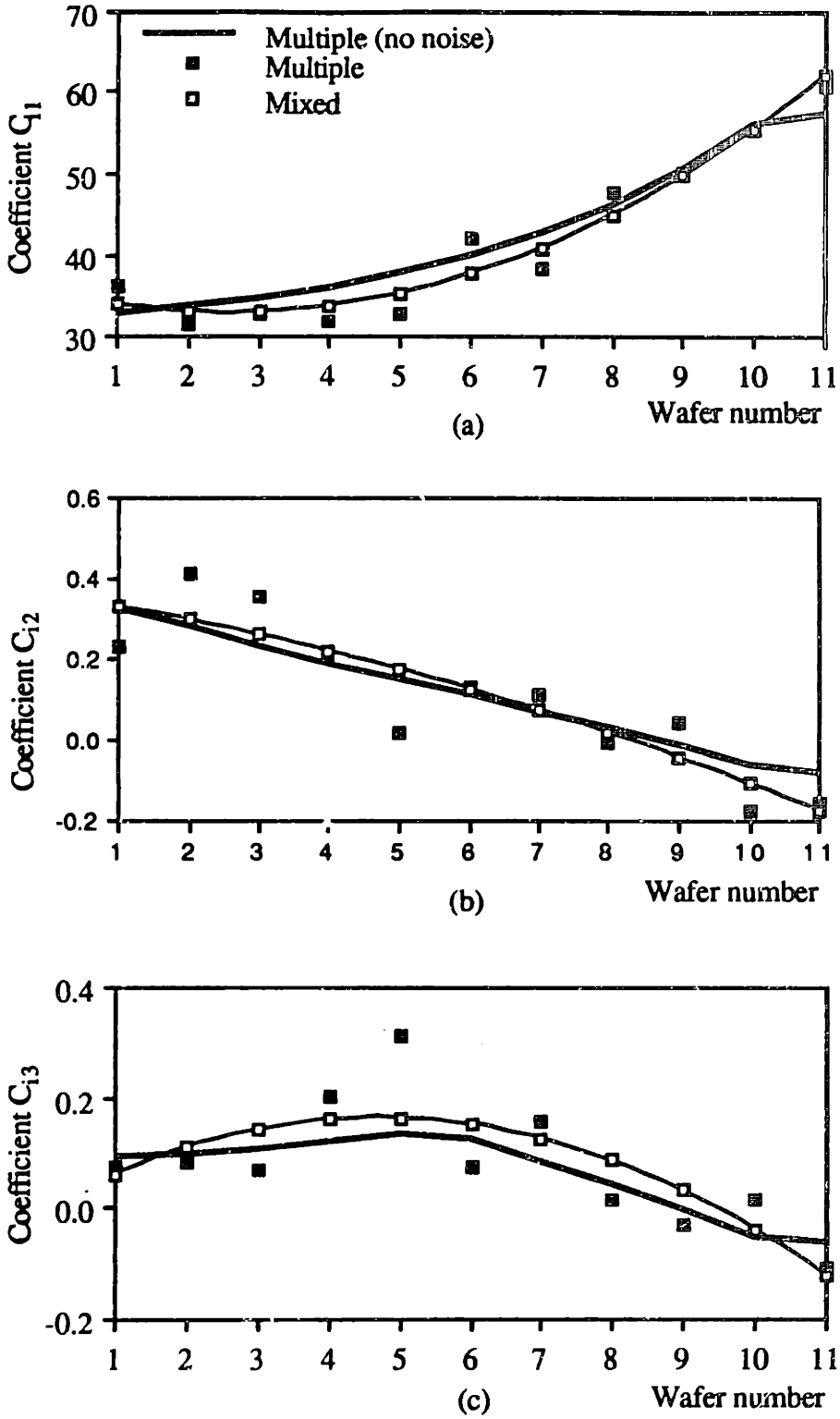

Fig. 7.2 Mixed model to smooth coefficients estimated from Multiple Response Surfaces.

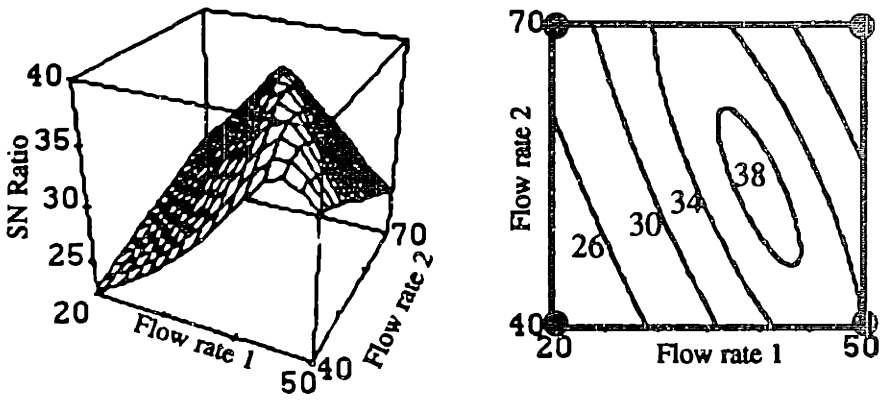

(a) True response estimated without noises superimposed

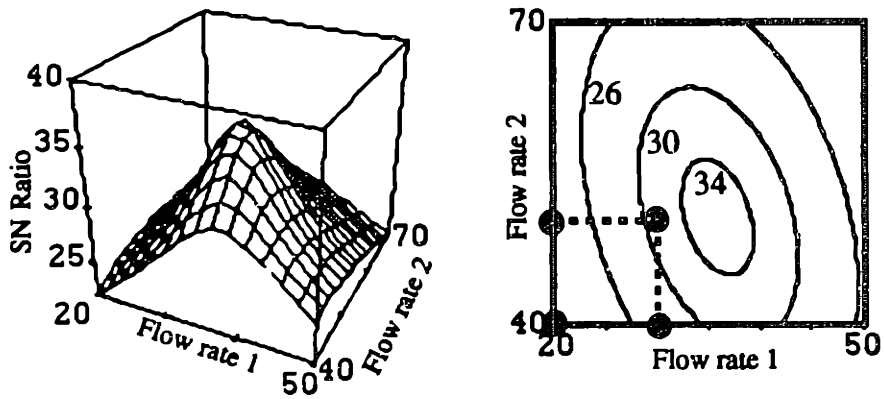

(b) Multiple Response Surfaces

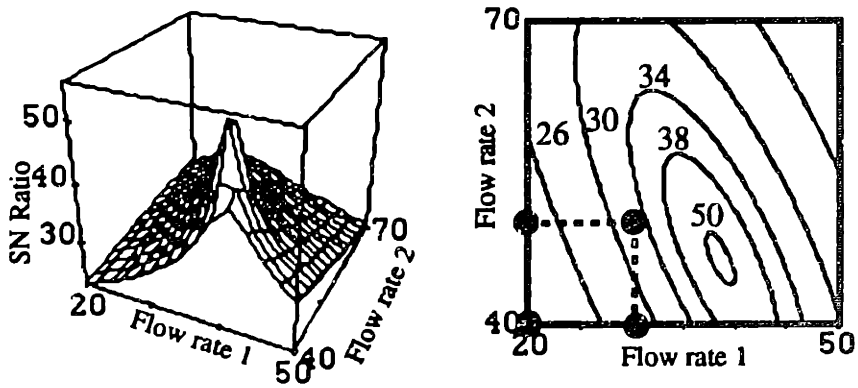

(c) Mixed model

Fig. 7.3 Predicted SN Ratio based on Multiple Response Surfaces and mixed model. Solid circles represent data points and dotted lines represent setting space used to create models.

In the second case study, the data points used to create models are at the corner of the setting space (interpolation) and the predictions of each coefficient obtained from Multiple Response Surfaces are very accurate. In this case, the mixed model has little effect on smoothing the coefficients (Fig. 7.4). When the multiple models are combined together, the prediction of SN Ratio based on mixed model is not as good as that based on Multiple Response Surfaces either, especially for the predicted optimum value (Fig. 7.5). In both case studies, it is possible that better results might be obtained by using different order of polynomial in Z; however, there is no way to know other than trial and error.

7.2 Neural Network

Most of the applications of neural network to modeling include the simultaneous modeling of several output characteristics of different types [40][41]. When modeling spatial uniformity using a neural network, it may be appropriate to apply the basic methodology of Multiple Response Surfaces and simultaneously model the output characteristics of the same type at several sites. Uniformity would then be calculated from the site predictions. Initial tests using a three-layer error-backpropagation neural network in application to the uniformity of etch rate in plasma etching, show that this method does produce better modeling results than directly modeling the uniformity [42].

There are several key differences between the neural network implementation of Multiple Response Surfaces and the first-order statistical model implementation discussed in this paper. Neural nets use a nonlinear threshold function [43] while this work has focused on linear models. Neural nets have a hidden layer which is a way to establish correlation among the output characteristics (see discussion of mixed model). The penalty associated with these virtues is that more data is needed than with multiple, first-order statistical models.

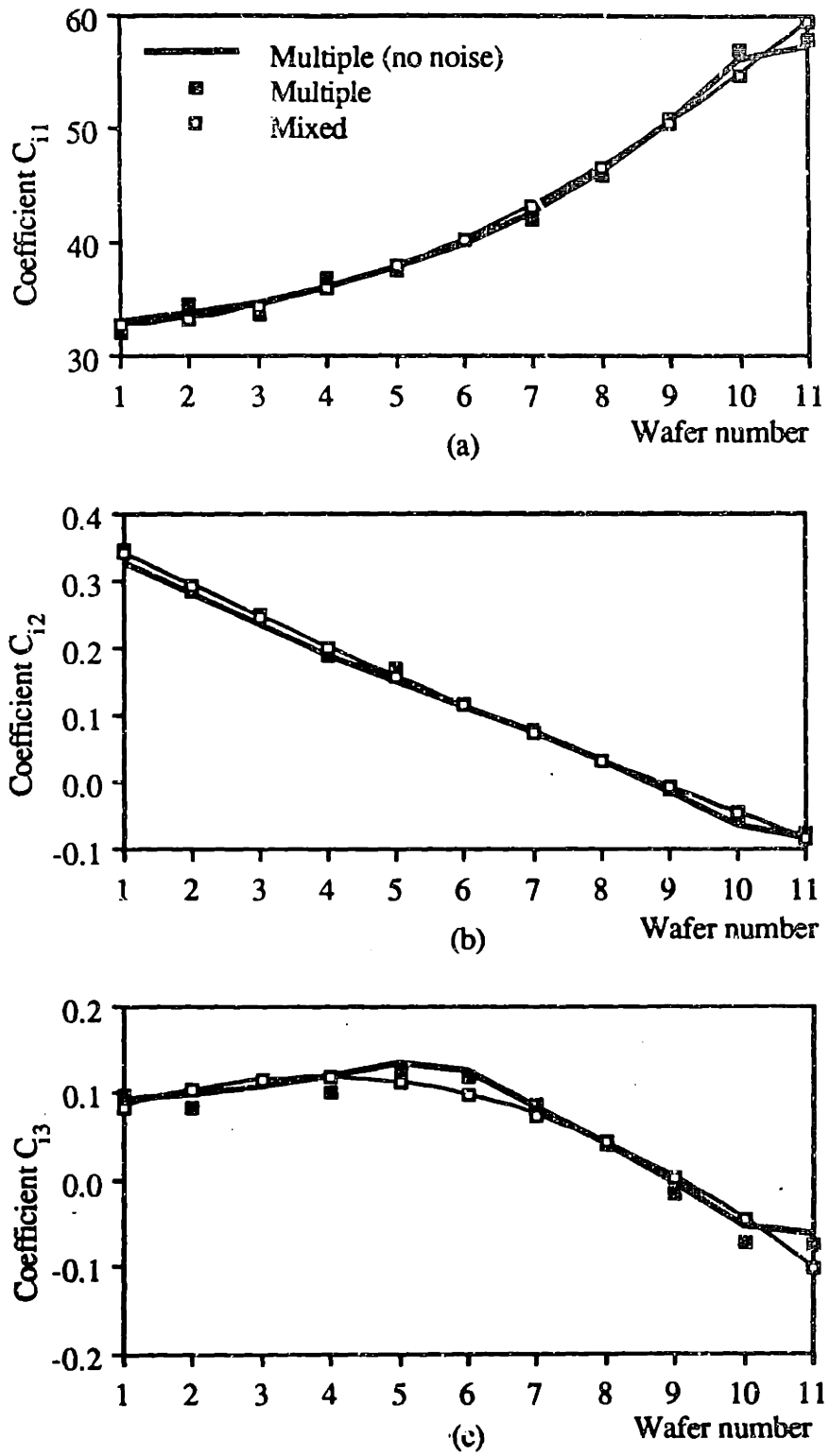

Fig. 7.4 Mixed model to smooth coefficients estimated from Multiple Response Surfaces.

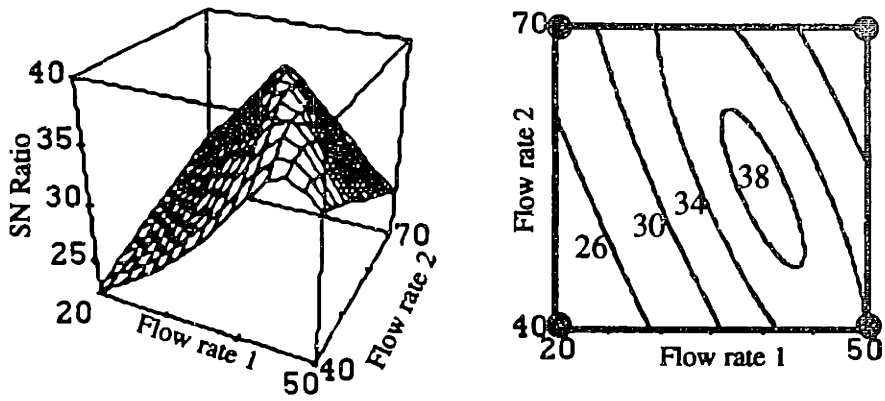

(a) True response estimated without noises superimposed

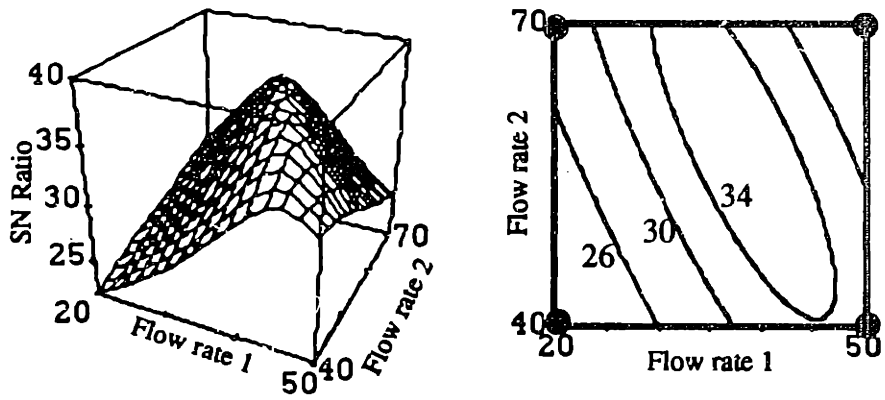

(b) Multiple Response Surfaces

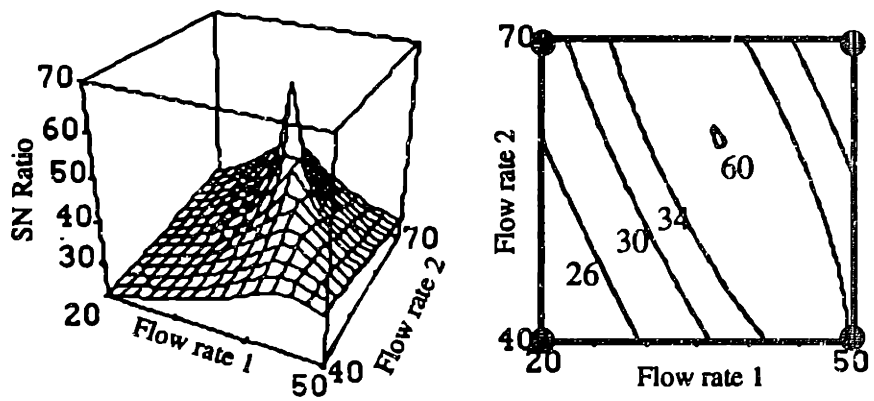

(c) Mixed model

Fig. 7.5 Predicted SN Ratio based on Multiple Response Surfaces and mixed model. Solid circles represent data points used to create models.

7.3 Difference Model

In the silicon epitaxy experiment, we used 15 measurement sites to calculate the uniformity. It was also found that the typical thickness variation can be characterized by two differences. The first is the thickness difference between the the top site of the top wafer and the bottom site of the bottom wafer on the same susceptor face (Fig. 5.1). The second is the average thickness difference between the left site and the right site of three wafers on the same face. Two difference models, (top-bottom) and (left-right), were created using first-order polynomials, and the fit of the models (adjusted R^2 is 99%)[10] is better than the fit of individual site models (adjusted R^2 are from 6% - 96%) (appendix D).

One advantage associated with models for the difference between sites is that if an equipment setting has the same effect on the two sites, it will have no effect on the difference. Thus, it is possible that models for the difference between sites will need fewer equipment settings than individual site models. Similarly, difference models can remove the effect of disturbances which act at both sites. This mechanism is thought to be responsible for the observation that the fit of the difference models reported above is better than the fit of most of the individual site models. Note that a linear model for the difference between two sites can be created by taking the difference between two linear site models. However, this procedure is less preferred to modeling the difference directly as no statistics such as adjusted R^2 or t-ratios will be available to help in interpreting the results.

---

[10] Note that models for the difference between two measured sites are still utilizing the Multiple Response Surfaces approach. This is clearly true in the case discussed above where two difference models are used to characterize the process. A degenerate case is where there are only two sites of interest and one difference model is created. In this case, the Multiple Response Surfaces approach is being practiced with only one model. The key point is that the sign of the difference is being retained, i.e., it is not squared, nor is its absolute value being modeled as would be the case with a Single Response Surface.

CHAPTER EIGHT

CONCLUSIONS AND FUTURE WORK

8.1 Conclusions

Spatial uniformity in manufacturing processes is a key issue in determining the overall quality of product. The modeling, optimization, and control of spatial uniformity has been an effort to develop a general process control system. The system is structured around three core modules. The Flexible Recipe Generator responds a new product design by delivering a best first guess about where to begin operations. The Run by Run Controller updates the recipe between product runs based on post-process and *in situ* measurements. The Run by Run Controller performs on-line optimization and control. The Real Time Controller accepts *in situ* measurements as inputs and modifies the equipment settings during a process step in order to bring the result as close as possible to target.

A new methodology called Multiple Response Surfaces has been developed and used to model, optimize, and control processes. Multiple, low-order polynomials are used to model the output characteristics at each of the measurement sites within a batch of product. The uniformity model is then obtained by combining these multiple models. This contrasts with the traditional approach of fitting a high-order polynomial to the uniformity directly.

Both simulation and experimental data have supported the use of Multiple Response Surfaces. The advantages include effective models from a small number of data, rapid adaptation of models after a process disturbance, immunity of models to the presence of noise, and compatibility of model forms with process knowledge.

The Multiple Response Surfaces approach is easily incorporated into standard techniques for parallel and sequential design of experiments. Further, the ability of the Multiple Response Surface models to adapt quickly to process changes makes the technique well suited to on-line, run by run process control [14].

8.2 Future Work

One of the major applications of Multiple Response Surfaces is to the on-line run by run process control. An important issue is to monitor and to control many output characteristics of the same type at the same time. For example, in an epitaxial process it might include a simultaneous control of the thickness uniformity across 15 measurement sites or a control of two thickness differences which characterize the major variation of one batch. In these cases, account must be made to correlate the outputs so that the detection of any change of the process is correct and efficient. The generalized SPC, as implemented in the Run by Run Controller, must be able to distinguish between the "slow" change and the "rapid" change of the process under such circumstances. The correlation might be explained through a variance-covariance matrix as implemented in multivariate statistics. In this work, we also suggest the use of spatial dimension as a parameter to partly explain the correlation. Another possibility is the use of neural network. In a more general case where the focus is to monitor and to control many output characteristics of different types, the correlation might be more complicated and the control will be even more challenging.

Another important issue related to run by run process control is the rapid adaptation of the models to a process disturbance. In this thesis, the change of constant terms of individual site models after a step disturbance is demonstrated useful. In an experimental work [33], it was found that the effect of a step disturbance was approximated well by the

change of the constant terms; however, there were still changes in the slope coefficients. A generalization of rapid model modification will consider the changes in other coefficients. A possible way is to update the constant terms right after a step disturbance. The newly updated models can be used to generate the recipe for the next run and the data of the following runs can be used for updating other slope coefficients.

The Multiple Response Surfaces is useful in tuning the uniformity of one batch of product. In practice, variation contains the component that must be minimized using robust design. As a result, the process should be made robust against noise first and the other tunable variation is then reduced as small as possible. The important issues are then the classification of process and equipment parameters into different categories for robustness, tuning, and adjustment purposes. Because of the decomposition of variation, the objective functions optimized in each step have different forms and need to be correctly defined [37].

REFERENCES

[1] S. Kalpakjian, *Manufacturing Engineering and Technology*. Addison-Wesley, 1989.

[2] S. Wolf and R.N. Tauber, *Silicon Processing for the VLSI Era, vol. 1: Process Technology*. Sunset Beach, CA, Lattice Press, 1986.

[3] D.C. Montgomery, *Design and Analysis of Experiments*. New York : Wiley, 1984.

[4] G.E. Box and N.R. Draper, *Empirical Model-Building and Response Surfaces*. New York : Wiley, 1987.

[5] R.H. Myers, A.I. Khuri, and W.H. Carter, "Response Surface Methodology : 1966-1988," Technometrics, vol. 31, no. 2, pp. 137-157, May 1989.

[6] G. Taguchi, *Introduction to Quality Engineering*. Asian Productivity Organization, 1986.

[7] M.S. Phadke, *Quality Engineering Using Robust Design*. Prentice Hall, 1989.

[8] R.J. Ross, *Taguchi Techniques for Quality Engineering*. McGraw-Hill, 1988.

[9] K. Dehnad, *Quality Control, Robust Design, and the Taguchi Method*. Wadsworth & Brooks/Cole, 1988.

[10] R. N. Kackar, "Off-line Quality Control, Parameter Design, and the Taguchi Method", Journal of Quality Technology, vol. 17, no. 4, pp. 176-209, Oct. 1985.

[11] H.M. Wadsworth, K.S. Stephens, and A.B. Godfrey, *Modern Methods for Quality Control and Improvement*. New York : Wiley, 1986.

[12] C.R.Shyamsundar, P.K.Mozumder, and A.J. Strojwas, "Statistical Control Of VLSI Fabrication Process : A Software System", IEEE Transactions on Semiconductor Manufacturing, vol. 1, no. 2, pp. 72-82, May 1988.

[13] E.M. Sachs, R. Guo, S. Ha, and A. Hu, "Process Control System for VLSI Fabrication", IEEE Transaction on Semiconductor Manufacturing, vol. 4, no. 2, May 1991.

[14] E.M. Sachs, A. Ingolfsson, and A. Hu, "Run by Run Process Control : Combining SPC and Feedback Control", to be submitted to IEEE Transactions on Semiconductor Manufacturing.

[15] J. M. Lucas and M.S. Saccucci, "Exponentially Weighted Moving Average Control Schemes", Technometrics, vol. 32, no. 1, pp. 1-29, February 1990.

[16] G.E. Box and T. Kramer, "Statistical Process Control and Automatic Process Control - A Discussion", Report no. 41, Center for Quality and Productivity Improvement, University of Wisconsin-Madison, January, 1990.

[17] B.J. Mandel, "The Regression Control Chart", Journal of Quality Technology, vol. 1, no. 1, pp. 1- 9, January, 1969.

[18] E.M. Sachs, G. Prueger, and R. Guerrieri, "An Equipment Model for Polysilicon LPCVD", to be published in IEEE Transactions on Semiconductor Manufacturing, February 1992.

[19] C.W. Moreno, "Continuous Process Improvement through Sequential Experimentation", P-Q System Annual Conference, Dayton, Ohio, 1989.

[20] C.W. Moreno, "Self-learning Optimizing Control Software", Instrument Society of America, Robotics and Expert Systems Conference, Houston, Texas, 1986.

[21] D.C. Montgomery, *Introduction to Statistical Quality Control.* New York : Wiley, 1991.

[22] D.S. Boning, M.B. McIlrath, P. Penfield Jr., and E.M. Sachs, "A General Semiconductor Process Modeling Framework", to be submitted to IEEE Transactions on Semiconductor Manufacturing.

[23] W.P. Wehrle, *Application of Dimensional Analysis to Statistical Process Modeling*. M.S. Thesis, Mechanical Eng., MIT, 1989.

[24] K. Wong, *Sequential Optimization Using Grouped Variables*, M.S. Thesis, Mechanical Eng., MIT, 1990.

[25] R.H. McCafferty, "Dimensionless Parameters of Reactive Ion Etching", in Proceedings of the 39th Electronic Components Conference, Houston, Texas, May 1989.

[26] D.J. Collins, *A Methodology for the Development of Semiconductor Equipment Models*. M.S. Thesis, Electrical and Computer Eng., CMU, 1989.

[27] K. Lin and C.J. Spanos, "Statistical Equipment Modeling for VLSI Manufacturing: An Application for LPCVD Process", IEEE Transactions on Semiconductor Manufacturing, Nov., 1990.

[28] G.E. Box and N.R. Draper, *Evolutionary Operation*. New York : Wiley, 1969.

[29] A. Adelman and W.F. Stevens, "Process Improvement by the Complex Method", AIChE Journal, vol.18, no.1, 1972.

[30] G.S. May, J. Huang, and C.J. Spanos, "Statistical Experimental Design in Plasma Etch Modeling", IEEE Transactions on Semiconductor Manufacturing, vol. 4, no. 2, May 1991.

[31] P.E. Riley and D.A. Hanson, "Study of Etch Rate Characteristics of SF6/He Plasmas by Response Surface Methodology : Effects of Interelectrode Spacing", IEEE Transactions on Semiconductor Manufacturing, vol. 2, no. 4, November 1989.

[32] W.G. Hunter and A.P. Jaworski, "A Useful Method for Model-Building II : Synthesizing Response Functions from Individual Components", Technometrics, vol. 28, no. 4, pp. 321-327, November 1986.

[33] E.M. Sachs, A. Hu, A. Ingolfsson, and P.H. Langer, "Modeling and Control of an Epitaxial Silicon Deposition Process with Step Disturbances", Advanced Semiconductor Manufacturing Conference and Workshop, Boston, MA, October 1991.

[34] P. Lee, J. Cronin, and C. Kaanta, "Chemical Vapor Deposition of Tungsten as Submicron Interconnection and Via Stud", Journal of Electrochemical Society, vol. 136, no. 7, pp. 2108-2112, July 1989.

[35] R.S. Rosler, J. Mendonca, and M.J. Rice Jr., "Tungsten CVD Characteristics Using SiH_4 in a Single Wafer System", Conference on Metals, Dielectrics, and Interfaces for VLSI - 1988.

[36] J.I. Ulacia F. and C. Werner, "Equipment Simulation: Part I", Solid State Technology, November 1990.

[37] S. Ha and E.M. Sachs, "Categories of Process Variables : Robustness Optimization, Uniformity Tuning and Mean Adjustment", in Proceedings for Microelectronic Processing Integration 91', International Society for Optical Engineering, San Jose, CA, September 1991.

[38] R.A. Johnson and D.W. Wichern, *Applied Multivariate Statistical Analysis*. Prentice Hall, 1988.

[39] E.F. Vonesh and R.L. Carter, "Efficient Inference for Random-Coefficient Growth Curve Models with Unbalanced Data", Biometrics, vol. 43, pp. 617-628, September 1987.

[40] F. Nadi, A.M. Agogino, and D.A. Hodges, "Use of Influence Diagrams and Neural Networks in Modeling Semiconductor Manufacturing Processes", IEEE Transaction on Semiconductor Manufacturing, vol. 4, no. 1, February 1991.

[41] G. Chryssolouris and M. Guillot, "A Comparison of Statistical and AI Approaches to the Selection of Process Parameters in Intelligent Machining", Transaction of the ASME, vol. 112, May 1990.

[42] T. Dalton, private communication.

[43] D.E. Rumelhart and J.L. McClelland, *Parallel Distribution Processing*. vol.1, Cambridge : MIT Press, 1986.

APPENDIX A

SADDLE POINT

Given a second-order model (A.1) with k equipment settings ($\mathbf{X}$), we obtain the canonical form (A.2) by rotating the axes and translating the origin,

$$F = b_0 + \mathbf{X}^T\mathbf{b} + \mathbf{X}^T\mathbf{B}\mathbf{X} \tag{A.1}$$

$$F = \tilde{b}_0 + \tilde{\mathbf{X}}^T\Lambda\tilde{\mathbf{X}} \tag{A.2}$$

where Λ contains the eigenvalues of the matrix **B**. (A.2) can be further expressed as :

$$F = \tilde{b}_0 + \lambda_1\tilde{X}_1^2 + \lambda_2\tilde{X}_2^2 + \cdots + \lambda_k\tilde{X}_k^2 \tag{A.3}$$

So, F has a minimum if and only if all λ are positive and has a maximum if and only if all λ are negative. There is a saddle point if some λ are positive and some are negative.

The analysis can be done in closed form for the case of normalized metrics. For illustration, a simple case which has three output characteristics and two equipment settings is examined :

$$\left(\frac{Y_1-\mu}{\mu}\right) = C_1 + C_2X_1 + C_3X_2 \tag{A.4}$$

$$\left(\frac{Y_2-\mu}{\mu}\right) = C_4 + C_5X_1 + C_6X_2 \tag{A.5}$$

$$\left(\frac{Y_3-\mu}{\mu}\right) = C_7 + C_8X_1 + C_9X_2 \tag{A.6}$$

(A.4), (A.5), and (A.6) are then substituted into (A.7)

$$\frac{\sigma}{\mu} = \sqrt{\frac{1}{2}\sum_{i=1}^{3}\left(\frac{Y_i - \mu}{\mu}\right)^2} = \sqrt{b_0 + \mathbf{X}^T\mathbf{b} + \mathbf{X}^T\mathbf{B}\mathbf{X}} \qquad (A.7)$$

and we have

$$\mathbf{B} = \frac{1}{2}\begin{bmatrix} C_2^2+C_5^2+C_8^2 & C_2C_3+C_5C_6+C_8C_9 \\ C_2C_3+C_5C_6+C_8C_9 & C_3^2+C_6^2+C_9^2 \end{bmatrix} \qquad (A.8)$$

The determinant of **B** is then calculated as follows :

$$|\mathbf{B}| = \frac{1}{2}\left[(C_2^2+C_5^2+C_8^2)(C_3^2+C_6^2+C_9^2) - (C_2C_3+C_5C_6+C_8C_9)^2\right]$$

$$= \frac{1}{2}\left[(C_2C_6-C_3C_5)^2+(C_2C_9-C_3C_8)^2+(C_5C_9-C_6C_8)^2\right] > 0 \qquad (A.9)$$

Since the first element of **B** is also larger than zero, **B** is a positive-definite matrix and both eigenvalues are positive. Thus (σ / μ) always has a minimum value and there is no saddle point.

APPENDIX B

CONFIDENCE INTERVAL

B.1 Single Response Surface

Suppose we have a regression model with (r+1) coefficients :

$$u = \frac{\sigma}{\mu} = C_0 + C_1D_1 + C_2D_2 + \cdots + C_rD_r + e \tag{B.1}$$

where D_i are the design elements like X_1, X_2, X_1^2, X_1X_2, etc, and e is an error term. C_i are the coefficients to be estimated. (B.1) can be expressed as a matrix form when there are n sets of data :

$$\mathbf{U}_{n\times 1} = \mathbf{D}_{n\times(r+1)}\mathbf{C}_{(r+1)\times 1} + \mathbf{e}_{n\times 1} \tag{B.2}$$

$$E(\mathbf{e}) = \mathbf{O}_{n\times 1} \text{ and } Cov(\mathbf{e}) = \sigma^2\mathbf{I}_{n\times n} \tag{B.3}$$

Let $\mathbf{D}_0 = [1, D_{01}, D_{02}, \cdots, D_{0r}]^T$, the 100(1-$\alpha$)% confidence interval for $E(u_0 \mid \mathbb{D}_0) = \mathbf{D}_0^T\mathbf{C}$ is given by

$$\mathbf{D}_0^T\hat{\mathbf{C}} \pm t_{n-r-1}\left(\frac{\alpha}{2}\right)\sqrt{(\mathbf{D}_0^T(\mathbf{D}^T\mathbf{D})^{-1}\mathbf{D}_0)s^2} \tag{B.4}$$

where $\hat{\mathbf{C}}$ is the estimated coefficient vector and s^2 is the estimate of σ^2, as given by

$$\hat{\mathbf{C}} = (\mathbf{D}^T\mathbf{D})^{-1}\mathbf{D}^T\mathbf{U} \tag{B.5}$$

$$s^2 = \frac{\mathbf{U}^T(\mathbf{I} - \mathbf{D}(\mathbf{D}^T\mathbf{D})^{-1}\mathbf{D}^T)\mathbf{U}}{n - r - 1} \tag{B.6}$$

B.2 Multiple Response Surfaces

In a process with m output characteristics, the multivariate regression model expressed in matrix form is

$$\mathbf{Y}_{n\times m} = \mathbf{D}_{n\times(r+1)}\mathbf{C}_{(r+1)\times m} + \mathbf{e}_{n\times m} \tag{B.7}$$

$$E(\mathbf{e}_i) = \mathbf{O}_{n\times 1} \quad \text{and} \quad \text{Cov}(\mathbf{e}_i,\mathbf{e}_j) = \Sigma_{m\times m} \qquad i, j = 1, 2, \cdots, m \tag{B.8}$$

The 100(1-α)% confidence hyperellipsoid for $E(\mathbf{Y}_0 \mid \mathbf{D}_0) = \mathbf{C}^T\mathbf{D}_0$ is given by

$$(\mathbf{Y}_0-\hat{\mathbf{C}}^T\mathbf{D}_0)^T\left(\frac{n\hat{\Sigma}}{n-r-1}\right)^{-1}(\mathbf{Y}_0-\hat{\mathbf{C}}^T\mathbf{D}_0) \le \mathbf{D}_0^T(\mathbf{D}^T\mathbf{D})^{-1}\mathbf{D}_0\left[\left(\frac{m(n-r-1)}{n-r-m}\right)F_{m,n-r-m}(\alpha)\right] \tag{B.9}$$

where $\hat{\mathbf{C}}$ is the estimated coefficient matrix and $\hat{\Sigma}$ is the estimate of Σ, as given by

$$\hat{\mathbf{C}} = (\mathbf{D}^T\mathbf{D})^{-1}\mathbf{D}^T\mathbf{Y} \tag{B.10}$$

$$\hat{\Sigma} = \frac{(\mathbf{Y} - \mathbf{D}\hat{\mathbf{C}})^T(\mathbf{Y} - \mathbf{D}\hat{\mathbf{C}})}{n} \tag{B.11}$$

APPENDIX C

POLYSILICON LPCVD SIMULATION

Experimental Design

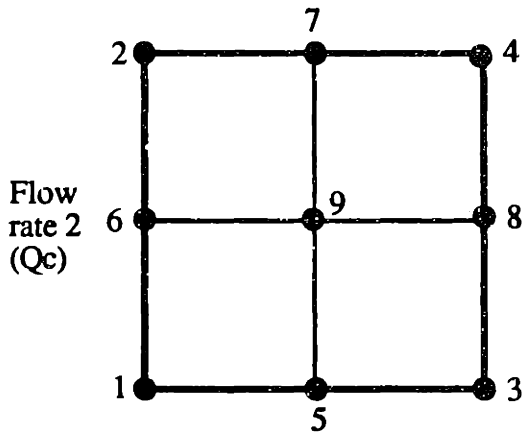

Setting point	Ql	Qc
1	20	40
2	20	70
3	50	40
4	50	70
5	35	40
6	20	55
7	35	70
8	50	55
9	35	55

Simulation Data (No Noise)

	Qi	Qc	Y1	Y2	Y3	Y4	Y5	Y6	Y7	Y8	Y9	Y10	Y11	SN Ratio
1	20	40	43.100	43.075	43.522	44.493	46.039	47.088	47.457	48.459	50.184	52.764	53.207	22.223
2	20	70	45.924	46.063	46.758	48.061	50.044	50.785	49.892	49.590	49.923	50.967	51.169	27.914
3	50	40	52.923	51.501	50.533	50.192	50.497	50.341	49.491	49.224	49.585	50.655	50.878	33.803
4	50	70	55.629	54.401	53.724	53.768	54.575	54.184	52.138	50.624	49.641	49.215	48.830	26.633
5	35	40	48.223	47.483	47.204	47.503	48.416	48.855	48.611	48.981	50.033	51.874	52.028	29.433
6	20	55	44.563	44.622	45.195	46.334	48.100	48.998	48.742	49.103	50.147	51.978	52.124	24.978
7	35	70	50.963	50.401	50.390	51.045	52.425	52.587	51.110	50.198	49.874	50.190	50.009	34.805
8	50	55	54.305	52.981	52.159	52.010	52.565	52.291	50.843	49.956	49.652	49.985	49.817	30.458
9	35	55	49.555	48.900	48.749	49.218	50.351	50.636	49.758	49.468	49.810	50.863	51.074	36.065

Uniformity Model

Dependent variable is: SN Ratio
R² = 89.0% R²(adjusted) = 70.8%
s = 2.526 with 9 - 6 = 3 degrees of freedom

Source	Sum of Squares	df	Mean Square	F-ratio
Regression	155.598	5	31.1	4.88
Residual	19.1473	3	6.38242	

Variable	Coefficient	s.e. of Coeff	t-ratio
Constant	-51.4266	27.05	-1.90
Ql	2.75519	0.6395	4.31
Qc	1.21082	0.8978	1.35
Ql^2	-0.025627	0.0079	-3.23
Qc^2	-0.006067	0.0079	-0.764
Ql*Qc	-0.014290	0.0056	-2.55

Deposition Rate Models

Dependent variable is: Y1
R² = 100.0% R²(adjusted) = 100.0%
s = 0.0590 with 4 - 3 = 1 degrees of freedom

Source	Sum of Squares	df	Mean Square	F-ratio
Regression	102.981	2	51.5	14792
Residual	0.003481	1	0.003481	

Variable	Coefficient	s.e. of Coeff	t-ratio
Constant	32.9335	0.1316	250
Q_l	0.325467	0.0020	165
Q_c	0.092167	0.0020	46.9

Dependent variable is: Y2
R² = 100.0% R²(adjusted) = 100.0%
s = 0.0440 with 4 - 3 = 1 degrees of freedom

Source	Sum of Squares	df	Mean Square	F-ratio
Regression	78.9251	2	39.46	20384
Residual	0.001936	1	0.001936	

Variable	Coefficient	s.e. of Coeff	t-ratio
Constant	33.5837	0.0981	342
Q_l	0.279400	0.0015	190
Q_c	0.098133	0.0015	66.9

Dependent variable is: Y3
R² = 100.0% R²(adjusted) = 100.0%
s = 0.0225 with 4 - 3 = 1 degrees of freedom

Source	Sum of Squares	df	Mean Square	F-ratio
Regression	59.1657	2	29.58	58435
Residual	0.000506	1	0.000506	

Variable	Coefficient	s.e. of Coeff	t-ratio
Constant	34.5896	0.0502	689
Q_l	0.232950	0.0007	311
Q_c	0.107117	0.0007	143

Deposition Rate Models

Dependent variable is: Y4
R² = 100.0% R²(adjusted) = 100.0%
s = 0.0040 with 4 - 3 = 1 degrees of freedom

Source	Sum of Squares	df	Mean Square	F-ratio
Regression	45.2834	2	22.64	1415106
Residual	0.000016	1	0.000016	

Variable	Coefficient	s.e. of Coeff	t-ratio
Constant	35.9263	0.0089	4028
Q_l	0.190100	0.0001	1426
Q_c	0.119067	0.0001	893

Dependent variable is: Y5
R² = 100.0% R²(adjusted) = 100.0%
s = 0.0365 with 4 - 3 = 1 degrees of freedom

Source	Sum of Squares	df	Mean Square	F-ratio
Regression	36.5343	2	18.27	13711
Residual	0.001332	1	0.001332	

Variable	Coefficient	s.e. of Coeff	t-ratio
Constant	37.6358	0.0814	462
Q_l	0.149817	0.0012	123
Q_c	0.134717	0.0012	111

Dependent variable is: Y6
R² = 100.0% R²(adjusted) = 99.9%
s = 0.0730 with 4 - 3 = 1 degrees of freedom

Source	Sum of Squares	df	Mean Square	F-ratio
Regression	25.2752	2	12.64	2371
Residual	0.005329	1	0.005329	

Variable	Coefficient	s.e. of Coeff	t-ratio
Constant	39.8075	0.1628	245
Q_l	0.110867	0.0024	45.6
Q_c	0.125667	0.0024	51.6

Deposition Rate Models

Dependent variable is: **Y7**
R² = 99.9% R²(adjusted) = 99.7%
s = 0.1060 with 4 - 3 = 1 degrees of freedom

Source	Sum of Squares	df	Mean Square	F-ratio
Regression	11.0363	2	5.518	491
Residual	0.011236	1	0.011236	

Variable	Coefficient	s.e. of Coeff	t-ratio
Constant	42.5893	0.2364	180
Ql	0.071333	0.0035	20.2
Qc	0.084700	0.0035	24.0

Dependent variable is: **Y8**
R² = 99.3% R²(adjusted) = 97.8%
s = 0.1345 with 4 - 3 = 1 degrees of freedom

Source	Sum of Squares	df	Mean Square	F-ratio
Regression	2.41059	2	1.2053	66.6
Residual	0.018090	1	0.018090	

Variable	Coefficient	s.e. of Coeff	t-ratio
Constant	46.1047	0.2999	154
Ql	0.029983	0.0045	6.69
Qc	0.042183	0.0045	9.41

Dependent variable is: **Y9**
R² = 89.1% R²(adjusted) = 67.2%
s = 0.1585 with 4 - 3 = 1 degrees of freedom

Source	Sum of Squares	df	Mean Square	F-ratio
Regression	0.204547	2	0.102273	4.07
Residual	0.025122	1	0.025122	

Variable	Coefficient	s.e. of Coeff	t-ratio
Constant	50.5351	0.3534	143
Ql	-0.014683	0.0053	-2.78
Qc	-0.003417	0.0053	-0.647

Deposition Rate Models

Dependent variable is: **Y10**
R² = 99.5% R²(adjusted) = 98.5%
s = 0.1785 with 4 - 3 = 1 degrees of freedom

Source	Sum of Squares	df	Mean Square	F-ratio
Regression	6.34637	2	3.1732	99.6
Residual	0.031862	1	0.031862	

Variable	Coefficient	s.e. of Coeff	t-ratio
Constant	56.1198	0.3980	141
Q_I	-0.064350	0.0059	-10.8
Q_C	-0.053950	0.0059	-9.07

Dependent variable is: **Y11**
R² = 100.0% R²(adjusted) = 100.0%
s = 0.0050 with 4 - 3 = 1 degrees of freedom

Source	Sum of Squares	df	Mean Square	F-ratio
Regression	9.62141	2	4.8107	192428
Residual	0.000025	1	0.000025	

Variable	Coefficient	s.e. of Coeff	t-ratio
Constant	57.4895	0.0111	5156
Q_I	-0.077800	0.0002	-467
Q_C	-0.068100	0.0002	-409

Simulation Data (Adding Noise)

#1	Qi	Qc	Y1	Y2	Y3	Y4	Y5	Y6	Y7	Y8	Y9	Y10	Y11	SN Ratio
1	20	40	42.376	42.477	43.405	43.631	46.335	46.633	47.398	48.206	49.927	52.123	52.882	22.033
2	20	70	45.445	45.265	46.563	47.391	50.278	51.137	49.292	49.001	49.368	50.199	50.869	27.217
3	50	40	52.879	52.253	50.663	49.499	51.200	50.497	50.032	49.154	49.590	50.882	51.301	32.848
4	50	70	55.430	54.391	53.629	53.522	54.803	53.782	52.020	51.267	49.286	48.771	48.460	26.356
5	35	40	48.506	47.072	47.100	47.134	48.165	48.939	48.666	48.985	50.050	52.128	51.713	29.011
6	20	55	44.113	44.745	45.143	46.550	48.059	49.055	48.948	49.172	50.255	52.230	52.050	24.726
7	35	70	51.009	50.504	51.019	50.953	52.377	52.984	50.779	49.837	50.281	50.352	50.530	34.787
8	50	55	54.086	52.798	52.457	52.395	52.354	52.460	51.144	49.384	49.492	50.212	49.709	30.214
9	35	55	48.860	48.621	48.458	48.839	50.181	50.332	49.835	49.384	50.064	50.634	51.004	35.121

#2	Qi	Qc	Y1	Y2	Y3	Y4	Y5	Y6	Y7	Y8	Y9	Y10	Y11	SN Ratio
1	20	40	43.169	43.127	43.944	44.670	46.275	47.269	47.920	48.607	50.416	52.750	53.553	22.245
2	20	70	45.827	45.885	46.649	47.877	50.110	50.743	49.660	49.902	50.198	50.641	51.103	27.711
3	50	40	52.509	51.786	50.133	51.014	50.642	49.959	49.410	49.483	49.994	50.674	50.545	34.596
4	50	70	55.856	54.618	53.888	54.551	55.007	54.666	51.890	50.548	49.113	49.443	48.935	25.938
5	35	40	48.145	47.187	46.372	47.203	48.096	47.876	48.461	48.853	49.712	51.495	51.754	29.041
6	20	55	44.500	44.875	45.767	46.918	48.195	49.147	48.751	48.796	50.459	52.044	52.397	25.169
7	35	70	51.602	50.266	50.608	51.016	52.937	52.000	50.981	50.296	49.702	50.390	49.688	34.275
8	50	55	54.498	52.914	52.589	52.492	52.991	52.559	51.034	49.439	50.025	49.565	49.966	29.634
9	35	55	48.721	49.284	48.691	48.982	49.927	50.055	49.548	49.708	49.963	50.748	50.774	36.781

#3	Qi	Qc	Y1	Y2	Y3	Y4	Y5	Y6	Y7	Y8	Y9	Y10	Y11	SN Ratio
1	20	40	43.281	43.215	43.020	44.528	45.772	46.595	47.248	49.098	50.278	52.934	52.968	22.092
2	20	70	45.988	45.687	46.902	48.475	50.153	51.326	49.370	49.219	50.195	50.628	50.485	28.008
3	50	40	53.306	51.675	49.687	50.752	51.313	50.155	49.263	48.657	49.964	51.145	51.501	31.777
4	50	70	54.972	54.579	53.371	53.192	54.213	54.366	51.696	50.485	48.886	48.976	48.016	26.579
5	35	40	48.468	47.266	46.860	48.037	48.812	48.833	48.500	48.440	50.203	52.183	52.407	28.700
6	20	55	44.687	44.194	45.551	46.327	48.119	47.926	49.260	49.088	50.195	52.243	52.032	24.850
7	35	70	51.134	49.859	50.427	50.943	53.007	52.511	50.577	50.196	49.551	50.235	49.351	32.878
8	50	55	54.552	53.253	52.978	51.705	53.185	52.525	50.530	50.548	49.748	50.475	50.067	30.190
9	35	55	49.807	49.131	48.308	49.689	50.307	50.732	50.326	49.470	50.306	51.122	51.234	35.163

#4	Qi	Qc	Y1	Y2	Y3	Y4	Y5	Y6	Y7	Y8	Y9	Y10	Y11	SN Ratio
1	20	40	42.929	43.370	43.216	44.712	45.744	47.249	47.401	48.476	50.034	53.226	53.688	21.875
2	20	70	45.717	46.301	46.726	47.677	49.953	50.978	49.208	49.334	49.952	50.659	51.054	28.023
3	50	40	53.189	52.327	50.762	50.262	51.322	50.935	48.861	48.972	50.032	51.151	51.072	31.942
4	50	70	56.300	54.500	54.228	53.386	54.574	54.307	52.271	50.665	49.266	49.392	49.143	26.311
5	35	40	47.846	46.871	46.984	47.469	47.936	47.934	48.302	48.900	50.329	52.110	52.061	28.280
6	20	55	44.463	44.836	44.950	45.171	46.333	49.566	48.295	49.215	49.721	51.642	52.250	24.621
7	35	70	51.247	50.591	50.801	51.497	52.311	52.468	51.257	49.911	50.020	49.871	49.885	34.590
8	50	55	53.799	53.252	51.345	50.984	53.045	51.747	50.599	49.450	49.574	49.636	49.187	29.619
9	35	55	49.371	48.883	49.194	49.253	51.105	49.838	49.780	50.248	50.459	50.935	51.155	35.772

Simulation Data (Adding Noise)

#5	Qi	Qc	Y1	Y2	Y3	Y4	Y5	Y6	Y7	Y8	Y9	Y10	Y11	SN Ratio
1	20	40	43.178	43.140	43.359	43.356	45.455	46.966	47.420	48.220	48.680	53.212	52.746	22.137
2	20	70	45.860	46.537	46.466	47.965	50.563	51.245	50.111	49.656	50.297	51.210	51.735	27.221
3	50	40	52.851	51.086	51.113	49.485	50.770	50.695	49.074	48.941	49.182	50.887	50.435	33.278
4	50	70	55.178	54.075	53.708	53.812	54.553	54.044	52.334	50.264	49.307	49.373	49.103	26.965
5	35	40	47.930	46.850	46.458	47.139	48.415	48.399	48.256	49.110	49.636	51.262	52.776	28.192
6	20	55	44.902	44.554	45.192	45.955	47.724	48.519	48.535	48.713	50.311	51.951	51.947	25.105
7	35	70	51.469	50.250	50.695	51.140	52.526	52.971	51.468	50.754	50.410	50.519	50.214	34.930
8	50	55	53.659	53.001	52.502	51.897	52.801	51.756	50.731	49.552	49.883	49.922	49.139	30.294
9	35	55	49.988	48.764	48.726	49.578	49.915	50.400	49.733	49.485	50.055	50.856	51.522	35.639

#6	Qi	Qc	Y1	Y2	Y3	Y4	Y5	Y6	Y7	Y8	Y9	Y10	Y11	SN Ratio
1	20	40	43.449	43.738	43.557	44.334	46.894	46.713	47.577	48.170	49.720	52.633	53.479	22.558
2	20	70	46.092	45.706	46.694	48.062	50.657	51.707	49.552	50.172	50.341	51.094	51.547	26.917
3	50	40	52.786	51.194	50.297	49.740	50.372	50.717	49.584	49.284	49.156	49.835	50.445	33.795
4	50	70	55.770	54.600	54.155	54.129	55.792	54.495	53.734	50.547	48.963	49.566	48.600	25.624
5	35	40	48.530	47.266	46.732	46.686	48.357	48.800	49.390	48.369	49.736	52.333	51.380	28.750
6	20	55	44.517	45.134	44.901	45.854	48.369	49.183	48.894	50.142	49.939	51.629	51.897	25.030
7	35	70	50.934	50.488	50.445	51.357	52.584	51.843	51.177	50.620	49.999	50.345	50.004	36.078
8	50	55	54.478	53.313	52.256	51.973	52.627	52.372	50.678	50.044	49.496	50.306	50.207	30.320
9	35	55	49.646	49.409	48.928	49.297	50.054	51.063	49.601	49.701	49.615	50.395	50.825	37.634

#7	Qi	Qc	Y1	Y2	Y3	Y4	Y5	Y6	Y7	Y8	Y9	Y10	Y11	SN Ratio
1	20	40	42.637	43.406	43.393	44.476	47.253	46.829	47.468	47.886	50.156	51.981	53.881	22.209
2	20	70	45.556	45.914	46.797	48.333	50.731	50.818	50.138	49.472	50.164	51.604	52.000	26.765
3	50	40	53.395	52.047	50.525	50.295	50.238	50.360	49.479	49.347	49.880	51.264	51.429	32.521
4	50	70	56.221	54.023	53.555	53.035	54.109	54.184	51.689	50.348	49.486	49.143	48.715	26.424
5	35	40	48.669	47.810	47.340	48.278	47.737	49.003	49.656	48.494	50.112	52.520	52.549	28.751
6	20	55	44.728	44.606	45.461	46.679	48.542	48.726	48.440	49.258	50.162	51.657	52.193	25.333
7	35	70	50.890	50.165	50.518	50.842	52.863	52.973	51.606	50.024	50.232	50.840	49.878	33.533
8	50	55	54.047	53.445	52.890	51.879	52.878	52.998	50.769	50.656	49.923	49.757	49.666	30.108
9	35	55	48.528	48.222	48.858	49.098	50.205	50.356	49.268	49.024	48.991	50.607	51.069	34.543

#8	Qi	Qc	Y1	Y2	Y3	Y4	Y5	Y6	Y7	Y8	Y9	Y10	Y11	SN Ratio
1	20	40	42.566	42.872	42.464	43.820	45.441	46.423	47.654	48.264	49.575	52.345	52.934	21.876
2	20	70	45.087	45.221	46.426	47.395	49.239	49.876	48.887	49.090	49.444	49.912	49.974	28.211
3	50	40	53.000	51.559	50.565	50.488	50.847	50.731	50.131	50.459	49.936	51.123	50.294	35.528
4	50	70	56.249	54.291	54.170	53.743	54.961	54.238	52.009	50.347	49.936	49.637	48.975	26.450
5	35	40	48.044	46.686	47.161	47.743	48.366	49.420	49.182	49.362	49.892	52.408	51.931	28.650
6	20	55	44.568	44.913	45.420	46.308	47.703	48.743	48.144	49.125	49.707	51.839	51.770	25.526
7	35	70	51.108	51.117	49.773	50.841	52.337	53.239	51.148	50.086	50.446	50.228	49.952	33.660
8	50	55	54.359	53.876	53.085	52.126	53.014	52.312	51.433	50.191	50.368	50.238	49.681	30.152
9	35	55	49.057	49.437	48.798	49.451	49.885	51.079	49.692	50.293	50.574	50.687	51.032	36.072

Simulation Data (Adding Noise)

#9	Qi	Qc	Y1	Y2	Y3	Y4	Y5	Y6	Y7	Y8	Y9	Y10	Y11	SN Ratio
1	20	40	43.381	43.009	43.569	44.419	46.383	47.314	47.625	48.247	51.059	53.021	53.398	22.000
2	20	70	46.245	46.201	46.700	48.593	50.325	51.324	50.012	49.146	49.432	51.113	51.212	27.973
3	50	40	53.134	52.241	50.537	50.697	50.394	50.668	48.973	48.937	49.648	50.868	51.281	32.061
4	50	70	56.202	53.547	53.787	54.031	54.439	53.790	51.657	50.842	49.848	49.504	48.082	26.388
5	35	40	48.412	47.347	46.914	48.015	48.432	48.247	46.968	49.046	49.641	51.653	52.124	29.569
6	20	55	44.312	44.594	45.071	46.139	48.706	49.178	49.889	48.463	50.661	51.942	51.963	24.617
7	35	70	50.345	49.466	50.232	50.257	52.296	52.008	51.040	50.052	49.818	49.879	49.827	34.760
8	50	55	54.073	52.584	51.905	51.821	52.561	51.686	50.830	49.673	48.856	49.448	49.889	30.055
9	35	55	49.808	49.385	49.167	49.445	50.800	51.315	50.283	49.283	50.598	51.158	51.883	34.614

#10	Qi	Qc	Y1	Y2	Y3	Y4	Y5	Y6	Y7	Y8	Y9	Y10	Y11	SN Ratio
1	20	40	43.632	43.152	43.710	44.559	46.631	47.319	47.778	48.835	49.944	52.208	53.166	22.732
2	20	70	45.865	45.807	47.039	48.216	49.011	51.029	49.885	49.315	50.082	50.664	51.280	27.929
3	50	40	53.088	51.672	50.704	49.704	50.162	50.157	49.711	49.721	48.993	50.551	50.957	33.031
4	50	70	55.879	54.820	53.993	53.113	54.755	54.395	52.083	50.097	49.008	49.011	48.586	25.718
5	35	40	47.907	47.875	47.504	47.930	48.348	49.354	48.392	48.938	49.536	51.711	52.621	29.444
6	20	55	44.776	44.794	45.095	45.510	47.302	49.769	49.572	49.597	49.731	51.930	52.012	24.730
7	35	70	49.872	49.642	49.860	50.742	51.555	52.208	49.953	49.892	50.423	49.017	49.533	34.616
8	50	55	53.974	52.693	52.280	52.312	53.137	52.199	50.727	50.326	49.833	50.085	49.822	30.929
9	35	55	49.606	49.101	49.241	48.872	50.645	49.900	49.699	49.061	49.945	51.287	51.180	35.463

#11	Qi	Qc	Y1	Y2	Y3	Y4	Y5	Y6	Y7	Y8	Y9	Y10	Y11	SN Ratio
1	20	40	43.746	43.621	43.915	44.924	46.223	47.453	48.188	48.466	49.572	53.149	53.018	22.800
2	20	70	46.277	45.492	46.736	47.686	50.078	50.263	50.201	49.436	49.746	50.709	50.900	27.999
3	50	40	53.307	51.736	51.177	50.140	50.109	49.591	49.968	49.971	49.983	51.211	51.101	33.331
4	50	70	55.882	54.314	53.750	54.057	54.409	54.694	51.651	50.474	49.230	48.894	48.520	25.848
5	35	40	48.745	47.357	47.378	48.116	47.839	48.684	48.685	48.573	49.411	51.522	51.524	30.629
6	20	55	44.466	44.417	45.132	46.260	48.102	49.014	49.248	48.367	51.159	52.854	52.400	24.083
7	35	70	51.134	50.714	50.423	50.694	52.692	52.459	50.917	51.345	50.028	49.801	49.888	34.506
8	50	55	54.482	53.180	51.590	52.247	53.564	52.353	51.303	50.485	49.738	49.895	49.342	29.725
9	35	55	50.159	48.870	49.353	49.253	50.252	51.009	50.273	49.528	49.376	51.089	50.957	36.094

#12	Qi	Qc	Y1	Y2	Y3	Y4	Y5	Y6	Y7	Y8	Y9	Y10	Y11	SN Ratio
1	20	40	42.874	42.860	43.940	43.755	45.546	46.969	48.063	48.211	49.725	52.935	53.031	22.067
2	20	70	46.186	46.173	46.785	47.688	50.467	50.350	49.536	48.955	50.494	50.936	50.449	28.373
3	50	40	53.339	51.844	50.386	50.379	50.011	49.453	49.144	49.299	49.356	51.340	50.553	31.881
4	50	70	55.695	53.856	52.798	54.130	54.789	54.462	51.992	50.829	49.521	49.415	48.683	26.621
5	35	40	48.017	47.353	46.843	47.856	48.700	48.644	48.259	49.253	50.222	51.889	51.762	29.339
6	20	55	44.572	44.578	45.070	46.360	47.438	48.847	49.282	48.841	49.908	53.200	52.502	24.200
7	35	70	50.546	50.641	50.407	50.932	52.055	52.952	51.174	50.266	50.449	49.855	50.972	35.249
8	50	55	53.784	52.818	52.360	51.399	52.409	51.833	50.788	49.070	49.197	49.874	50.027	30.320
9	35	55	48.845	48.723	48.369	49.167	50.570	50.225	49.587	49.361	49.479	51.747	51.489	33.046

Simulation Data (Adding Noise)

#13	Qi	Qc	Y1	Y2	Y3	Y4	Y5	Y6	Y7	Y8	Y9	Y10	Y11	SN Ratio
1	20	40	43.143	43.245	43.189	44.810	45.455	47.290	47.445	48.244	49.624	52.430	53.353	22.353
2	20	70	46.484	46.691	46.575	47.973	50.163	51.104	50.487	49.177	50.220	51.387	50.882	28.165
3	50	40	53.462	51.825	50.154	50.486	50.572	50.984	49.342	49.467	49.104	50.713	50.505	32.272
4	50	70	56.013	54.845	53.627	54.212	54.567	53.937	52.360	51.190	49.449	49.570	48.737	26.489
5	35	40	47.930	46.950	46.751	48.079	48.571	48.397	48.295	48.945	50.157	51.159	51.727	29.729
6	20	55	45.245	44.705	46.240	46.413	48.863	49.428	48.870	48.707	50.798	52.382	52.095	25.337
7	35	70	50.612	49.701	49.920	50.280	51.607	52.597	51.534	49.880	49.578	50.237	49.259	33.823
8	50	55	53.930	53.183	52.216	51.638	52.431	53.328	50.866	49.358	50.624	50.029	49.179	29.962
9	35	55	49.685	48.571	48.706	48.768	50.272	50.639	49.978	50.164	49.615	50.937	51.245	34.802

#14	Qi	Qc	Y1	Y2	Y3	Y4	Y5	Y6	Y7	Y8	Y9	Y10	Y11	SN Ratio
1	20	40	43.123	42.810	43.607	44.461	45.708	47.261	47.643	48.741	50.452	53.364	53.374	21.741
2	20	70	45.923	45.809	46.969	47.788	49.493	51.021	50.080	49.625	49.436	50.925	51.735	27.517
3	50	40	53.304	50.708	51.093	50.706	50.971	50.356	49.498	48.713	49.427	50.696	50.586	32.642
4	50	70	55.781	55.207	54.783	53.784	54.794	55.263	52.480	50.532	49.654	50.111	49.101	26.292
5	35	40	48.352	47.324	47.298	47.258	48.191	48.819	47.909	49.061	49.355	52.185	52.448	28.587
6	20	55	44.213	44.949	44.632	46.234	47.968	48.810	48.663	49.782	50.209	52.314	51.972	24.549
7	35	70	51.632	50.254	50.116	51.502	51.666	52.409	51.252	49.508	49.430	49.577	50.835	33.894
8	50	55	54.242	53.248	52.575	51.807	52.146	52.086	51.100	50.515	49.622	50.118	50.159	31.065
9	35	55	49.609	49.087	48.653	49.097	50.599	50.573	48.909	49.452	49.483	50.591	50.570	36.370

#15	Qi	Qc	Y1	Y2	Y3	Y4	Y5	Y6	Y7	Y8	Y9	Y10	Y11	SN Ratio
1	20	40	42.721	42.901	43.932	44.159	45.710	46.690	47.235	48.286	50.308	51.959	52.813	22.455
2	20	70	45.276	46.498	46.480	48.433	50.014	51.000	50.163	49.278	50.076	51.471	51.056	27.313
3	50	40	52.938	51.438	50.900	49.857	50.205	49.872	49.264	48.807	49.602	50.173	50.944	32.843
4	50	70	55.742	54.692	54.145	53.912	55.028	54.322	52.587	51.155	50.061	49.741	48.551	26.647
5	35	40	48.471	46.782	47.603	47.364	48.134	49.423	47.973	47.966	50.463	51.326	51.084	29.136
6	20	55	44.876	44.745	45.527	46.540	48.537	48.809	49.431	49.643	50.531	52.488	51.961	25.006
7	35	70	51.187	50.141	50.528	51.666	51.818	52.574	50.745	50.533	50.072	50.051	50.392	35.776
8	50	55	54.008	52.953	51.430	51.846	53.079	51.683	51.122	49.435	50.067	50.355	49.725	30.816
9	35	55	49.279	48.570	48.560	49.061	50.078	49.955	50.412	48.939	49.616	50.274	51.257	35.361

#16	Qi	Qc	Y1	Y2	Y3	Y4	Y5	Y6	Y7	Y8	Y9	Y10	Y11	SN Ratio
1	20	40	43.141	42.805	43.522	44.781	46.615	46.365	47.347	48.558	50.291	52.894	53.023	22.212
2	20	70	45.917	46.152	46.615	47.753	49.694	51.317	49.768	49.568	49.699	50.889	51.704	27.472
3	50	40	53.554	51.609	50.874	50.493	50.570	50.378	49.916	49.638	50.220	50.799	50.794	33.689
4	50	70	54.970	54.574	54.298	53.323	55.227	55.012	52.246	50.935	49.456	48.616	48.585	25.933
5	35	40	49.089	47.395	48.472	48.473	48.746	48.782	48.659	49.326	50.215	51.627	52.449	30.425
6	20	55	44.686	44.026	45.069	47.046	49.050	49.838	48.938	48.997	50.810	52.482	52.893	24.108
7	35	70	50.732	49.898	49.836	50.733	52.449	52.530	51.000	49.665	49.570	50.333	49.980	33.749
8	50	55	54.715	52.662	51.968	52.194	51.934	52.921	51.235	50.090	49.259	50.668	50.251	30.501
9	35	55	48.915	48.575	48.224	48.753	49.805	50.170	49.446	49.449	48.928	50.987	51.085	34.357

Simulation Data (Adding Noise)

#17	QI	Qc	Y1	Y2	Y3	Y4	Y5	Y6	Y7	Y8	Y9	Y10	Y11	SN Ratio
1	20	40	43.263	42.469	43.065	44.223	45.833	46.970	47.106	48.665	50.145	52.374	52.556	22.248
2	20	70	46.924	45.617	47.532	47.968	49.816	51.565	50.395	49.798	49.681	51.059	51.424	27.973
3	50	40	52.419	52.049	50.298	50.032	50.613	50.373	49.142	48.922	49.416	50.556	50.466	33.347
4	50	70	54.881	54.085	53.741	53.831	54.094	54.169	51.601	49.939	49.662	49.354	48.645	26.878
5	35	40	48.778	48.073	47.708	47.186	48.333	49.053	48.517	48.243	49.238	51.939	51.694	30.170
6	20	55	44.351	44.382	45.396	45.505	48.053	48.610	48.911	48.973	50.007	51.507	51.506	25.153
7	35	70	50.292	49.967	49.987	50.727	52.339	52.993	51.178	49.479	49.031	50.016	50.106	32.535
8	50	55	54.577	52.731	51.659	52.323	52.183	51.860	49.643	49.730	49.417	49.674	49.348	29.393
9	35	55	48.961	48.591	48.500	49.076	50.621	50.003	49.458	49.689	50.335	50.840	51.035	34.863

#18	QI	Qc	Y1	Y2	Y3	Y4	Y5	Y6	Y7	Y8	Y9	Y10	Y11	SN Ratio
1	20	40	42.706	43.282	43.375	44.681	46.062	47.535	47.896	48.625	50.260	52.656	52.911	22.281
2	20	70	45.972	45.879	46.804	47.877	50.110	50.099	49.769	49.257	49.050	50.120	50.801	28.751
3	50	40	53.177	51.887	50.823	49.638	50.122	50.396	49.508	49.553	50.303	50.812	51.170	33.221
4	50	70	55.550	54.333	54.116	53.850	54.121	54.487	52.041	50.820	49.432	49.154	48.754	26.517
5	35	40	48.625	47.639	47.291	47.807	47.961	48.477	49.194	49.427	49.922	51.814	51.938	29.808
6	20	55	44.440	45.319	45.343	46.099	48.539	48.642	49.264	49.165	50.195	51.711	52.305	25.194
7	35	70	50.307	50.003	50.917	51.117	52.578	52.446	51.258	50.274	49.417	49.600	49.362	33.105
8	50	55	53.534	52.852	52.515	51.591	52.773	52.794	50.253	50.033	49.238	50.176	49.850	30.506
9	35	55	49.961	48.039	48.576	49.556	49.407	50.610	49.241	49.424	49.732	50.607	50.727	35.384

#19	QI	Qc	Y1	Y2	Y3	Y4	Y5	Y6	Y7	Y8	Y9	Y10	Y11	SN Ratio
1	20	40	43.009	43.285	43.344	44.189	45.736	46.807	47.331	48.429	49.690	52.139	52.844	22.554
2	20	70	46.487	46.317	46.957	48.041	50.133	50.899	50.149	49.814	50.224	51.492	51.241	28.105
3	50	40	52.134	51.753	50.488	50.063	50.989	50.657	49.666	49.226	48.897	50.389	50.557	34.252
4	50	70	54.875	53.963	53.462	53.160	55.022	54.034	52.423	50.334	49.282	48.558	48.087	26.127
5	35	40	47.692	47.366	46.645	47.623	47.714	48.524	47.554	49.067	49.935	51.055	51.140	30.022
6	20	55	44.435	44.348	44.858	46.820	48.685	49.389	49.013	49.338	50.445	51.726	51.589	24.939
7	35	70	51.049	50.447	50.374	50.972	52.396	52.473	50.460	49.798	50.044	49.490	50.294	34.410
8	50	55	54.039	52.405	51.437	51.666	52.638	52.398	50.027	49.921	49.684	50.197	49.394	30.610
9	35	55	50.039	48.794	48.246	49.173	50.213	50.077	50.574	49.916	50.120	50.904	51.219	35.006

#20	QI	Qc	Y1	Y2	Y3	Y4	Y5	Y6	Y7	Y8	Y9	Y10	Y11	SN Ratio
1	20	40	42.938	42.959	43.504	44.574	45.417	46.687	47.529	47.859	50.298	51.976	53.670	22.156
2	20	70	45.085	45.911	46.531	48.175	50.267	50.977	50.214	49.123	49.221	51.202	51.015	27.020
3	50	40	52.687	51.384	50.907	50.033	50.594	50.898	49.366	49.212	49.480	51.024	50.898	33.893
4	50	70	55.524	54.585	53.844	53.418	53.687	53.786	52.167	50.549	50.108	48.993	48.819	27.023
5	35	40	48.454	47.413	47.519	48.364	48.864	48.993	48.998	49.590	49.876	52.936	52.660	28.635
6	20	55	43.873	44.772	45.413	46.703	48.116	49.240	48.186	49.253	50.227	51.812	52.332	24.797
7	35	70	50.744	50.859	50.389	50.988	52.104	53.375	51.097	50.315	49.754	50.814	50.846	34.426
8	50	55	54.098	52.517	51.363	51.916	52.646	51.502	50.265	49.987	49.257	50.540	49.968	31.005
9	35	55	49.539	49.241	48.990	48.925	50.219	49.806	49.439	49.253	49.712	50.279	51.247	37.283

Simulation Data (Adding Noise)

#21	Qi	Qc	Y1	Y2	Y3	Y4	Y5	Y6	Y7	Y8	Y9	Y10	Y11	SN Ratio
1	20	40	42.679	42.641	43.613	44.801	45.709	46.615	47.880	48.082	49.559	53.982	53.631	21.554
2	20	70	46.024	45.182	46.563	47.149	49.840	50.268	49.619	49.413	49.867	50.545	50.746	27.662
3	50	40	52.471	50.959	49.606	49.844	50.078	50.131	49.126	48.482	49.123	50.282	51.170	33.076
4	50	70	55.518	54.266	53.192	53.496	54.180	54.376	51.936	50.862	49.648	50.459	49.370	27.208
5	35	40	48.198	47.553	47.190	47.992	48.513	48.498	48.745	48.391	50.742	52.083	52.365	28.618
6	20	55	44.377	44.810	45.097	46.621	47.821	49.984	47.760	48.587	50.114	53.013	52.583	24.230
7	35	70	50.695	50.035	49.654	51.241	51.743	52.193	51.746	50.086	49.280	50.068	49.622	34.065
8	50	55	54.429	53.095	51.469	51.600	51.585	52.593	50.868	50.032	49.065	50.285	49.899	30.300
9	35	55	50.295	48.918	48.453	49.547	50.043	50.541	49.399	49.275	49.927	50.695	50.565	36.662

#22	Qi	Qc	Y1	Y2	Y3	Y4	Y5	Y6	Y7	Y8	Y9	Y10	Y11	SN Ratio
1	20	40	43.563	43.352	43.361	44.413	46.583	46.713	46.557	48.544	50.041	52.014	53.314	22.604
2	20	70	45.953	46.239	46.670	47.951	50.278	51.507	50.268	49.365	49.426	51.107	51.130	27.567
3	50	40	53.379	51.750	50.862	49.687	50.672	50.001	49.696	49.454	49.843	49.867	50.795	32.647
4	50	70	55.607	53.948	54.079	54.149	55.052	54.723	52.101	50.844	49.407	49.695	49.321	26.740
5	35	40	48.716	47.717	46.468	47.631	47.715	48.851	48.440	48.218	49.405	52.355	51.843	28.744
6	20	55	44.614	43.995	45.341	46.654	47.823	48.650	48.967	48.817	49.764	51.502	51.650	25.336
7	35	70	31.665	50.096	49.869	50.325	52.528	52.674	51.091	50.242	50.355	50.686	50.075	34.171
8	50	55	54.670	52.184	52.326	51.854	52.672	52.563	50.616	49.049	49.788	50.015	49.748	29.638
9	35	55	49.800	48.856	48.320	49.178	50.950	50.997	49.718	48.966	50.058	50.458	51.704	33.583

#23	Qi	Qc	Y1	Y2	Y3	Y4	Y5	Y6	Y7	Y8	Y9	Y10	Y11	SN Ratio
1	20	40	42.390	43.040	43.312	44.943	45.368	46.960	46.859	48.542	50.274	53.509	52.523	21.889
2	20	70	45.876	46.419	46.439	48.284	49.647	50.510	49.940	50.064	49.705	50.405	50.760	28.513
3	50	40	51.703	50.973	50.309	50.350	50.864	50.292	49.305	49.178	49.689	50.978	50.793	36.303
4	50	70	55.604	54.202	53.852	53.397	54.303	53.912	52.134	50.271	49.729	48.861	48.696	26.561
5	35	40	48.162	47.716	47.743	47.527	49.317	49.519	48.908	49.028	50.347	51.960	52.475	29.409
6	20	55	44.613	43.936	44.482	46.412	47.670	48.963	48.755	49.386	49.857	51.963	51.795	24.593
7	35	70	51.252	50.643	50.502	50.995	52.289	52.297	51.017	50.488	50 004	51.161	49.715	35.896
8	50	55	54.540	52.435	52.701	51.826	53.148	52.131	51.025	49.905	49.586	49.807	50.010	30.052
9	35	55	49.451	47.343	48.273	49.193	49.634	50.397	48.831	48.680	49.571	50.791	51.270	32.770

#24	Qi	Qc	Y1	Y2	Y3	Y4	Y5	Y6	Y7	Y8	Y9	Y10	Y11	SN Ratio
1	20	40	42.550	42.895	43.686	44.751	46.436	46.706	47.051	48.544	50.235	52.867	52.850	22.186
2	20	70	45.709	45.939	46.173	47.638	50.127	50.484	50.419	49.793	50.149	51.105	51.486	26.984
3	50	40	52.559	51.050	50.477	50.135	50.297	50.563	49.435	49.059	49.493	50.227	50.265	34.623
4	50	70	55.438	54.295	53.399	54.084	54.367	53.400	52.096	50.380	49.773	49.395	48.765	26.987
5	35	40	48.260	47.457	46.998	47.568	48.623	48.914	48.715	49.098	50.047	51.980	51.686	29.593
6	20	55	44.627	45.259	45.058	45.993	47.787	49.472	48.265	48.577	50.699	52.288	52.429	24.693
7	35	70	50.833	50.182	49.768	50.560	51.870	52.201	50.208	50.505	49.921	50.002	49.488	35.482
8	50	55	53.641	52.229	52.420	51.999	53.520	52.404	50.954	49.884	50.536	49.921	50.606	31.707
9	35	55	49.324	49.211	48.936	49.412	50.499	50.443	49.923	49.745	49.792	50.332	51.053	37.765

APPENDIX D

SILICON EXITAXY EXPERIMENT

Experimental Design

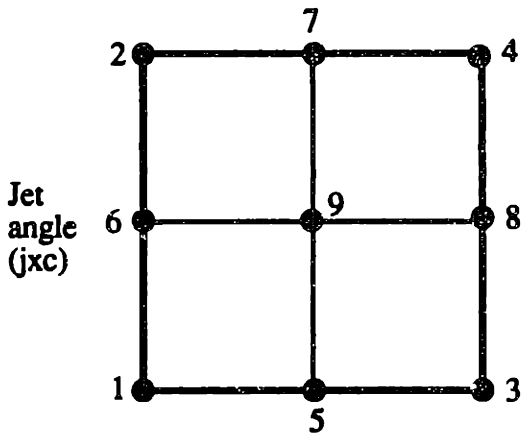

Flow balance (blc)

Setting point	blc	jxc
1	-1	-1
2	-1	1
3	1	-1
4	1	1
5	0	-1
6	-1	0
7	0	1
8	1	0
9	0	0

15 measurement sites

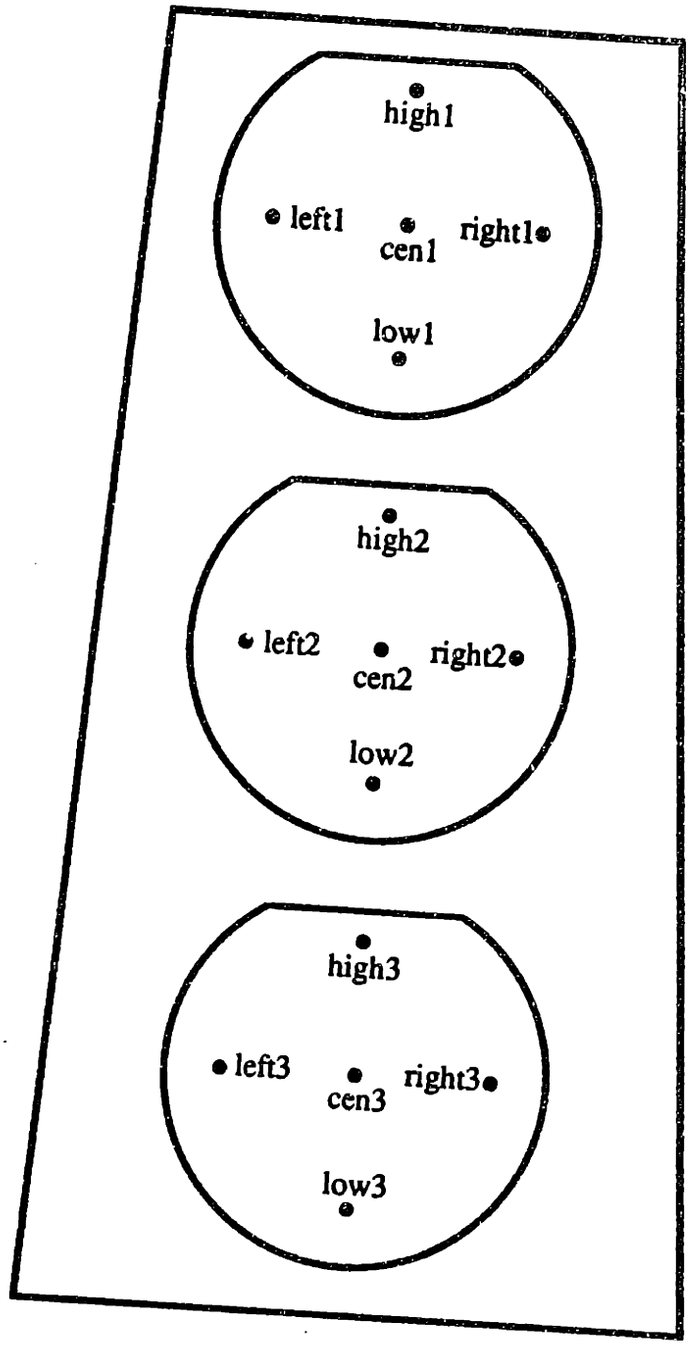

Experimental Data

Setting point	Experimental data															
	high1	low1	cen1	right1	left1	high2	low2	cen2	right2	left2	high3	low3	cen3	right3	left3	σ/μ (%)
1	8.11	6.92	7.43	8.36	7.49	6.90	6.23	6.51	7.45	6.65	6.23	5.87	5.95	6.88	6.29	10.96
	8.16	6.96	7.48	8.55	7.61	6.93	6.27	6.54	7.77	6.67	6.29	5.81	5.95	6.99	6.24	11.77
2	7.27	6.90	7.04	7.29	6.82	6.96	7.13	7.00	7.48	6.67	7.19	7.66	7.35	8.29	7.22	5.42
	7.22	6.93	6.94	7.21	6.87	6.88	7.12	6.98	7.56	6.71	7.27	7.60	7.31	8.28	7.25	5.40
	7.20	6.84	6.91	7.17	6.81	6.87	7.18	6.95	7.49	6.58	7.26	7.62	7.34	8.22	7.18	5.57
	7.11	6.78	6.83	7.07	6.74	6.84	7.03	6.90	7.39	6.50	7.24	7.54	7.25	8.07	7.11	5.38
3	7.90	6.95	7.38	7.31	8.22	6.79	6.30	6.46	6.60	7.61	6.24	6.02	6.04	6.27	7.08	10.04
	7.84	6.84	7.26	7.24	8.24	6.68	6.17	6.37	6.69	7.53	6.16	5.88	5.95	6.25	7.01	10.41
	8.23	7.22	7.66	7.77	8.46	6.91	6.77	6.81	6.83	7.59	6.45	6.52	6.44	6.56	7.45	9.09
	8.24	7.26	7.64	7.68	8.50	6.98	6.59	6.72	6.81	7.94	6.49	6.36	6.35	6.48	7.46	9.90
4	7.09	6.76	6.87	6.76	7.12	6.84	7.05	6.87	6.60	7.49	7.09	7.54	7.20	7.19	8.21	5.64
	6.95	6.73	6.70	6.75	7.04	6.74	6.87	6.79	6.57	7.40	7.12	7.51	7.18	7.23	8.18	5.89
5	8.21	7.17	7.65	8.03	7.91	7.10	6.48	6.71	7.12	7.28	6.41	6.10	6.19	6.75	6.81	9.36
	7.87	7.05	7.48	7.88	7.91	7.00	6.39	6.66	7.05	7.27	6.42	6.10	6.14	6.72	6.82	8.66
6	7.86	7.14	7.42	7.71	7.18	7.18	6.91	6.99	7.69	6.64	6.98	7.03	6.93	7.88	6.91	5.37
	7.66	7.15	7.30	7.70	7.20	7.18	6.88	7.03	7.67	6.69	7.09	6.98	6.90	7.81	6.98	4.76
7	6.81	6.55	6.61	6.70	6.64	6.63	6.91	6.71	6.83	6.76	7.00	7.44	7.15	7.57	7.54	4.99
	6.97	6.66	6.73	6.78	6.86	6.71	6.94	6.79	6.90	6.81	7.07	7.33	7.12	7.65	7.51	4.26
8	7.72	6.95	7.30	7.14	7.67	7.03	6.75	6.81	6.50	7.72	6.89	6.90	6.77	6.67	7.97	6.35
	7.55	6.94	7.25	7.15	7.70	6.95	6.64	6.76	6.54	7.70	6.80	6.96	6.74	6.63	7.96	6.35
9	7.57	6.97	7.21	7.13	7.28	7.04	6.97	6.96	7.05	7.14	7.02	7.22	7.05	7.35	7.52	2.70
	7.49	6.98	7.20	7.12	7.33	7.01	6.90	6.92	6.94	7.21	7.01	7.18	6.98	7.32	7.47	2.75
	7.40	6.90	7.08	7.11	7.21	6.95	6.87	6.86	6.90	6.99	6.84	7.12	6.95	7.22	7.35	2.56
	7.40	6.88	7.04	7.15	7.22	6.87	6.87	6.84	6.97	7.04	6.96	7.07	6.88	7.22	7.36	2.59

Uniformity Model

Dependent variable is: **uniformity**
R² = 95.4% R²(adjusted) = 94.1%
s = 0.6849 with 24 - 6 = 18 degrees of freedom

Source	Sum of Squares	df	Mean Square	F-ratio
Regression	174.807	5	35.0	74.5
Residual	8.44427	18	0.469126	

Variable	Coefficient	s.e. of Coeff	t-ratio
Constant	3.17500	0.2873	11.1
blc	-0.025000	0.1768	-0.141
jxc	-2.36000	0.1768	-13.3
blc^2	2.00750	0.3091	6.49
jxc^2	3.12250	0.3091	10.1

Difference Models

top-bottom = high1 - low3

left-right = (left1+left2+left3-right1-right2-right3)/3

Dependent variable is: **top-bottom**
R² = 99.3% R²(adjusted) = 99.2%
s = 0.1169 with 12 - 3 = 9 degrees of freedom

Source	Sum of Squares	df	Mean Square	F-ratio
Regression	18.0778	2	9.039	661
Residual	0.123012	9	0.013668	

Variable	Coefficient	s.e. of Coeff	t-ratio
Constant	0.782500	0.0337	23.2
blc	-0.134375	0.0358	-3.75
jxc	-1.26563	0.0358	-35.4

Dependent variable is: **left-right**
R² = 99.0% R²(adjusted) = 98.7%
s = 0.0948 with 12 - 3 = 9 degrees of freedom

Source	Sum of Squares	df	Mean Square	F-ratio
Regression	7.81750	2	3.9087	435
Residual	0.080824	9	0.008980	

Variable	Coefficient	s.e. of Coeff	t-ratio
Constant	0.023056	0.0274	0.843
blc	0.800833	0.0290	27.6
jxc	-0.018333	0.0290	-0.632

Thickness Models

Dependent variable is: **high1**
R² = 94.2% R²(adjusted) = 92.9%
s = 0.1358 with 12 - 3 = 9 degrees of freedom

Source	Sum of Squares	df	Mean Square	F-ratio
Regression	2.69674	2	1.3484	73.2
Residual	0.165863	9	0.018429	

Variable	Coefficient	s.e. of Coeff	t-ratio
Constant	7.61000	0.0392	194
blc	-0.065625	0.0416	-1.58
jxc	-0.491875	0.0416	-11.8

Dependent variable is: **cen1**
R² = 85.9% R²(adjusted) = 82.7%
s = 0.1394 with 12 - 3 = 9 degrees of freedom

Source	Sum of Squares	df	Mean Square	F-ratio
Regression	1.06495	2	0.53247	27.4
Residual	0.175017	9	0.019446	

Variable	Coefficient	s.e. of Coeff	t-ratio
Constant	7.17833	0.0403	178
blc	-0.028750	0.0427	-0.673
jxc	-0.306250	0.0427	-7.17

Dependent variable is: **low1**
R² = 40.4% R²(adjusted) = 27.1%
s = 0.1416 with 12 - 3 = 9 degrees of freedom

Source	Sum of Squares	df	Mean Square	F-ratio
Regression	0.122075	2	0.061037	3.04
Residual	0.180417	9	0.020046	

Variable	Coefficient	s.e. of Coeff	t-ratio
Constant	6.92417	0.0409	169
blc	0.002500	0.0434	0.058
jxc	-0.100000	0.0434	-2.31

Thickness Models

Dependent variable is: **right1**
R² = 87.6% R²(adjusted) = 84.9%
s = 0.2201 with 12 - 3 = 9 degrees of freedom

Source	Sum of Squares	df	Mean Square	F-ratio
Regression	3.08845	2	1.5442	31.9
Residual	0.435950	9	0.048439	

Variable	Coefficient	s.e. of Coeff	t-ratio
Constant	7.43000	0.0635	117
blc	-0.346250	0.0674	-5.14
jxc	-0.503750	0.0674	-7.48

Dependent variable is: **left1**
R² = 94.8% R²(adjusted) = 93.7%
s = 0.1743 with 12 - 3 = 9 degrees of freedom

Source	Sum of Squares	df	Mean Square	F-ratio
Regression	4.99495	2	2.4975	82.2
Residual	0.273317	9	0.030369	

Variable	Coefficient	s.e. of Coeff	t-ratio
Constant	7.49333	0.0503	149
blc	0.268750	0.0534	5.04
jxc	-0.503750	0.0534	-9.44

Dependent variable is: **high2**
R² = 23.3% R²(adjusted) = 6.2%
s = 0.0880 with 12 - 3 = 9 degrees of freedom

Source	Sum of Squares	df	Mean Square	F-ratio
Regression	0.021137	2	0.010569	1.37
Residual	0.069629	9	0.007737	

Variable	Coefficient	s.e. of Coeff	t-ratio
Constant	6.86167	0.0254	270
blc	-0.044375	0.0269	-1.65
jxc	-0.018125	0.0269	-0.673

Thickness Models

Dependent variable is: **cen2**
R² = 68.8% R²(adjusted) = 61.9%
s = 0.1352 with 12 - 3 = 9 degrees of freedom

Source	Sum of Squares	df	Mean Square	F-ratio
Regression	0.363138	2	0.181569	9.93
Residual	0.164629	9	0.018292	

Variable	Coefficient	s.e. of Coeff	t-ratio
Constant	6.74167	0.0390	173
blc	-0.015625	0.0414	-0.377
jxc	0.168125	0.0414	4.06

Dependent variable is: **low2**
R² = 80.1% R²(adjusted) = 75.7%
s = 0.1941 with 12 - 3 = 9 degrees of freedom

Source	Sum of Squares	df	Mean Square	F-ratio
Regression	1.36871	2	0.68436	18.2
Residual	0.338979	9	0.037664	

Variable	Coefficient	s.e. of Coeff	t-ratio
Constant	6.72583	0.0560	120
blc	0.013125	0.0594	0.221
jxc	0.341875	0.0594	5.75

Dependent variable is: **right2**
R² = 95.5% R²(adjusted) = 94.5%
s = 0.1061 with 12 - 3 = 9 degrees of freedom

Source	Sum of Squares	df	Mean Square	F-ratio
Regression	2.16814	2	1.0841	96.3
Residual	0.101329	9	0.011259	

Variable	Coefficient	s.e. of Coeff	t-ratio
Constant	7.10333	0.0306	232
blc	-0.443125	0.0325	-13.6
jxc	-0.069375	0.0325	-2.14

Thickness Models

Dependent variable is: low3
R² = 94.5% R²(adjusted) = 93.2%
s = 0.2104 with 12 - 3 = 9 degrees of freedom

Source	Sum of Squares	df	Mean Square	F-ratio
Regression	6.81543	2	3.4077	76.9
Residual	0.398600	9	0.044289	

Variable	Coefficient	s.e. of Coeff	t-ratio
Constant	6.82750	0.0608	112
blc	0.068750	0.0644	1.07
jxc	0.773750	0.0644	12.0

Dependent variable is: right3
R² = 96.4% R²(adjusted) = 95.6%
s = 0.1666 with 12 - 3 = 9 degrees of freedom

Source	Sum of Squares	df	Mean Square	F-ratio
Regression	6.73688	2	3.3684	121
Residual	0.249817	9	0.027757	

Variable	Coefficient	s.e. of Coeff	t-ratio
Constant	7.22583	0.0481	150
blc	-0.387500	0.0510	-7.60
jxc	0.525000	0.0510	10.3

Dependent variable is: left3
R² = 95.3% R²(adjusted) = 94.3%
s = 0.1428 with 12 - 3 = 9 degrees of freedom

Source	Sum of Squares	df	Mean Square	F-ratio
Regression	3.73210	2	1.8660	91.5
Residual	0.183567	9	0.020396	

Variable	Coefficient	s.e. of Coeff	t-ratio
Constant	7.22333	0.0412	175
blc	0.497500	0.0437	11.4
jxc	0.467500	0.0437	10.7

Simulated Experimental Data (Adding Noise)

Setting point	Simulated experimental data (adding noise)															
	high1	low1	cen1	right1	left1	high2	low2	cen2	right2	left2	high3	low3	cen3	right3	left3	σ/μ(%)
1	7.40	6.52	7.28	8.54	6.90	6.47	6.44	6.52	7.11	6.63	6.73	5.62	5.81	6.80	6.07	10.48
	8.98	7.56	7.99	8.02	7.93	6.25	6.39	6.68	6.67	6.85	6.33	5.39	6.18	7.15	6.29	13.56
2	7.36	6.45	7.25	7.61	6.87	7.24	6.76	6.99	6.18	6.65	7.09	7.14	7.46	8.38	7.39	7.23
	7.28	6.79	6.57	7.55	7.11	6.64	6.99	7.67	7.23	6.43	7.30	7.60	7.56	7.92	6.87	6.23
	7.17	6.72	6.95	7.30	6.87	6.44	7.26	7.12	7.99	6.15	7.11	7.19	6.77	8.54	6.97	8.12
	6.35	5.99	6.79	7.36	6.62	7.07	6.79	6.79	7.95	6.88	7.06	7.56	7.48	7.90	6.88	7.71
3	7.98	7.42	7.53	7.27	8.90	7.28	6.27	6.39	6.73	7.34	6.17	6.01	5.67	5.50	7.16	13.31
	7.34	6.91	7.11	7.21	8.59	7.10	6.48	6.27	6.90	7.70	5.34	5.62	5.98	6.56	6.69	12.16
	8.10	7.26	7.68	7.47	8.77	6.81	6.45	6.58	6.48	7.41	6.25	6.61	6.70	6.30	7.23	10.22
	7.73	7.10	8.22	7.49	9.38	6.68	6.29	6.27	6.93	8.36	6.54	6.31	6.07	6.26	7.65	13.51
4	6.70	6.79	6.74	6.61	7.37	6.79	7.13	6.42	6.70	7.22	7.44	7.16	7.24	7.13	8.11	6.05
	6.83	6.69	6.76	7.12	6.91	6.28	6.36	6.80	7.14	7.76	7.08	7.76	7.61	7.06	8.80	8.96
5	8.26	7.45	7.35	7.61	7.41	7.19	6.86	6.70	7.20	7.61	6.37	6.36	6.29	6.51	6.77	8.08
	8.07	7.14	7.02	7.63	7.66	6.41	6.22	6.67	7.42	7.01	6.49	6.65	5.76	6.83	6.75	8.78
6	7.49	7.43	7.32	8.50	7.75	7.18	6.94	7.04	7.91	6.38	6.96	6.83	6.79	7.35	6.83	7.28
	7.58	7.24	6.66	6.80	6.87	7.27	6.96	7.85	7.33	6.62	6.96	6.91	7.25	7.44	7.06	4.85
7	6.80	6.09	6.94	6.42	7.10	7.21	7.34	6.49	7.78	6.54	6.90	7.20	6.60	7.68	7.08	6.09
	6.76	6.54	6.69	6.98	6.85	6.65	7.28	6.87	6.98	6.78	7.03	7.23	6.53	7.52	7.58	4.73
8	7.45	7.24	6.74	7.33	8.38	6.83	6.22	6.35	6.85	6.60	7.24	6.98	6.71	7.09	7.59	7.65
	7.45	7.22	7.25	7.17	8.07	6.58	6.74	6.82	6.53	7.78	6.94	6.92	7.19	6.23	7.98	7.46
9	7.83	7.37	6.43	6.87	6.54	6.41	6.56	7.07	7.14	7.41	7.58	7.46	6.69	7.39	7.53	6.62
	7.26	7.15	6.72	7.22	6.94	6.63	7.10	6.57	6.82	6.50	6.46	7.48	6.57	7.57	7.18	5.23
	7.36	6.79	7.22	7.06	7.42	6.83	6.84	7.24	6.63	7.07	7.30	6.99	7.08	7.35	7.55	3.72
	7.90	6.45	6.79	6.61	7.23	7.08	7.36	6.41	7.17	7.47	6.06	6.95	7.39	7.27	7.24	6.85

APPENDIX E

TUNGSTEN CVD EXPERIMENT

Experimental Design

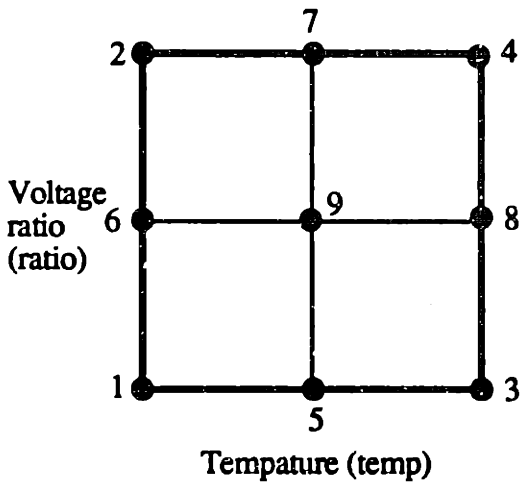

Setting point	temp	ratio
1	280	0.5
2	280	2.5
3	320	0.5
4	320	2.5
5	300	0.5
6	280	1.5
7	300	2.5
8	320	1.5
9	300	1.5

Experimental Data

Setting point	1			2			3		
Meas. Temp.	280			280			320		
Meas. Volt. Ratio	0.486			2.490			0.479		
Measurement	thickness	sheet resis.	resistivity	thickness	sheet resist	resistivity	thickness	sheet resist	resistivity
Unit	angstrom	ohm/sq	uohm-cm	angstrom	ohm/sq	uohm-cm	angstrom	ohm/sq	uohm-cm
Measu. #1	3758	0.55	20.6690	3771	0.46	17.3466	4284	0.30	12.8520
Measu. #2	3823	0.49	18.7327	3893	0.45	17.5185	4312	0.30	12.9360
Measu. #3	3845	0.51	19.6095	3905	0.43	16.7915	4358	0.30	13.0740
Measu. #4	3843	0.52	19.9836	3868	0.45	17.4060	4321	0.30	12.9630
Measu. #5	3835	0.49	18.7915	3831	0.46	17.6226	4241	0.30	12.7230
Measu. #6	3890	0.55	21.3950	4172	0.43	17.9396	4765	0.32	15.2480
Measu. #7	3910	0.54	21.1140	4136	0.44	18.1984	4737	0.31	14.6847
Measu. #8	3875	0.55	21.3125	4098	0.46	18.8508	4730	0.29	13.7170
Measu. #9	3944	0.52	20.5088	4144	0.43	17.8192	4746	0.26	13.2888
Average	3858	0.52	20.2352	3980	0.45	17.7215	4499	0.30	13.4985
Uniformity %			5.0451			3.2878			6.6066

Setting point	4			5			6		
Meas. Temp.	320			300			280		
Meas. Volt. Ratio	2.571			0.495			1.468		
Measurement	thickness	sheet resist	resistivity	thickness	sheet resist	resistivity	thickness	sheet resist	resistivity
Unit	angstrom	ohm/sq	uohm-cm	angstrom	ohm/sq	uohm-cm	angstrom	ohm/sq	uohm-cm
Measu. #1	4430	0.26	11.5180	3780	0.42	15.8760	3741	0.52	19.4532
Measu. #2	4465	0.26	11.6090	3822	0.42	16.0524	3793	0.52	19.7236
Measu. #3	4476	0.26	11.6376	3815	0.41	15.6415	3779	0.50	18.8950
Measu. #4	4458	0.26	11.5908	3796	0.41	15.5636	3791	0.53	20.0923
Measu. #5	4396	0.26	11.4296	3781	0.41	15.5021	3768	0.52	19.5936
Measu. #6	4833	0.25	12.0825	4104	0.46	18.8784	3950	0.50	19.7500
Measu. #7	4842	0.26	12.5892	4126	0.42	17.3292	4006	0.49	19.6294
Measu. #8	4761	0.26	12.3786	4050	0.46	18.6300	3923	0.52	20.3996
Measu. #9	4750	0.25	11.8750	4088	0.44	17.9872	3999	0.51	20.3949
Average	4601	0.26	11.8567	3929	0.43	16.8289	3861	0.51	19.7702
Uniformity %			3.4485			8.2226			2.4061

Setting point	7			8			9		
Meas. Temp.	300			320			300		
Meas. Volt. Ratio	2.654			1.506			1.500		
Measurement	thickness	sheet resist	resistivity	thickness	sheet resist	resistivity	thickness	sheet resist	resistivity
Unit	angstrom	ohm/sq	uohm-cm	angstrom	ohm/sq	uohm-cm	angstrom	ohm/sq	uohm-cm
Measu. #1	4085	0.34	13.8890	4375	0.29	12.6875	3772	0.39	14.7108
Measu. #2	4141	0.32	13.2512	4415	0.28	12.3620	3816	0.39	14.8824
Measu. #3	4128	0.32	13.2096	4433	0.28	12.4124	3872	0.38	14.7136
Measu. #4	4095	0.33	13.5135	4426	0.28	12.3928	3859	0.30	15.0501
Measu. #5	4087	0.32	13.0784	4413	0.28	12.3564	3852	0.39	15.0228
Measu. #6	4490	0.32	14.3680	4793	0.29	13.8997	4040	0.39	15.7560
Measu. #7	4446	0.32	14.2272	4782	0.30	14.3460	4104	0.38	15.5952
Measu. #8	4408	0.33	14.5464	4754	0.28	13.3112	4076	0.39	15.8964
Measu. #9	4421	0.32	14.1472	4745	0.28	13.2860	4109	0.38	15.6142
Average	4256	0.32	13.8034	4571	0.28	13.0060	3944	0.39	15.2491
Uniformity %			4.0035			5.7231			3.0503

Uniformity Model

Dependent variable is: uniformity
R^2 = 78.8% R^2(adjusted) = 43.5%
s = 1.436 with 9 - 6 = 3 degrees of freedom

Source	Sum of Squares	df	Mean Square	F-ratio
Regression	23.0254	5	4.605	2.23
Residual	6.18475	3	2.06158	

Variable	Coefficient	s.e. of Coeff	t-ratio
Constant	-155.276	229.0	-0.678
temp	1.02898	1.528	0.673
ratio	0.046086	10.82	0.004
temp**2	-0.001601	0.0025	-0.629
ratio**2	1.25800	0.9269	1.36
temp*ratio	-0.017842	0.0351	-0.508

Resistivity Models

Dependent variable is: r 1
R² = 97.9% R²(adjusted) = 93.8%
s = 1.044 with 4 - 3 = 1 degrees of freedom

Source	Sum of Squares	df	Mean Square	F-ratio
Regression	51.8697	2	25.93	23.8
Residual	1.08989	1	1.08989	

Variable	Coefficient	s.e. of Coeff	t-ratio
Constant	68.1511	7.872	8.66
temp*	-0.169529	0.0261	-6.49
ratio*	-1.12587	0.5096	-2.21

Dependent variable is: r 2
R² = 100.0% R²(adjusted) = 100.0%
s = 0.0291 with 4 - 3 = 1 degrees of freedom

Source	Sum of Squares	df	Mean Square	F-ratio
Regression	35.8755	2	17.94	21190
Residual	0.000847	1	0.000847	

Variable	Coefficient	s.e. of Coeff	t-ratio
Constant	59.8602	0.2194	273
temp*	-0.145753	0.0007	-200
ratio*	-0.620715	0.0142	-43.7

Dependent variable is: r 3
R² = 98.6% R²(adjusted) = 95.8%
s = 0.7363 with 4 - 3 = 1 degrees of freedom

Source	Sum of Squares	df	Mean Square	F-ratio
Regression	38.6205	2	19.31	35.6
Residual	0.542184	1	0.542184	

Variable	Coefficient	s.e. of Coeff	t-ratio
Constant	60.3804	5.552	10.9
temp*	-0.145164	0.0184	-7.88
ratio*	-1.03095	0.3595	-2.87

Resistivity Models

Dependent variable is: r 4
R² = 99.1% R²(adjusted) = 97.3%
s = 0.6450 with 4 - 3 = 1 degrees of freedom

Source	Sum of Squares	df	Mean Square	F-ratio
Regression	45.0369	2	22.52	54.1
Residual	0.416000	1	0.416000	

Variable	Coefficient	s.e. of Coeff	t-ratio
Constant	64.7969	4.864	13.3
temp*	-0.159562	0.0161	-9.89
ratio*	-0.957542	0.3149	-3.04

Dependent variable is: r 5
R² = 100.0% R²(adjusted) = 100.0%
s = 0.0358 with 4 - 3 = 1 degrees of freedom

Source	Sum of Squares	df	Mean Square	F-ratio
Regression	39.1044	2	19.55	15263
Residual	0.001281	1	0.001281	

Variable	Coefficient	s.e. of Coeff	t-ratio
Constant	61.8616	0.2699	229
temp*	-0.152712	0.0009	-171
ratio*	-0.601523	0.0175	-34.4

Dependent variable is: r 6
R² = 99.9% R²(adjusted) = 99.7%
s = 0.2160 with 4 - 3 = 1 degrees of freedom

Source	Sum of Squares	df	Mean Square	F-ratio
Regression	46.9580	2	23.48	503
Residual	0.046666	1	0.046666	

Variable	Coefficient	s.e. of Coeff	t-ratio
Constant	63.6655	1.629	39.1
temp*	-0.148556	0.0054	-27.5
ratio*	-1.61417	0.1055	-15.3

Resistivity Models

Dependent variable is: r 7
R² = 99.5% R²(adjusted) = 98.5%
s = 0.4638 with 4 - 3 = 1 degrees of freedom

Source	Sum of Squares	df	Mean Square	F-ratio
Regression	42.4622	2	21.23	98.7
Residual	0.215086	1	0.215086	

Variable	Coefficient	s.e. of Coeff	t-ratio
Constant	63.2885	3.497	18.1
temp*	-0.149354	0.0116	-12.9
ratio*	-1.21855	0.2264	-5.38

Dependent variable is: r 8
R² = 99.3% R²(adjusted) = 98.0%
s = 0.6023 with 4 - 3 = 1 degrees of freedom

Source	Sum of Squares	df	Mean Square	F-ratio
Regression	53.0379	2	26.52	73.1
Residual	0.362804	1	0.362804	

Variable	Coefficient	s.e. of Coeff	t-ratio
Constant	70.4511	4.542	15.5
temp*	-0.174994	0.0151	-11.6
ratio*	-0.921442	0.2940	-3.13

Dependent variable is: r 9
R² = 99.4% R²(adjusted) = 98.1%
s = 0.5286 with 4 - 3 = 1 degrees of freedom

Source	Sum of Squares	df	Mean Square	F-ratio
Regression	44.9470	2	22.47	80.4
Residual	0.279455	1	0.279455	

Variable	Coefficient	s.e. of Coeff	t-ratio
Constant	65.1731	3.986	16.3
temp*	-0.159949	0.0132	-12.1
ratio*	-0.923020	0.2581	-3.58

APPENDIX F

PLASMA ETCHING EXPERIMENT

Screening Experiments

D-Optimal Design + Replicates at setting points 1, 2, 3, 5

Setting point	D-Optimal Design					
	Pressure	Power	Gap	He	CHF3	CF4
1	2.7	500	0.3	100	15	45
2	3.3	900	0.4	150	45	135
3	2.7	900	0.4	150	15	135
4	3.3	500	0.3	100	45	45
5	2.7	500	0.3	150	45	135
6	3.3	900	0.4	100	15	45
7	3.3	500	0.4	100	45	135
8	2.7	900	0.3	150	15	45
9	2.7	900	0.4	100	45	45
10	3.3	500	0.3	150	15	135
11	3.3	500	0.4	150	15	45
12	2.7	900	0.3	100	45	135

Measurement Sites

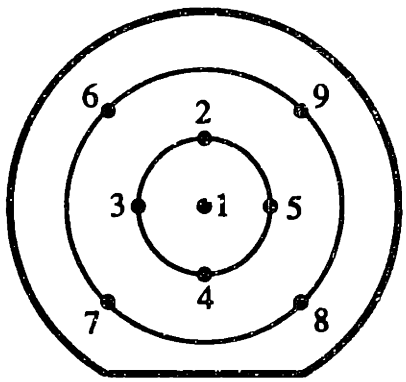

$$\text{Normalized metric - 1} = \frac{Y_1 - \mu}{\mu}$$

$$\text{Normalized metric - 2} = \frac{\overline{Y}_2 - \mu}{\mu}$$

$$\text{Normalized metric - 3} = \frac{\overline{Y}_3 - \mu}{\mu}$$

Experimental Data

Setting point	Experimental data								
	Y1	Y2	Y3	Y4	Y5	Y6	Y7	Y8	Y9
1	141.55	130.95	143.45	161.30	160.65	103.55	140.20	150.40	130.05
	108.50	103.90	113.35	127.10	124.50	88.60	104.30	109.60	102.35
2	98.55	106.30	105.65	112.40	113.40	110.50	122.85	124.50	119.90
	103.05	106.95	110.85	116.60	115.85	109.65	136.35	132.05	116.25
3	111.40	106.90	111.25	114.25	113.30	101.15	115.35	119.90	103.80
	112.75	107.75	112.45	115.75	114.10	100.10	113.95	121.10	106.70
4	63.00	58.70	66.25	78.65	74.80	54.15	74.00	76.95	60.05
5	120.70	130.10	135.45	146.45	146.10	115.45	146.55	149.60	134.20
	116.50	124.20	129.75	132.45	130.95	126.30	142.15	135.30	135.00
6	195.40	197.65	201.25	223.65	223.30	158.40	194.90	206.35	194.70
7	60.50	59.50	63.65	73.05	72.40	59.45	71.20	79.15	69.10
8	184.80	178.65	201.65	207.05	201.60	143.05	191.80	196.65	153.60
9	165.45	167.45	179.40	193.40	188.75	145.65	182.90	188.35	172.40
10	111.85	112.40	114.50	126.80	127.35	88.70	117.45	122.95	115.90
11	144.65	164.30	172.50	179.15	176.55	157.70	169.55	163.60	160.05
12	163.95	159.90	171.15	191.10	180.85	144.70	176.40	179.35	164.95

Normalized Metric Models

Dependent variable is: **Normalized metric -1**
R² = 87.4% R²(adjusted) = 81.0%
s = 0.0230 with 16 - 6 = 10 degrees of freedom

Source	Sum of Squares	df	Mean Square	F-ratio
Regression	0.036513	5	0.007303	13.8
Residual	0.005285	10	0.000528	

Variable	Coefficient	s.e. of Coeff	t-ratio
Constant	0.207149	0.0521	3.98
Power	0.000128	0.0000	3.85
Gap	-0.463194	0.1332	-3.48
He	-0.001021	0.0003	-3.53
CHF3	-0.002933	0.0004	-6.53
CF4	0.000305	0.0002	1.77

Dependent variable is: **normalized metric -2**
R² = 89.3% R²(adjusted) = 84.0%
s = 0.0135 with 16 - 6 = 10 degrees of freedom

Source	Sum of Squares	df	Mean Square	F-ratio
Regression	0.015232	5	0.003046	16.7
Residual	0.001821	10	0.000182	

Variable	Coefficient	s.e. of Coeff	t-ratio
Constant	0.212579	0.0306	6.95
Power	0.000009	0.0000	0.451
Gap	-0.271015	0.0782	-3.47
He	-0.000282	0.0002	-1.66
CHF3	-0.001036	0.0003	-3.93
CF4	-0.000317	0.0001	-3.13

Dependent variable is: **Normalized metric -3**
R² = 94.0% R²(adjusted) = 90.9%
s = 0.0129 with 16 - 6 = 10 degrees of freedom

Source	Sum of Squares	df	Mean Square	F-ratio
Regression	0.025840	5	0.005168	31.1
Residual	0.001662	10	0.000166	

Variable	Coefficient	s.e. of Coeff	t-ratio
Constant	-0.264367	0.0292	-9.05
Power	-0.000041	0.0000	-2.19
Gap	0.386813	0.0747	5.18
He	0.000537	0.0002	3.31
CHF3	0.001769	0.0003	7.03
CF4	0.000240	0.0001	2.49

Etch Rate Models

Dependent variable is: Y1
R² = 55.1% R²(adjusted) = 32.7%
s = 31.70 with 16 - 6 = 10 degrees of freedom

Source	Sum of Squares	df	Mean Square	F-ratio
Regression	12351.1	5	2470	2.46
Residual	10050.6	10	1005.06	

Variable	Coefficient	s.e. of Coeff	t-ratio
Constant	156.999	71.82	2.19
Power	0.121370	0.0459	2.64
Gap	-232.522	183.7	-1.27
He	0.107386	0.3990	0.269
CHF3	-0.482924	0.6192	-0.780
CF4	-0.362700	0.2379	-1.52

Dependent variable is: Y2
R² = 44.5% R²(adjusted) = 16.8%
s = 36.00 with 16 - 6 = 10 degrees of freedom

Source	Sum of Squares	df	Mean Square	F-ratio
Regression	10396.6	5	2079	1.60
Residual	12961.6	10	1296.16	

Variable	Coefficient	s.e. of Coeff	t-ratio
Constant	115.831	81.56	1.42
Power	0.104155	0.0522	2.00
Gap	-157.130	208.6	-0.753
He	0.316797	0.4531	0.699
CHF3	-0.238365	0.7032	-0.339
CF4	-0.430936	0.2702	-1.60

Dependent variable is: Y3
R² = 49.8% R²(adjusted) = 24.7%
s = 36.66 with 16 - 6 = 10 degrees of freedom

Source	Sum of Squares	df	Mean Square	F-ratio
Regression	13349.4	5	2670	1.99
Residual	13441.9	10	1344.19	

Variable	Coefficient	s.e. of Coeff	t-ratio
Constant	140.238	83.06	1.69
Power	0.115972	0.0531	2.18
Gap	-219.363	212.5	-1.03
He	0.343467	0.4614	0.744
CHF3	-0.223812	0.7161	-0.313
CF4	-0.508748	0.2751	-1.85

Etch Rate Models

Dependent variable is: Y4
R² = 48.5% R²(adjusted) = 22.8%
s = 39.27 with 16 - 6 = 10 degrees of freedom

Source	Sum of Squares	df	Mean Square	F-ratio
Regression	14545.7	5	2909	1.89
Residual	15423.7	10	1542.37	

Variable	Coefficient	s.e. of Coeff	t-ratio
Constant	183.412	88.97	2.06
Power	0.120604	0.0569	2.12
Gap	-247.334	227.6	-1.09
He	0.147506	0.4943	0.298
CHF3	-0.284171	0.7671	-0.370
CF4	-0.501384	0.2947	-1.70

Dependent variable is: Y5
R² = 47.1% R²(adjusted) = 20.7%
s = 38.83 with 16 - 6 = 10 degrees of freedom

Source	Sum of Squares	df	Mean Square	F-ratio
Regression	13427.4	5	2685	1.78
Residual	15077.0	10	1507.70	

Variable	Coefficient	s.e. of Coeff	t-ratio
Constant	173.233	87.96	1.97
Power	0.112413	0.0563	2.00
Gap	-217.850	225.0	-0.968
He	0.174496	0.4887	0.357
CHF3	-0.325664	0.7584	-0.429
CF4	-0.488392	0.2914	-1.68

Dependent variable is: Y6
R² = 37.7% R²(adjusted) = 6.5%
s = 30.72 with 16 - 6 = 10 degrees of freedom

Source	Sum of Squares	df	Mean Square	F-ratio
Regression	5709.70	5	1142	1.21
Residual	9436.69	10	943.669	

Variable	Coefficient	s.e. of Coeff	t-ratio
Constant	46.6697	69.59	0.671
Power	0.077086	0.0445	1.73
Gap	-44.6579	178.0	-0.251
He	0.439079	0.3866	1.14
CHF3	0.170614	0.6000	0.284
CF4	-0.349605	0.2305	-1.52

Etch Rate Models

Dependent variable is: **Y7**
R² = 45.0% R²(adjusted) = 17.5%
s = 34.91 with 16 - 6 = 10 degrees of freedom

Source	Sum of Squares	df	Mean Square	F-ratio
Regression	9960.48	5	1992	1.63
Residual	12188.5	10	1218.85	

Variable	Coefficient	s.e. of Coeff	t-ratio
Constant	103.390	79.09	1.31
Power	0.113052	0.0506	2.24
Gap	-185.041	202.3	-0.915
He	0.444414	0.4394	1.01
CHF3	0.207224	0.6819	0.304
CF4	-0.454123	0.2620	-1.73

Dependent variable is: **Y8**
R² = 46.7% R²(adjusted) = 20.1%
s = 34.40 with 16 - 6 = 10 degrees of freedom

Source	Sum of Squares	df	Mean Square	F-ratio
Regression	10383.7	5	2077	1.75
Residual	11835.3	10	1183.53	

Variable	Coefficient	s.e. of Coeff	t-ratio
Constant	128.681	77.93	1.65
Power	0.118845	0.0498	2.38
Gap	-190.870	199.4	-0.957
He	0.275703	0.4330	0.637
CHF3	-0.001635	0.6720	-0.002
CF4	-0.411564	0.2582	-1.59

Dependent variable is: **Y9**
R² = 31.0% R²(adjusted) = -3.5%
s = 36.86 with 16 - 6 = 10 degrees of freedom

Source	Sum of Squares	df	Mean Square	F-ratio
Regression	6101.26	5	1220	0.898
Residual	13587.2	10	1358.72	

Variable	Coefficient	s.e. of Coeff	t-ratio
Constant	101.780	83.50	1.22
Power	0.088113	0.0534	1.65
Gap	-94.5476	213.6	-0.443
He	0.217310	0.4639	0.468
CHF3	0.015794	0.7200	0.022
CF4	-0.326759	0.2766	-1.18